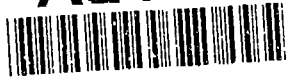


AD-A249 739



FJSRL-TR-92-0001

FRANK J. SEILER RESEARCH LABORATORY

**ACTIVE CONTROL OF THE  
SEPARATION REGION ON A  
TWO-DIMENSIONAL AIRFOIL**

DTIC  
SELECTE  
APR 29 1992  
S B D

92-11164



DR J.A. LOVATO

APPROVED FOR PUBLIC RELEASE  
DISTRIBUTION UNLIMITED.



MARCH 1992

AIR FORCE SYSTEMS COMMAND

UNITED STATES AIR FORCE

**FJSRL-TR-92-0001**

This document was prepared by the Aerospace Sciences Division, Frank J. Seiler Research Laboratory, United States Air Force Academy, CO. The research was conducted under Project Work Unit Number 2800/FF/07, Unsteady Aerodynamics. Dr J.A. Lovato was the Project Scientist in charge of the work.

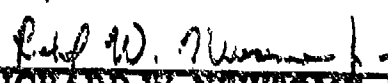
When U.S. Government drawings, specifications or other data are used for any purpose other than a definitely related government procurement operation, the government thereby incurs no responsibility nor any obligation whatsoever, and the fact that the government may have formulated, furnished or in any way supplied the said drawings, specifications or other data is not to be regarded by implication or otherwise, as in any manner licensing the holder or any other person or corporation or conveying any rights or permission to manufacture, use or sell any patented invention that may in any way be related thereto.

Inquiries concerning the technical content of this document should be addressed to the Frank J. Seiler Research Laboratory (AF3C), FJSRL/NA, USAF Academy, CO 80841-3528. Phone (719) 472-2812.

[This report has been reviewed by the Technical Director and is releasable to the National Technical Information Service (NTIS). At NTIS it will be available to the general public, including foreign nations.]

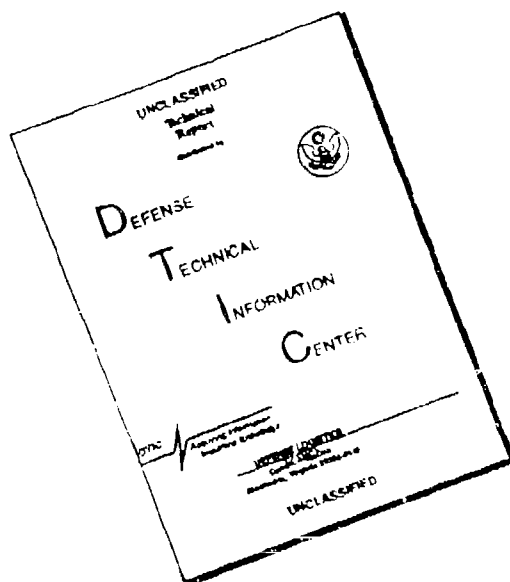
This technical report has been reviewed and is approved for publication.

  
**JUDE A. LOVATO**  
NRC Research Fellow

  
**RICHARD W. NEWSOME, Jr.**  
Lt Col, USAF  
Chief, Aerospace Sciences Division

  
**JOHN E. WILK**  
Technical Director

# DISCLAIMER NOTICE



THIS DOCUMENT IS BEST QUALITY AVAILABLE. THE COPY FURNISHED TO DTIC CONTAINED A SIGNIFICANT NUMBER OF PAGES WHICH DO NOT REPRODUCE LEGIBLY.

| REPORT DOCUMENTATION PAGE  |  |  | Form Approved<br>OMB No. 0704-0188 |  |
|--|--|--|------------------------------------|--|
| <small>Public reporting burden for this collection of information is estimated to average 1 hour per response, including the time for reviewing instructions, searching existing data sources, gathering and maintaining the data needed, and completing and reviewing the collection of information. Send comments regarding this burden estimate or any other aspect of this collection of information, including suggestions for reducing this burden, to Washington Headquarters Services, Directorate for Information Operations and Reports, 1215 Jefferson Davis Highway, Suite 1204, Arlington, VA 22202-4302, and to the Office of Management and Budget, Paperwork Reduction Project (0704-0188), Washington, DC 20503.</small>  |  |  |                                    |  |
| 1. AGENCY USE ONLY (Leave blank)   | 2. REPORT DATE<br>March 1992                             | 3. REPORT TYPE AND DATES COVERED<br>Technical Report             |                                    |  |
| 4. TITLE AND SUBTITLE<br><br>Active Control of the Separation Region on a Two-Dimensional Airfoil  |  | 5. FUNDING NUMBERS<br><br>2300/FF/07                             |                                    |  |
| 6. AUTHOR(S)<br><br>Julie A. Lovato  |  |  |                                    |  |
| 7. PERFORMING ORGANIZATION NAME(S) AND ADDRESS(ES)<br><br>Frank J. Seiler Research Laboratory<br>USAF Academy CO 80840-6528  |  | 8. PERFORMING ORGANIZATION REPORT NUMBER<br><br>FJSRL-TR-92-0001 |                                    |  |
| 9. SPONSORING/MONITORING AGENCY NAME(S) AND ADDRESS(ES)  |  | 10. SPONSORING/MONITORING AGENCY REPORT NUMBER                   |                                    |  |
| 11. SUPPLEMENTARY NOTES  |  |  |                                    |  |
| 12a. DISTRIBUTION/AVAILABILITY STATEMENT<br><br>Distribution Unlimited   |  | 12b. DISTRIBUTION CODE   |                                    |  |
| 13. ABSTRACT (Maximum 200 words)<br><p>This experimental analysis presents a comprehensive study of the separating boundary layer over a static airfoil under natural and actively controlled conditions. Near-surface hot-film and surface pressure measurements, as well as flow visualization are used to analyze the large-scale nature of the flow over a two-dimensional NACA-0015 airfoil and determine forcing effects. Results from the static study are then extended for an initial evaluation of unsteady airfoil control.</p> <p>Results show that the fundamental frequency associated with free shear layer instabilities for this case is an integral multiple of the frequency associated with wake structures. The static separating boundary layer response to active control confirms that it is a boundary layer transitioning to a free shear layer. Qualitative analyses show that significant reduction in overall static separation can be achieved under forcing conditions. Upper airfoil surface suction values are also significantly increased over the natural values. Applying tangential pulsed air control at static fundamental frequencies to a dynamic airfoil results in delay of the dynamic stall vortex formation and a delay of dynamic stall. These discoveries indicate that the developed control methodology may prove successful in increasing unsteady aircraft maneuverability.</p> |  |  |                                    |  |
| 14. SUBJECT TERMS<br>Static Airfoil Control; Separation Control;<br>Unsteady Aerodynamics; Boundary Layer Control  |  |  | 15. NUMBER OF PAGES<br>154         |  |
|  |  |  | 16. PRICE CODE                     |  |
| 17. SECURITY CLASSIFICATION OF REPORT<br>UNCLASSIFIED  | 18. SECURITY CLASSIFICATION OF THIS PAGE<br>UNCLASSIFIED | 19. SECURITY CLASSIFICATION OF ABSTRACT<br>UNCLASSIFIED          | 20. LIMITATION OF ABSTRACT<br>NONE |  |

## GENERAL INSTRUCTIONS FOR COMPLETING SF 298

The Report Documentation Page (RDP) is used in announcing and cataloging reports. It is important that this information be consistent with the rest of the report, particularly the cover and title page. Instructions for filling in each block of the form follow. It is important to **stay within the lines** to meet optical scanning requirements.

### Block 1. Agency Use Only (Leave blank).

**Block 2. Report Date.** Full publication date including day, month, and year, if available (e.g. 1 Jan 88). Must cite at least the year.

**Block 3. Type of Report and Dates Covered.** State whether report is interim, final, etc. If applicable, enter inclusive report dates (e.g. 10 Jun 87 - 30 Jun 88).

**Block 4. Title and Subtitle.** A title is taken from the part of the report that provides the most meaningful and complete information. When a report is prepared in more than one volume, repeat the primary title, add volume number, and include subtitle for the specific volume. On classified documents enter the title classification in parentheses.

**Block 5. Funding Numbers.** To include contract and grant numbers; may include program element number(s), project number(s), task number(s), and work unit number(s). Use the following labels.

|                      |                              |
|----------------------|------------------------------|
| C - Contract         | PR - Project                 |
| G - Grant            | TA - Task                    |
| PE - Program Element | WU - Work Unit Accession No. |

**Block 6. Author(s).** Name(s) of person(s) responsible for writing the report, performing the research, or credited with the content of the report. If editor or compiler, this should follow the name(s).

**Block 7. Performing Organization Name(s) and Address(es).** Self-explanatory.

**Block 8. Performing Organization Report Number.** Enter the unique alphanumeric report number(s) assigned by the organization performing the report.

**Block 9. Sponsoring/Monitoring Agency Name(s) and Address(es).** Self-explanatory.

**Block 10. Sponsoring/Monitoring Agency Report Number.** (If known)

**Block 11. Supplementary Notes.** Enter information not included elsewhere such as: Prepared in cooperation with ..., Trans. of...; To be published in... When a report is revised, include a statement whether the new report supersedes or supplements the older report.

**Block 12a. Distribution/Availability Statement.** Denotes public availability or limitations. Cite any availability to the public. Enter additional limitations or special markings in all capitals (e.g. NOFORN, REL, ITAR)

**DOD** - See DoDD 5230.24, "Distribution Statements on Technical Documents."

**DOE** - See authorities.

**NASA** - See Handbook NHB 2200.2.

**NTIS** - Leave blank.

### Block 12b. Distribution Code.

**DOD** - Leave blank.

**DOE** - Enter DOE distribution categories from the Standard Distribution for Unclassified Scientific and Technical Reports.

**NASA** - Leave blank.

**NTIS** - Leave blank.

**Block 13. Abstract.** Include a brief (**Maximum 200 words**) factual summary of the most significant information contained in the report.

**Block 14. Subject Terms.** Keywords or phrases identifying major subjects in the report.

**Block 15. Number of Pages.** Enter the total number of pages.

**Block 16. Price Code.** Enter appropriate price code (**NTIS only**).

**Blocks 17. - 19. Security Classifications.** Self-explanatory. Enter U.S. Security Classification in accordance with U.S. Security Regulations (i.e., UNCLASSIFIED). If form contains classified information, stamp classification on the top and bottom of the page.

**Block 20. Limitation of Abstract.** This block must be completed to assign a limitation to the abstract. Enter either UL (unlimited) or SAR (same as report). An entry in this block is necessary if the abstract is to be limited. If blank, the abstract is assumed to be unlimited.

## EXTENDED ABSTRACT

The effectiveness of combat aircraft depends in part on their ability to maintain high lift under extreme conditions. Examples of such conditions include the high angle of attack, rapid pitch motions necessary for combat maneuvers. A well known phenomena occurring on airfoils undergoing such high angle of attack motions is the formation of a leading edge vortex. This vortex is preceded by significant increases in lift, but is also accompanied by subsequent rapid loss of lift and the ensuing dynamic stall.

Prior to dynamic stall vortex formation, the unsteady separating boundary layer resembles the separating boundary layer over a static airfoil. Before developing control methodologies for unsteady flows, it is necessary to obtain a thorough understanding of the controlled flow over a static airfoil. This experimental analysis presents a comprehensive study of the separating boundary layer over a static airfoil under natural and actively controlled conditions. Near-surface hot-film and surface pressure measurements, as well as flow visualization are used to analyze the large-scale nature of the flow and determine forcing effects. Results from the static study are then extended for an initial evaluation of unsteady airfoil control.

The fundamental frequency for a two-dimensional NACA-0015 airfoil is found to be an integral multiple of the frequency associated with wake structures. The static separating boundary layer response to active control confirms that it is a boundary layer transitioning to a free shear layer. Qualitative analyses show that significant reduction in overall static separation can be achieved under forcing

conditions. Upper airfoil surface suction values are also significantly increased over the natural values. Applying tangential pulsed air control at static fundamental frequencies to a dynamic airfoil results in delay of the dynamic stall vortex formation and a delay of dynamic stall. These discoveries indicate that the developed control methodology may prove successful in increasing unsteady aircraft maneuverability.

|                      |                                     |
|----------------------|-------------------------------------|
| <b>Accession For</b> |                                     |
| NTIS GRA&I           | <input checked="" type="checkbox"/> |
| DTIC TAB             | <input type="checkbox"/>            |
| Unannounced          | <input type="checkbox"/>            |
| Justification        |                                     |
| By                   |                                     |
| Distribution/        |                                     |
| Availability Codes   |                                     |
| Dist                 | Avail and/or<br>Special             |
| A-1                  |                                     |



## ACKNOWLEDGEMENTS

I would like to thank the members of my committee, Dr. B. R. Ramaprian, Dr. C. Pezeshki, and Dr. M. Chaudhry. Very special thanks are due to Dr. T. R. Troutt for his patience and guidance as my committee chairman.

The Air Force Office of Scientific Research deserves appreciation for their financial support under contracts F49620-85-C-0013, F49620-88-C-0053, F49620-90-C-0076, and AFOSR-90-0131.

Additional appreciation goes to Bob and Minnie Lovato, Dr. Ngozi Kamalu, Captains Scott Schreck and Dave Bunker, and Dr. Tom Henshaw for their help and special contributions.

Thanks are due to all the men and women of the Frank J. Seiler Research Laboratory and the DFAN Aeronautics Laboratory at the US Air Force Academy for their invaluable assistance throughout this research project. Special thanks go to the following people:

- Mr. Bobby Hatfield, for assistance in design and construction of the experimental apparatus.
- TSgt Young Paek and Mr. Jim Smith for their help in the design and fabrication of the pulsed-air system.
- CIC Ed Figueroa and CIC Tim Jung for their assistance in obtaining the dynamic pressure data.
- Ms. Leah Kelly, for her constant support.

I would also like to thank Jan Danforth, Darlene Magallon, and Danielle Bishop at Washington State University for keeping me organized.

My heartfelt appreciation goes to Nikita and Cherie, for their constant companionship through all the late nights.



## TABLE OF CONTENTS

|   |            |
|---|------------|
| <b>EXTENDED ABSTRACT.....</b>                                   | <b>i</b>   |
| <b>ACKNOWLEDGEMENTS.....</b>                                    | <b>iii</b> |
| <b>LIST OF FIGURES.....</b>                                     | <b>vi</b>  |
| <b>NOMENCLATURE LIST.....</b>                                   | <b>xii</b> |
| <b>1. LITERATURE REVIEW.....</b>                                | <b>1</b>   |
| 1.1 Motivation.....   | 1          |
| 1.2 Comparison Between Steady and Unsteady Separation.....      | 3          |
| 1.3 Characteristics of Steady Airfoil Flows.....                | 8          |
| 1.4 Characteristics of Unsteady Airfoil Flows.....              | 9          |
| 1.5 Active Control of Free Shear Flows.....                     | 18         |
| <b>2. RESEARCH OBJECTIVES .....</b>                             | <b>26</b>  |
| 2.1 Static Airfoil.....   | 26         |
| 2.2 Dynamic Airfoil.....  | 27         |
| <b>3. EXPERIMENTAL METHODS.....</b>                             | <b>28</b>  |
| 3.1 Introduction.....   | 28         |
| 3.2 Flow Visualization.....                                     | 29         |
| 3.3 Hot-Film Anemometry.....                                    | 30         |
| 3.4 Flow Modification.....                                      | 31         |
| 3.5 Pressure Measurements.....                                  | 32         |
| <b>4. ACOUSTIC CONTROL RESULTS – STEADY.....</b>                | <b>39</b>  |
| 4.1 Determination of Fundamental Frequency.....                 | 39         |
| 4.2 Acoustic Manipulation of the Separating Boundary Layer..... | 45         |

|           |  |            |
|-----------|--|------------|
| <b>5.</b> | <b>INTERNAL TANGENTIAL PULSED AIR CONTROL</b>                                  |            |
|           | <b>RESULTS – STEADY.....</b>   | <b>55</b>  |
| 5.1       | Pulsed Air Manipulation of the Separating Boundary Layer.....                  | 55         |
| 5.2       | Qualitative Response of Pulsed Air Control.....                                | 64         |
| 5.3       | Effect of Reynolds Number on Control Response.....                             | 70         |
| 5.4       | Effect of Pulsed Air Control on Surface Pressures.....                         | 74         |
| <b>6.</b> | <b>DYNAMIC FLOW CONTROL.....</b>   | <b>87</b>  |
| 6.1       | Pulsed Air Control of an Unsteady Separating Boundary<br>Layer.....            | 87         |
| 6.2       | Qualitative Control Response of the Unsteady Separating Boundary<br>Layer..... | 101        |
| 6.3       | Control Effects on Unsteady Airfoil Performance.....                           | 103        |
| <b>7.</b> | <b>DISCUSSION AND CONCLUSIONS.....</b>   | <b>111</b> |
| 7.1       | Discussion – Static Airfoil.....   | 111        |
| 7.2       | Discussion – Dynamic Airfoil.....  | 113        |
| 7.3       | Conclusions – Static and Dynamic Airfoil.....                                  | 114        |
| <b>8.</b> | <b>RECOMMENDATIONS.....</b>  | <b>116</b> |
|           | <b>BIBLIOGRAPHY.....</b>   | <b>118</b> |
|           | <b>APPENDIX</b>  |            |
| <b>A.</b> | <b>LIST OF COMPUTER PROGRAMS.....</b>  | <b>129</b> |

## LIST OF FIGURES

|            |   |    |
|------------|---|----|
| Figure 1-1 | Flow visualization comparison of flow over a static and dynamic NACA-0015 airfoil. $R_c=24,000$ .....   | 6  |
| Figure 1-2 | Comparison between static and dynamic lift coefficients.....  | 7  |
| Figure 3-1 | Flow visualization schematic.....   | 33 |
| Figure 3-2 | Hot-film anemometry data acquisition process.....   | 34 |
| Figure 3-3 | Acoustic control schematic.....   | 35 |
| Figure 3-4 | Tangential-pulsed air control schematic.....  | 36 |
| Figure 3-5 | Velocity profile of tangential-pulsed air control at the slot exit.....   | 37 |
| Figure 3-6 | Pressure airfoil configuration.....   | 38 |
| Figure 4-1 | Velocity fluctuations in the separating boundary layer on a static airfoil with respect to distance from the airfoil surface, $\alpha=20^\circ$ ..... | 42 |
| Figure 4-2 | Power spectra at varying frequencies. $\alpha=20^\circ$ , $R_c=57,000$ .....  | 43 |
| Figure 4-3 | Maximum power spectral values at varying control frequencies. $\alpha=20^\circ$ , $R_c=57,000$ .....  | 44 |
| Figure 4-4 | Velocity fluctuations with respect to time and the corresponding power spectra. Acoustic control, $\alpha=10^\circ$ . $R_c=24,000$ .....              | 48 |
| Figure 4-5 | Velocity fluctuations with respect to time and the corresponding power spectra. Acoustic control. $\alpha=15^\circ$ . $R_c=24,000$ .....              | 49 |

|             |  |    |
|-------------|--|----|
| Figure 4-6  | Velocity fluctuations with respect to time and the<br>corresponding power spectra. Acoustic control. $\alpha=20^\circ$ .<br>$R_c=24,000$ .....   | 50 |
| Figure 4-7  | Velocity fluctuations with respect to time and the<br>corresponding power spectra. Acoustic control. $\alpha=25^\circ$ .<br>$R_c=24,000$ .. ..   | 51 |
| Figure 4-8  | Velocity fluctuations with respect to time and the<br>corresponding power spectra. Acoustic control. $\alpha=30^\circ$ .<br>$R_c=24,000$ .....   | 52 |
| Figure 4-9  | Change in free shear layer velocity fluctuations at<br>increasing angles of attack. Acoustic control.<br>$R_c=24,000$ .....                      | 53 |
| Figure 4-10 | Comparison of experimental and theoretical fundamental<br>frequencies with respect to angle of attack.....                                       | 54 |
| Figure 5-1  | Velocity fluctuations with respect to time and the<br>corresponding power spectra. Pulsed air control. $\alpha=10^\circ$ .<br>$R_c=24,000$ ..... | 58 |
| Figure 5-2  | Velocity fluctuations with respect to time and the<br>corresponding power spectra. Pulsed air control. $\alpha=15^\circ$ .<br>$R_c=24,000$ ..... | 59 |
| Figure 5-3  | Velocity fluctuations with respect to time and the<br>corresponding power spectra. Pulsed air control. $\alpha=20^\circ$ .<br>$R_c=24,000$ ..... | 60 |

|             |  |    |
|-------------|--|----|
| Figure 5-4  | Velocity fluctuations with respect to time and the corresponding power spectra. Pulsed air control. $\alpha=25^\circ$ . $R_c=24,000$ .....   | 61 |
| Figure 5-5  | Changes in free shear layer velocity fluctuations at increasing angle of attack. Pulsed air control. $R_c=24,000$ ....                       | 62 |
| Figure 5-6  | Flow receptivity to forcing with increasing angle of attack. Pulsed air control. $\alpha=20^\circ$ and $25^\circ$ . $R_c=24,000$ .....       | 63 |
| Figure 5-7  | Leading edge smoke flow visualization of a static airfoil. Pulsed air control. $R_c=24,000$ .....  | 67 |
| Figure 5-8  | Smoke flow visualization of the entire flow field over a static airfoil. Pulsed air control. $R_c=24,000$ .....                              | 68 |
| Figure 5-9  | Smoke flow visualization of a static airfoil undergoing increasing pulsed air control frequencies. $R_c=24,000$ , $\alpha=25^\circ$ .....    | 69 |
| Figure 5-10 | Velocity fluctuations with respect to time and the corresponding power spectra. Pulsed air control. $R_c=57,000$ . $\alpha=20^\circ$ .....   | 72 |
| Figure 5-11 | Comparison between the velocity fluctuations with respect to time for 24,000 and 57,000. Pulsed air control. $\alpha=20^\circ$ .....         | 73 |
| Figure 5-12 | Upper surface pressure coefficients for a one second period. Pulsed air control. $\alpha=10^\circ$ , $R_c=57,000$ .....                      | 77 |
| Figure 5-13 | Average pressure coefficients for a static airfoil with respect to port location. Pulsed air control. $\alpha=10^\circ$ , $R_c=57,000$ ..... | 78 |
| Figure 5-14 | Upper surface pressure coefficients for a one second period. Pulsed air control. $\alpha=15^\circ$ , $R_c=57,000$ .....                      | 79 |

|             |  |
|-------------|--|
| Figure 5-15 | Upper surface pressure coefficients for a one second period.<br>Pulsed air control. $\alpha=15^\circ$ , $R_c=57,000$ .....80   |
| Figure 5-16 | Average pressure coefficients for a static airfoil with respect<br>to port location. Pulsed air control. $\alpha=15^\circ$ , $R_c=57,000$ .....81                                |
| Figure 5-17 | Upper surface pressure coefficients for a one second period.<br>Pulsed air control. $\alpha=20^\circ$ , $R_c=57,000$ .....82   |
| Figure 5-18 | Upper surface pressure coefficients for a one second period.<br>Pulsed air control. $\alpha=20^\circ$ , $R_c=57,000$ ... ..83  |
| Figure 5-19 | Average pressure coefficients for a static airfoil with respect<br>to port location. Pulsed air control. $\alpha=20^\circ$ , $R_c=24,000$ .....84                                |
| Figure 5-20 | Upper surface pressure coefficients for a one second period.<br>Pulsed air control. $\alpha=25^\circ$ , $R_c=57,000$ .....85   |
| Figure 5-21 | Upper surface pressure coefficients for a one second period.<br>Pulsed air control. $\alpha=25^\circ$ , $R_c=57,000$ .....86   |
| Figure 5-22 | Average pressure coefficients for a static airfoil with respect<br>to port location. Pulsed air control. $\alpha=25^\circ$ , $R_c=57,000$ .....87                                |
| Figure 6-1  | Instantaneous velocity fluctuations over dynamic airfoil<br>with respect to angle of attack. Natural flow. $\alpha^+=0.05$ ,<br>$R_c=24,000$ . $X/C=0.10$ .....92                |
| Figure 6-2  | Instantaneous velocity fluctuations over dynamic airfoil<br>with respect to angle of attack. Pulsed air control at<br>20 Hz. $\alpha^+=0.05$ , $R_c=24,000$ . $X/C=0.10$ .....93 |
| Figure 6-3  | Instantaneous velocity fluctuations over dynamic airfoil<br>with respect to angle of attack. Pulsed air control at<br>10 Hz. $\alpha^+=0.05$ , $R_c=24,000$ . $X/C=0.10$ .....94 |

|             |  |     |
|-------------|--|-----|
| Figure 6-4  | Instantaneous velocity fluctuations over dynamic airfoil with respect to angle of attack. Pulsed air control at 5 Hz. $\alpha^+ = 0.05$ , $R_c = 24,000$ . $X/C = 0.10$ .....  | 95  |
| Figure 6-5  | Instantaneous velocity increases with respect to distance from the airfoil surface. Pulsed air control. $\alpha^+ = 0.05$ . $R_c = 24,000$ . $X/C = 0.10$ .....                | 96  |
| Figure 6-6  | Instantaneous velocity fluctuations over dynamic airfoil with respect to angle of attack. Natural flow. $\alpha^+ = 0.05$ , $R_c = 24,000$ . $X/C = 0.30$ .....                | 97  |
| Figure 6-7  | Instantaneous velocity fluctuations over dynamic airfoil with respect to angle of attack. Pulsed air control at 20 Hz. $\alpha^+ = 0.05$ , $R_c = 24,000$ . $X/C = 0.30$ ..... | 98  |
| Figure 6-8  | Instantaneous velocity fluctuations over dynamic airfoil with respect to angle of attack. Pulsed air control at 10 Hz. $\alpha^+ = 0.05$ , $R_c = 24,000$ . $X/C = 0.30$ ..... | 99  |
| Figure 6-9  | Instantaneous velocity fluctuations over dynamic airfoil with respect to angle of attack. Pulsed air control at 5 Hz. $\alpha^+ = 0.05$ , $R_c = 24,000$ . $X/C = 0.30$ .....  | 100 |
| Figure 6-10 | Instantaneous velocity increases with respect to distance from the airfoil surface. Pulsed air control. $\alpha^+ = 0.05$ , $R_c = 24,000$ . $X/C = 0.30$ .....                | 101 |
| Figure 6-11 | Smoke flow visualization of a dynamic airfoil under natural and pulsed air forced conditions. $R_c = 24,000$ .....   | 103 |

|             |   |     |
|-------------|---|-----|
| Figure 6-12 | Instantaneous surface pressure coefficients on a dynamic airfoil under natural conditions (a) and pulsed-air forced conditions at 30 Hz. $\alpha^+ = 0.05$ , $R_c = 57,000$ ..... | 107 |
| Figure 6-13 | Instantaneous surface pressure coefficients on a dynamic airfoil under pulsed air forcing. Column 1 = 15 Hz and Column 2 = 7.5 Hz. $\alpha^+ = 0.05$ , $R_c = 57,000$ .....       | 108 |
| Figure 6-14 | Lift coefficients with respect to angle of attack on a dynamic airfoil. $\alpha^+ = 0.05$ , $R_c = 57,000$ .....  | 109 |
| Figure 6-15 | Drag coefficients with respect to angle of attack on a dynamic airfoil. $\alpha^+ = 0.05$ , $R_c = 57,000$ .....  | 110 |



# NOMENCLATURE LIST

|                |   |
|----------------|---|
| $c$            | Airfoil chordlength, cm   |
| $C_D$          | Pressure drag coefficient   |
| $C_L$          | Pressure lift coefficient   |
| $C_P$          | Surface pressure coefficient  |
| $C_\mu$        | Blowing momentum coefficient, $(U_{\text{slot}})^2/(U_\infty)^2 \times (\text{slot width})/c$ |
| $F$            | Control frequency, hz   |
| $R_c$          | Chord Reynolds number   |
| $St$           | Strouhal Number, defined as $fc/U_\infty$ unless otherwise specified                          |
| $V$            | Composite velocity measured on a pitching airfoil by the hot-film                             |
| $u$            | Instantaneous free shear layer velocity, m/s  |
| $u'$           | Free shear layer fluctuating velocity component, m/s  |
| $U_\infty$     | Freestream velocity, m/s  |
| $X$            | Distance along the chordwise direction of the airfoil, cm                                     |
| $Y$            | Distance away from the airfoil, perpendicular to the surface, cm                              |
| $\alpha$       | Airfoil angle of attack, degrees  |
| $\dot{\alpha}$ | Actual dynamic pitch rate, radians/second   |
| $\alpha^+$     | Non-dimensional pitch rate, defined as $\dot{\alpha}c/U_\infty$                               |

## CHAPTER ONE

### LITERATURE REVIEW

#### 1.1 Motivation

The ability of high performance aircraft to perform in combat situations is governed in part by aircraft maneuverability and stability. Design changes in air to air weapons have increased the need for fighter-aircraft to execute difficult maneuvers in which the best possible instantaneous turning performance is essential to combat superiority. The development of all-aspect short-range infrared guided missiles and all-aspect capability guns coupled with aircraft position controls has caused the emphasis in close air combat design to shift to enhanced maneuverability (Herbst, 1985a & 1985b). These post-stall regime maneuvers utilize thrust control to achieve rapid attitude changes. Such conditions may result in unsteady separation on the wing. This situation can lead to increased drag, wind buffeting, and stability and control problems which degrade combat effectiveness and could cause the loss of the aircraft (Whitford 1987). Unsteady forces can also impose loads on helicopter blades and marine propellers which affect performance and longevity (McCroskey, 1982).

Unsteady separation does generate large transient aerodynamic forces which hold promise in augmenting aircraft performance. Jumper, Dardis, and Stephen (1988) noted that, where range and maneuverability attributes conflict in vehicle design, unsteady separation manipulation may be used to fulfill the maneuverability requirements, allowing the range requirements to be fulfilled by

design. The flow over airfoils undergoing constant pitching or oscillating motions exhibit lift coefficients of up to five times static values (Carr, et al, 1977). This complex, unsteady flow process is characterized in general as "dynamic stall flow", and has been the subject of numerous investigations (McCroskey, 1982, & Carr, 1988). The angle of attack of dynamic stall, or the point at which the lift curve begins to decrease, is significantly extended over the static values. These attributes can contribute to aircraft maneuverability, reducing the need for maneuverability design specifications. The difficulty in this lies in the transient nature of the enhanced aerodynamic parameters associated with dynamic stall. Therefore an efficient means of controlling these parameters is necessary.

For the study discussed here, an analogy is drawn between the separating boundary layer on a static airfoil and a free shear layer. It is known that, on a static airfoil, the laminar boundary layer undergoes a transition to a turbulent, separated shear layer as the angle of attack is increased (Lissaman, 1983). This experimental study evaluates the similarities between this separated shear layer and a free shear layer, as well as the response of the airfoil shear layer to active control methods proven successful in manipulating a free shear layer.

An experimental analysis of an oscillating two dimensional airfoil done by Conger (1992) has shown that large scale structures appear, grow, and develop as the angle of attack is increased. Near the leading edge of the airfoil, a number of these vortical structures coalesce to form the dynamic stall vortex at sufficiently high angles of attack. Since these unsteady shear layer structures bear at least a qualitative similarity to those present in both a free shear layer and the separating boundary layer on a static airfoil, it may be possible to successfully apply a control methodology focused on manipulating the growth and development of shear layer

structures to an unsteady airfoil. Numerous efforts, which will be outlined in this review, have shown success in applying active control methods to both free shear flows and static airfoils. This background review will first discuss the similarities between steady and unsteady airfoil flows, then summarize the known aerodynamic performance enhancements associated with a pitching airfoil. Studies concerning shear layer development and control will then be outlined. A subsequent overview of steady and unsteady airfoil control techniques to date will also be made.

## 1.2 Comparison Between Steady and Unsteady Separation

An important aspect of this study is that similarities exist between static and dynamic airfoil flows. Currier and Fung (1991) determined computationally that the flow prior to unsteady boundary layer separation and dynamic stall formation is quasi-steady. There is, however, a difference between the two separation mechanisms which should be mentioned. In steady separation, the flow is sufficiently retarded due to an adverse pressure gradient, and the momentum of the fluid particles is reduced. The retarded particles cannot penetrate into the high pressure region due to their reduced kinetic energy. The boundary layer is deflected away from the wall and separates from it. The point of separation is defined as the point where the wall shear vanishes (Schlichting 1955). In unsteady separation, the separation point does not necessarily coincide with the point of vanishing wall shear (Rott 1956). Rather, the unsteady separation point is determined by the simultaneous vanishing of the wall shear and the profile velocity at a point just above the wall as seen by an observer moving with the separation velocity (Moore, 1958, Sears and Telionis, 1975). This is known as the MRS criterion. If the

observer is fixed at a point on the airfoil surface, it is possible to observe zero velocity or zero shear stress and not have unsteady separation. The separation is caused by an abrupt thickening of the boundary layer, which results in the retarded fluid in the boundary layer being ejected into the potential flow.

Figure 1-1 compares the flow over a static and a dynamic airfoil. Except for the fact that the unsteady flow remains attached for higher angles of attack, the two flows are qualitatively similar up to the formation of the unsteady dynamic stall vortex. As the angle of attack increases, the flow transitions from a quasi-steady, symmetric flow to a separating flow with an increase in the strength of the trailing edge vortices. As the separation zone grows a shear layer interaction between the separating boundary layer and the separated flow produces a number of small clockwise vortices. This continues until, on the steady airfoil, the entire upper surface flow has separated and the airfoil is stalled.

Flow over the dynamic airfoil, pitched at a non-dimensional pitch rate,  $\alpha^+$ , of 0.05, initially follows the same qualitative pattern as in the static case. By an angle of attack of  $10^\circ$ , the flow is beginning to separate and numerous clockwise vortical structures are evident in the separating boundary layer. As the angle of attack increases, the separation point moves upstream along the airfoil surface until, at an angle of attack of  $20^\circ$ , a leading edge vortex can be seen developing on the upper surface. This leading edge vortex, known as the dynamic stall vortex, continues to grow with increasing angle of attack. Eventually, the dynamic stall vortex detaches from the airfoil surface and convects downstream.

Figure 1-2 shows an example of lift curves for both a static and a dynamic NACA-0015 airfoil. Separation on the steady airfoil results in a rapid loss of lift at the early angle of attack of  $15^\circ$ . Pitching the airfoil at a non-dimensional pitch rate

( $\alpha^+$ ) of 0.2 results in both a significant increase in lift coefficient magnitude and a delay in airfoil stall until the angle of attack of  $30^\circ$ , as indicated by the sudden loss of lift over the airfoil surface. The beneficial nature of the unsteady flow is evident in the increased lift. However, the transient characteristics of this high lift belies its practical application.

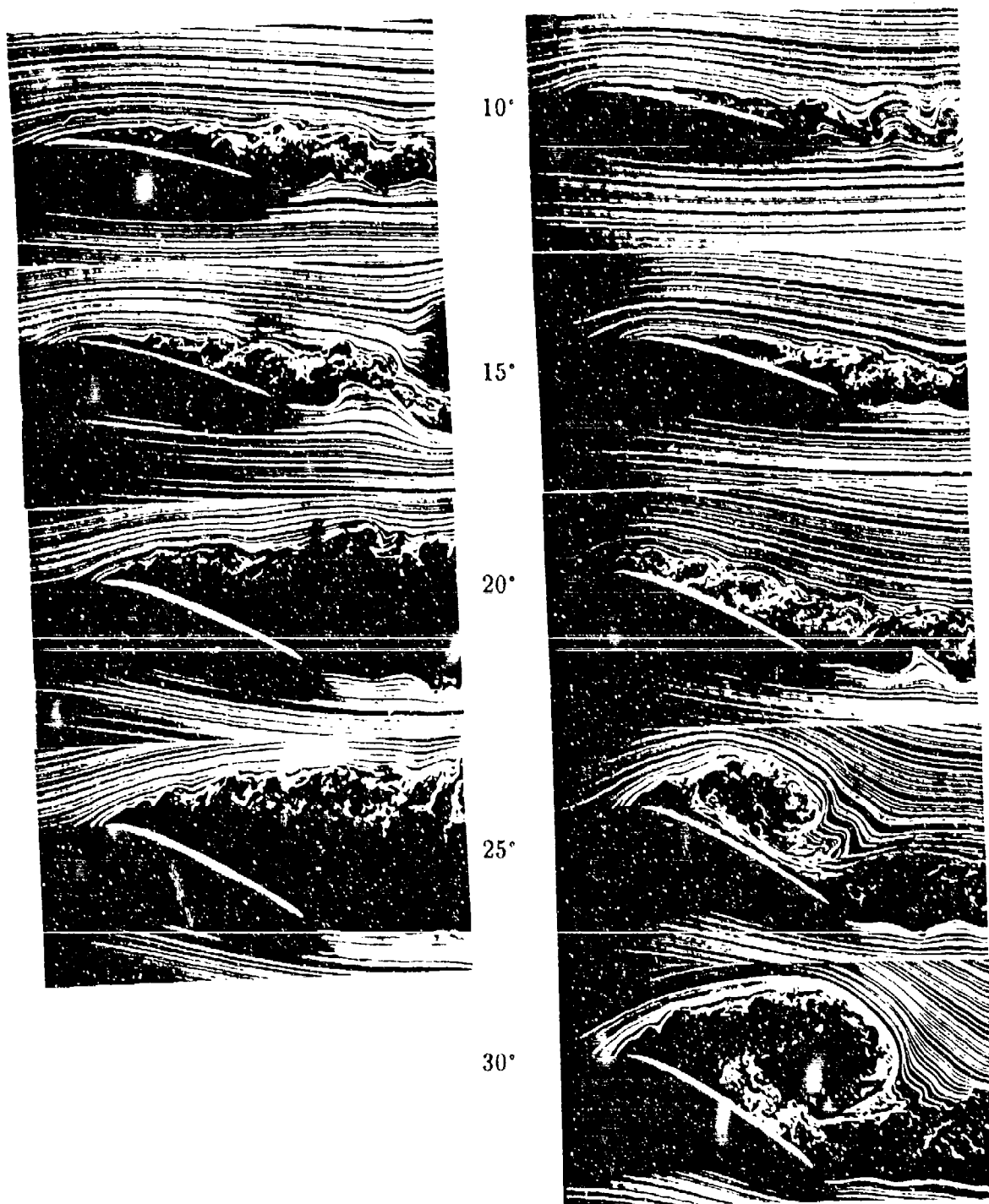


Figure 1-1.

Flow visualization comparison of flow over a static and dynamic ( $\alpha^+ = 0.05$ ) NACA-0015 airfoil.  $P_c = 24,000$ .

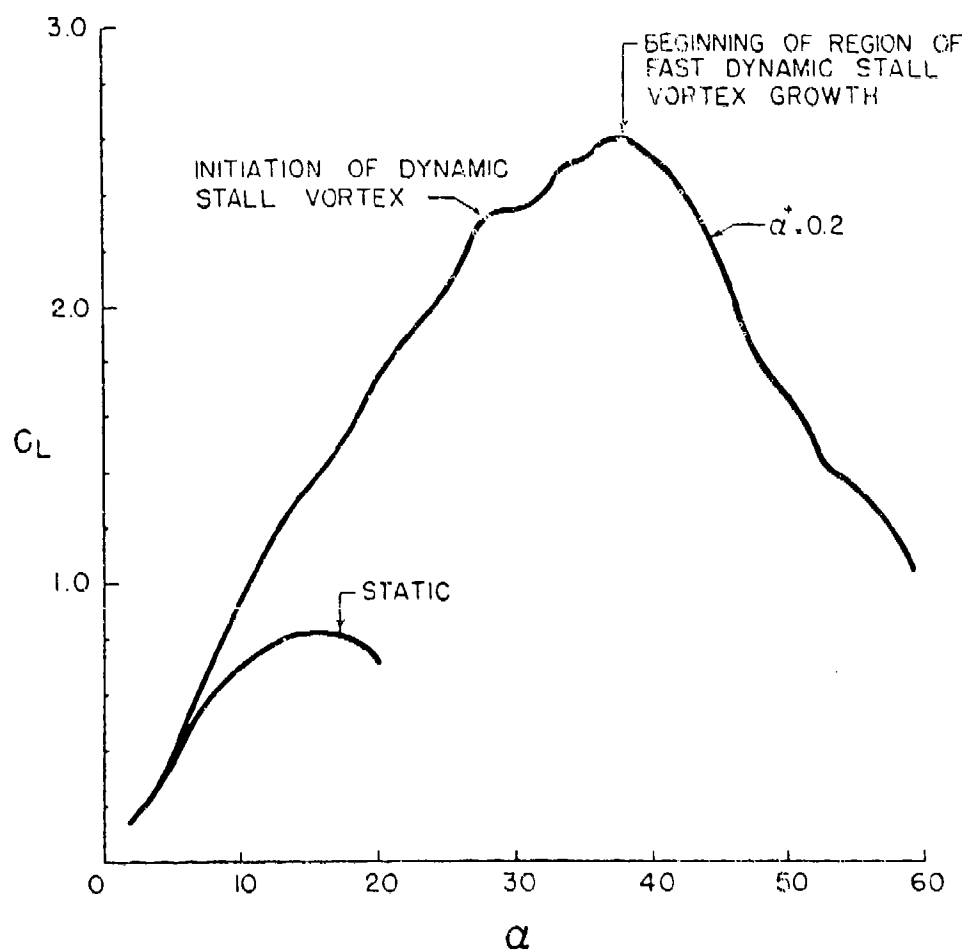


Figure 1-2. Comparison between static and dynamic lift coefficients. From Albertson, et al, (1987).



### 1.3 Characteristics of Steady Airfoil Flows

The first part of this experimental analysis is to evaluate the flow over a static airfoil. There are three specific types of stall, as discussed by **Currier and Fung (1991)**. The first is leading edge stall, where the flow separates initially near the leading edge but reattaches almost immediately due to rapid transition to turbulence. This reattachment occurs when the pressure nearly equals the value that would exist if the boundary layer was turbulent and attached (**Mueller and Batill, 1982**). This region between separation and reattachment is comparable in size to the thickness of the boundary layer. As the stall angle is approached, the region grows shorter until the adverse pressure gradient results in airfoil separation. The separation/reattachment region is significant because it determines the initial conditions of the boundary layer downstream (**Van den Berg, 1981**). It is this type of stall which occurs on a static airfoil. According to **Lissaman, (1983)**, the region between separation and reattachment, known as a laminar separation bubble, occurs only on airfoils below a chord Reynolds number of 50,000. Above this point, the airfoil is physically too short for reattachment to occur.

The second type of stall, thin-airfoil stall, is characterized by laminar flow separation at the airfoil leading edge and coinciding reattachment at some point downstream. The reattachment location moves downstream along the airfoil surface as the angle of attack is increased, creating what is known as a long separation bubble. This concept will be elaborated on in a later section. The third kind of stall is trailing edge stall, which involves the forward movement of a turbulent

separation point from the trailing edge. This kink of stall occurs on unsteady airfoils.

For all Reynolds numbers, the flow over a static airfoil separates at a sufficiently high angle of attack (Zaman and McKizzie, 1991). At Reynolds numbers below about 100,000, extensive separation on the upper airfoil surface may be possible even at low angles of attack. For these cases, the laminar boundary layer fails to overcome the adverse pressure gradient and separates, forming an unattached free shear layer. According to Mueller and Batill (1982), the lift and drag on a static airfoil increases as  $R_c$  increases. The angle of attack corresponding to airfoil stall also increases, but only slightly.

#### 1.4 Characteristics of Unsteady Airfoil Flows

Experimental investigations into the unsteady separated regime date back to the early 1930's. Looking at the effects of a single gust on airfoil performance, Kramer (1932) found that increases in lift were possible as the angle of attack changed. By varying the direction of the freestream with respect to a static airfoil, he discovered that the maximum lift increased at a linear rate. Lippisch (1935) was successful in obtaining smoke flow visualization of an airfoil pitched in a constant freestream. Although he noted a delay in upper surface flow separation past the static stall angle, there is no indication of the formation of a leading edge vortex. Unsteady airfoil flows are characterized by a reduced frequency, whose concept was developed by Birnbaum (1923). Today this frequency is referred to in the literature regarding constant-rate pitch studies as a non-dimensional pitch rate,  $\alpha^+$ , defined as  $\dot{\alpha}c/U_\infty$ , where  $\dot{\alpha}$  is the actual pitch rate,  $c$  is the airfoil chord length, and  $U_\infty$  is

the freestream velocity. **Cook (1987)** showed that, for inertia force dominated flows, the non-dimensional pitch rate could provide effects that are orders of magnitude greater than the Reynolds number effects.

In contrast to the early work in Germany, American efforts at the time concerning unsteady separation experimentation focused towards practical aircraft applications. **Silverstein et al (1938)** explored the changes in lift coefficient of an aircraft pitching at constant rates. Significant increases in maximum lift coefficient were found in both wind tunnel tests and flight tests using the same full scale aircraft pitched at an equivalent non-dimensional pitch rate of 0.01. **Harper and Flanigan (1948)** extended this work into the compressible range using a comparable non-dimensional pitch rate. Close corroboration was found between flight tests of a full scale aircraft and wind tunnel tests of a 1/20 scale model. They also noted that the transitory increases in lift with non-dimensional pitch rate varied with the Mach number.

Although significant in their results, these first investigations into the unsteady realm failed to address the actual physics of the flow leading to the enhanced lift. The majority of interest in constant rate pitching evolved from unsteady separation on helicopter rotors. **Ham and Gardlick (1968)** first explored the physical cause for dynamic stall, attempting to explain the extreme transient mechanical loads imposed on helicopter blades during linear attitude changes. What they found was that the peak lift was primarily a function of pitch rate, with the angle of attack at which dynamic stall occurred dependent primarily upon the pivot point of the airfoil.

Recent efforts have concentrated on evaluating the initiation and the growth of the dynamic stall vortex and the extensive variations in the upper surface

pressure field that accompany it. Francis and Keesee (1985) conducted an analysis of the pressure field on a constantly pitched airfoil. They found that, although there is significant dependence on non-dimensional pitch rate, the qualitative features of the surface pressure field are similar in various dynamic stall cases. At attack angles lower than the corresponding static stall values, the configuration of the pressure distributions resembles quasisteady (static) flow, except for a lag in pressure coefficient magnitudes. As the angle of attack passes the static stall point, the pressure distribution for an attached flow persists, again with pressure coefficient magnitudes in excess of steady flow values. The peak in pressure magnitude detaches from the leading edge region and moves downstream along the upper airfoil surface as the angle of attack continues to increase. Comparing the behavior of the upper surface pressure field with flow visualization data by Walker, Helin, and Strickland (1985) reveals that the pressure coefficient peak position corresponds approximately to the location of the dynamic stall vortex center on the airfoil surface. This was confirmed by Albertson, et al (1987) in a digital image analysis study tracking vortex movement over the airfoil.

The manifestation of these increased pressure coefficient magnitudes for unsteady airfoil flow results in accentuated lift and drag values as compared to static cases. Lift coefficients more than double the static stall values have been determined for non-dimensional pitch rates as low as 0.05 (Carr, et al, 1977, Albertson, Troutt, and Kedzie, 1988). Drag coefficient values were found to increase correspondingly, although analysis of the lift to drag ratios showed airfoil performance enhancements well above static airfoil experiments.

The non-dimensional pitch rate,  $\alpha^+$ , has been identified numerous times as a characteristic descriptive parameter for dynamic stall flows. The variation in the

flow field with respect to  $\alpha^+$  can be categorized into three areas: 1) flow visualization, 2) surface pressure measurements, and 3) surface velocity field measurements. In a comprehensive flow visualization analysis, **Walker, Helin, and Strickland (1985)** found that increasing  $\alpha^+$  from 0.2 to 0.6 both delayed flow separation and dynamic stall vortex formation. In addition, at the higher  $\alpha^+$  value, significant secondary vortical structures appear. **Albertson, et al (1987)** used digital image analysis to quantify the growth and movement of the leading edge vortex with respect to angle of attack. They determined that, for both  $\alpha^+$  values of 0.1 and 0.2, the dynamic stall vortex experiences a short period of slow growth, suggesting a quasi-stable period, followed by rapid growth and eventual vortex detachment. The angle of attack at which the vortex commences enhanced growth coincides closely to the point when dynamic stall occurs. It was also ascertained that the commencement of rapid vortex growth coincides with the attack angle at which the vortex center is located approximately over the quarter chord position. This connection has not been studied further to date.

The effect of non-dimensional pitch rate change on the upper surface pressure field has been the subject of several pressure surface studies. Experimental analyses performed by **Walker, Helin, and Chou (1985)** indicated that lift enhancement associated with the unsteady airfoil motion magnifies with increasing pitch rate. Observing the flow over a range from  $\alpha^+ = 0.05$  to 0.6, they determined that both the magnitude of maximum lift and the angle of attack at which it occurs (dynamic stall angle) increase with  $\alpha^+$ . As expected, an increase in the initial slope of the lift coefficient curve accompanies these trends. **Francis and Keesee (1985)** showed that the relationship between the maximum lift coefficient and  $\alpha^+$  over a pitch rate range from zero to 0.4 follows the same trend as the attack angle at which

dynamic stall occurs. **Strickland and Graham (1986)** introduced a stall delay angle, defined as:

$$\Delta\alpha_{N \text{ stall}} = \alpha_{N \text{ dyn. stall}} - \alpha_{\text{static stall}}$$

where  $\alpha_{N \text{ dyn. stall}}$  is the angle of attack corresponding to dynamic stall and  $\alpha_{\text{static stall}}$  is the angle of attack corresponding to static stall. Dynamic stall is defined as the angle of attack at which the separation point reaches the leading edge. They found that the stall delay angle at the nose,  $\Delta\alpha_{N \text{ stall}}$ , is proportional to the square root of the non-dimensional pitch rate. Based upon research that the maximum lift coefficient follows the same trend as the pitch angle corresponding to dynamic stall, it can be deduced that  $C_{L-\text{Max}}$  should follow the same trend. This has not been analyzed.

The connection between the surface velocity field over a constantly pitched airfoil and the non-dimensional pitch rate was investigated by **Walker, Helin, and Strickland (1985)** and by **Walker and Chou (1987)**. **Walker, Helin, and Strickland** discovered reverse flow velocities directly under the dynamic stall vortex to be over 140%  $U_{\infty}$  for an  $\alpha^+$  of 0.2 and over 210%  $U_{\infty}$  for an  $\alpha^+$  of 0.6. It was also noted that the leading edge vortex initially produces a much higher reverse flow velocity than the trailing edge vortex does. **Walker and Chou** confirmed these results, and additionally disclosed that the upper surface velocity reaches a sub-peak corresponding to the point of dynamic stall vortex initiation, and then resumes an increasing trend rapidly to the primary velocity peak.

It has been demonstrated that the airfoil pivot location has a substantial effect on the unsteady flow field development. **Helin and Walker (1985)** found that

as the pivot point moves downstream along the chord, the onset of dynamic stall is delayed. The subsequent rapid development and movement of the vortex over the airfoil has no appreciable qualitative variation with pivot location. **Stephen, et al (1989)** confirmed that the flow develops independently of pitch axis location after the leading edge vortex forms. In their comparative study of a two-dimensional NACA 0015 airfoil pitched about axes from half a chord length forward of the airfoil to half a chord length aft of the airfoil, they determined that the size of the vortical disturbances are similar. This indicates that the vortex strength may be comparable in each case. Although moving the pitch axes aft does delay the flow development, the magnitude of the pressure peak and thus of the aerodynamic pressure forces decreases. In both the non-dimensional pitch rates studied,  $\alpha^+ = 0.1$  and  $0.15$ , the delay due to an increase in  $\alpha^+$  was greater than the delay due to changing pitch axis. The trade off between dynamic stall delay and enhanced airfoil performance has not been thoroughly investigated to date.

The choice to study a two-dimensional, NACA-0015 airfoil under static and constant-rate pitched conditions in this study bears explanation. Numerous studies have been conducted on both constant-rate and oscillating airfoils, such that the airfoil performance is well documented. While an oscillating motion is the most likely to be applied in a practical situation, it induces somewhat complicated phase effects into all airfoil parameters. Specifically, the development of vortical structures is much more involved for the oscillating case due to phase relationships with airfoil motion (**Klinge, Schreck, and Luttges, 1990**). A constant-rate motion is chosen here to eliminate these phase relationships and simplify free shear layer structure development. It is felt that a clear understanding of this less complicated flow is necessary prior to extension to oscillatory motions.

The choice of the two-dimensional NACA-0015 airfoil is similarly due to the need for flow simplicity. In a comprehensive experimental study of unsteady flow over varying types of airfoils, **Gad-el-Hak and Ho, (1986)** discuss the variation in flow characteristics due to airfoil configuration. On a rectangular wing with a sharp leading edge, a secondary, counter-rotating vortex is present upstream of the dynamic stall vortex. These two structures interact with each other as the angle of attack changes. With a blunt leading edge, NACA-0012 wing, there is no counter-rotating vortex. On a swept wing, the leading edge separation vortex (dynamic stall vortex) is stationary for a portion of the pitch cycle. Each of these cases demonstrates the complexity of unsteady flows over wings. Keeping the experiment confined to a symmetrical, two dimensional airfoil allows concentration on the forcing effects applied to the development of the dynamic stall vortex specifically. This vortex plays a key role in both two and three-dimensional flows.

The preceding discussions concerning dependence of airfoil aerodynamic performance and flow complexity on varying parameters and those considered in this study can be summarized by the functional relationship  $P = F(\alpha, \alpha^+, R_c, \text{pivot location, airfoil shape, flow dimensionality, and control parameters})$ , where  $P$  represents both airfoil qualitative and quantitative behavior. Table 1 gives an example of the specific dependence on the varying flow parameters. As discussed in **Carr (1988)**, moving the pitch axis rearward produces some similarity to increasing the pitch rate, in that the formation of the dynamic stall vortex is delayed to a greater angle of attack. However, there are significant variations in vortex dynamics. Increasing the pitch rate itself results not only in the delay in dynamic stall vortex generation but in a delay in stall with respect to angle of attack and an increase in maximum lift and drag coefficients. **Walther and Chou (1987)**



determined that the chord Reynolds number effects are secondary to changes in the flow due to alterations in the non-dimensional pitch rate  $\alpha^+$  at Reynolds numbers below 150,000.

Carr also discusses the three dimensional effects on dynamic stall. Numerous dynamic stall characteristics are similar on two and three-dimensional airfoils, but there are important differences which must be considered. Structures generated on the tips of oscillating and constant-rate pitch wings can at times, depending on airfoil geometry and pitch rate, interact substantially with the dynamic stall vortex and alter both the qualitative and quantitative nature of the flow. The study here focuses only on the effects of control and angle of attack changes, simplifying the flow so that a basic understanding of static and dynamic control can be obtained. The reader is referred to **McLaughlin (1992)** for a detailed functional relationship of the specific parameters involved in constant-rate and oscillating airfoil flows.

TABLE I: Dynamic Airfoil Performance under Varying Conditions

| <u>Parameter</u>             | <u>Increasing <math>\alpha</math></u> | <u>Increasing <math>\alpha^+</math></u>           | <u>Increasing <math>R_c</math></u> | <u>Pivot Location (Increasing <math>X/C</math>)</u>           |
|------------------------------|---------------------------------------|---|------------------------------------|---|
| $C_P$                        | increases                             | increases   | decreases                          | independent   |
| $C_L$                        | increases                             | increases   | decreases                          | independent   |
| $C_D$                        | increases                             | increases   | decreases                          | independent   |
| $\alpha_{C_L-\max}$          | increases                             | increases   | decreases                          | increases asymptotically<br>(secondary to $\alpha^+$ effects) |
| $\alpha_{C_D-\max}$          | increases                             | increases   | decreases                          | increase asymptotically<br>(secondary to $\alpha^+$ effects)  |
| $u_{\max}(X/C=0.4)$          | independent                           | increases   |                                    |   |
| $\alpha_{u_{\max}}(X/C=0.4)$ | increases                             |   |                                    |   |
| Vortex dwell<br>Time         | increases                             | increases   | decreases                          | independent   |
| Vortex<br>Nature             | tighter                               | tighter, multiple<br>vortices at $\alpha^+ > 0.4$ |                                    | independent   |

## 1.5 Active Control of Free Shear Flows

Although significantly more energetic and complex, the unsteady flow around a constantly pitched, two-dimensional airfoil in part bears resemblance to free shear flows. The laminar free shear layer is susceptible to small perturbations via the Kelvin-Helmholtz instabilities. The two-dimensional waves grow exponentially with downstream distance and roll up into vortices (Ho and Huerre, 1984). Prior to formation of the leading edge stall vortex in the case of a constantly pitching airfoil, large-scale vortical structures appear in the interface layer between the unsteady boundary layer and the viscous separation region on the upper airfoil surface (Conger, 1992). Since the instability nature of a free shear layer can be manipulated to either reduce or enhance large-scale structure development (Oster and Wygnanski, 1982, and Wu, Wu, and Wu, 1992), a control method successful in affecting the large scale structure free shear layer is a reasonable idea to evaluate.

The plane mixing layer was first shown to contain large scale structures by the experiments of Brown and Roshko (1974). Winant and Browand (1974) added that the growth of the mixing layer was due to the propagation of the instability waves, which then roll up into discrete two-dimensional vortex structures. The subsequential growth of the mixing layer is due to the interaction between these large scale vortex structures, known as "vortex pairing". The vortical nature of these large scale structures was confirmed by Browand and Weidman (1976). Numerous studies have quantified the frequency associated with the initial instability occurring at the trailing edge of the splitter plate (Ho and Huang, 1982, Oster and Wygnanski, 1982, Monkewitz, 1988, and Tordella and Christiansen, 1989). Browand (1986) showed that the initial instability frequency

fluctuates in time by as much as 10%, and that there is actually a broad band of frequencies present.

The spanwise nature of the large scale vortex structures in plane mixing layers has been the subject of numerous investigations. Browand and Troutt (1980, 1985) showed that the structures are initially aligned in the spanwise direction. Pairing interactions do introduce three-dimensional distortions of spanwise nature, but these disturbances disappear as the pairing process is completed and the structures regain their spanwise alignment. A flow visualization study on the evolution of streamwise vortical structures in a plane free shear layer done by Lasheras, Cho, and Maxworthy (1986) found evidence of streamwise vortical structures. These streamwise vortices were a result of the unstable response of the shear layer to three dimensional perturbations. In a mixing layer without these upstream disturbances a primarily two dimensional structure was maintained.

It has been conclusively demonstrated that the large scale vortex structures present in the mixing layer can be modified by external forcing. Ho and Huang (1982) and Oster and Wygnanski (1982) showed that the pairing interactions between the large scale structures, and thus mixing layer growth, can be modified by introducing coherent perturbations at the initiation of mixing. By controlling the pairing interactions, the spreading rate of the mixing layer can be enhanced or inhibited, in some extents even changing the signs of the Reynolds stress values and reducing turbulent energy. Ho and Huang (1982) specifically determined that the mechanisms by which vortex pairing is controlled depends upon the frequency at which the flow is controlled. They found that forcing the flow at the fundamental frequency inhibits large scale structure pairing, forcing at one half the fundamental frequency causes two vortices to pair at once, forcing at one third the fundamental

frequency causes every three vortices to eventually coalesce, and so on. Ho and Huerre (1984) give a comprehensive study of the modification of large scale structures by acoustic forcing. The methods of vortex pairing control has been extended to include the shear layer of a reattaching, separated flow. Troutt, Scheelke, and Norman (1984) verified that large scale structures similar to those present in the mixing layer are also characteristic of the reattaching, separated flow over a downstream facing step. Bhattacharjee, Scheelke, and Troutt (1986) and Roos and Kegelmann (1986) explored control of the flow over a downstream facing step using two separate control mechanisms. Bhattacharjee, Scheelke, and Troutt (1986) used a hot-wire probe to ascertain the fundamental frequency associated with the initial instabilities. Power spectra of the signal yielded a broad peak that gradually shifts towards lower frequencies with downstream position. This shift is attributed to the large-scale vortex amalgamations occurring in the separated shear layer. Acoustic forcing at the fundamental initial vortex passage frequency produces a sharp spike in the power spectra at the natural flow frequency. This coincides with increased temporal and spatial correlation in the spanwise flow and a considerable reduction in reattachment length. Forcing between Strouhal numbers of 0.2 and 0.4 is the most effective forcing range over a large range of Reynolds number. Strouhal number,  $St$ , is defined as the frequency, multiplied by the characteristic length and divided by the free stream velocity. Roos and Kegelmann (1986) confirmed these results using an oscillating flap at the step edge to excite the flow.

The key assumption in this research effort is that, since the initial reattaching, separated region over the upper airfoil surface resembles a free shear layer, it should be possible to actively control it by methods proven successful in

controlling the free shear layer. The active control means reviewed in the previous pages have been shown to manipulate pairing of the shear layer vortices, growth of the shear layer, and reduction of the reattachment length in reattaching separated flows. Forcing applied to the reattaching separated layer over a static airfoil has delayed stall and enhanced lift (Gad-el-Hak and Bushnell (1991). Since it has been determined that the lift enhancement and stall delay associated with dynamic flows embodies itself prior to the development of the dynamic stall vortex (Albertson, Troutt, and Kedzie, 1988), it follows that the initial unsteady separation region, prior to dynamic stall vortex formation, is what must be focused upon when evaluating active controls. It is necessary for initial stall to have occurred, since it is the separating boundary layer, or shear layer, that is the focus of the proposed research analysis. Furthermore, it has been determined that active control, specifically acoustic forcing, modulates a free shear layer by manipulating the free shear layer itself, and not the upstream boundary layer (Zaman and Rice 1992). Therefore, it is concluded that, by linking the control frequencies with the initial Kelvin-Helmholtz instability frequencies, active forcing can be successfully applied to a two-dimensional, constantly pitched airfoil.

The nature of the frequencies associated with the wake from a static lifting surface has been explored previously. Roshko (1954) found that a universal Strouhal number based on wake frequencies has the value of  $St = 0.15-0.18$ , with the corresponding angle of attack—modified Strouhal number being represented by  $St = f \sin \alpha / U_\infty$ , where  $f$  in this case corresponds to the frequency associated with the large scale structures emanating from the wake. Katz (1981) showed that the large scale wake structures generated by a NACA-0012 airfoil are shed at an angle of attack—based Strouhal number of approximately 0.18.

Several experimental analyses have been performed on static airfoils under varying control conditions. **Ahuja and Burrin (1984)** used high frequency external acoustic control over a cambered airfoil to improve lift coefficients by over 50% relative to natural conditions. The most effective frequency was noted to be a multiple of the fundamental flow frequency associated with the shear layer instabilities. By internally injecting acoustic forcing near the fundamental flow frequency, **Collins (1981)** was able to partially reattach the upper surface separation and increase lift coefficients by 20%. **Maestrello (1986)** confirmed this with external acoustic forcing, and in addition determined that velocity perturbation magnitudes in the region of transition could be reduced significantly. An alternate forcing method employed by **Bar-Sever (1989)** involved an oscillating wire on the airfoil surface. This was successful in reducing separation and enhancing the static lift coefficient magnitudes.

**Zaman, Bar-Sever, and Mangalam (1987)** were able to reduce laminar separation completely by low frequency ( $St \leq 5$ ) external acoustic oscillations over a smooth airfoil. In addition, lift enhancements were achieved with large amplitude, high frequency excitation ( $St = 4-25$ ) in the post-stall regime. Tunnel cross-resonances induce large transverse velocity fluctuations near the airfoil that enhance the separation control. However, these fluctuations would not be present in the open flow over an aircraft in actual flight. The authors suggest that the excitation mechanisms which produce reduced separation must hinge on the instability of the separated shear layer, but are also be influenced by the presence of the solid boundary and the separation location. **Huang, Maestrello, and Bryant (1987)** discovered that the shear layer was extremely sensitive to sound excitation in the vicinity of the separation point. In their study of internal acoustic

excitation of a static airfoil, they also verified that the most beneficial forcing frequencies are those of the instability waves. Forcing at the fundamental shedding frequency or its harmonic increases entrainment in the early part of the shear layer and drastically reduces the extent of separation. **Zaman and McKinzie (1991)** developed a modified Strouhal number, represented by  $St/R_c^{1/2}$ . They determined that the optimum forcing effect occurs when the modified Strouhal number, based on the excitation frequency, falls in the range 0.02–0.03. In addition, detailed flowfield data indicated that a separation region still exists under forcing. This suggests that the excitation imposed perturbation effects on the downstream shear layer and not on the upstream boundary layer. **Hsiao, Shyu, and Chang (1990)** confirmed that at low frequency forcing, which would have been in the range of free shear layer fundamental frequencies for their experimental parameters, relied on enhancement of the free shear layer instability for separation control. At greater frequencies, the acoustically induced transverse velocity fluctuations played a greater role.

A second control methodology explored in this research project involves surface air injection. Blowing has been applied successfully by numerous researchers to simulate the enhanced lift created in unsteady flows. The initial interest in this particular method of control arose from the need to manipulate the flow over static delta wings, which are characterized by continuing leading edge vortex growth and breakdown. Both **Bradley and Wray (1974)** and **Campbell (1976)** found that blowing a stream of high-pressure air over a wing surface, parallel to the leading edge, delayed leading edge vortex growth and thus the deleterious effects of vortex breakdown at the higher angles of attack. This delay is accompanied by lift increases of up to 50% over uncontrolled flows. The delay of vortex breakdown



postpones static stall of the lifting surface as well. **Seginer and Salomon (1986)** used spanwise blowing over a canard-wing configuration for static angles of attack to augment both lift and lift-to-drag ratios, and delay static stall.

Using a slightly different means, **Roberts, et al (1988)** and **Wood and Roberts (1988)** used tangential mass injection through a slot along the leading edge of a static delta wing. Direct control of the primary separation allows significant control of the vortex flow up to sixty degrees angle of attack. The primary effect of tangential leading edge blowing is to reduce the strength of the vortical flow, resulting in an extended regime of stable, controlled vortical flow over the upper surface of the wing. In addition, the separation line relocates to an in-board position under the forcing.

Successful attempts have been made to control unsteady flows such as the one discussed here. **Carr and McAlister (1983)** used a leading edge slot on an oscillating airfoil to produce a flow that remains attached to the airfoil for angles of attack well above those characteristic of the natural flow. The dynamic stall was significantly delayed, while, at the same time, the severity of the stall was reduced. **Luttges, Robinson, and Kennedy (1985)** were able to obtain similar results by introducing single air pulses through a two-dimensional slot located at  $0.2c$  on an oscillating NACA 0015 surface. The flow control was effective only when the pulse corresponded to periods of high shear and large accumulations of vorticity. The primary difference between these studies and the research summarized here is that the current control methods are tied to the natural characteristics of the flow. Since the greatest enhancement to airfoil performance characteristic occurs prior to dynamic stall vortex formation, and the flow prior to the vortex resembles that of a reattaching, separated flow, it follows that proven control techniques which affect

the vortical nature of a shear layer will also be successful in controlling the pre-vortex dynamic flow. Thus, a clear understanding of an actively controlled static flow is obtained first. The results from the static analysis are then applied to a dynamic airfoil to obtain a preliminary evaluation of control effects on unsteady airfoil separation and stall.

## CHAPTER TWO

### RESEARCH OBJECTIVES

The purpose of this effort is to experimentally investigate the nature of the separating boundary layer on a two-dimensional airfoil, and to determine the effects of active control on airfoil flow characteristics. This investigation focuses first on a static airfoil and then extends the results to a dynamic airfoil. The results are used to evaluate the following:

#### 2.1 Static Airfoil

- The value of the fundamental forcing frequency and its relationship with large-scale wake structure frequencies.
- The nature of the large-scale structures present in the separating boundary layer.
- The effects of active control on the transient nature of the separating boundary layer.
- The effects on flow separation/reattachment and aerodynamic performance due to active control.

## 2.2 Dynamic Airfoil

- The extent of flow similarities between a static airfoil separation region and the pre--dynamic stall vortex dynamic airfoil separation region.
- The active control efficiency in delaying dynamic stall vortex formation and enhancing airfoil aerodynamic performance.
- The control effectiveness on reducing the severity of dynamic stall.

## CHAPTER THREE

### EXPERIMENTAL METHODS

#### 3.1 Introduction

A qualitative and quantitative understanding of an actively controlled, two-dimensional airfoil is obtained using three experimental methods. These methods include hot-film anemometry, surface pressure measurements, and flow field visualization. The hot-film anemometry is used to evaluate the large-scale nature of the flows under natural and forced conditions. The surface pressure measurements allow determination of airfoil performance augmentation due to active control. Flow field visualization yields a concise qualitative description of the flow which, when tied to the quantitative data, gives a more comprehensive picture of the flow mechanisms involved.

The experiments are conducted in the Frank J. Seiler Research Laboratory's open return, low speed wind tunnel at the U. S. Air Force Academy. The wind tunnel has a 0.91 m x 0.91 m test section designed for use with flow visualization and flow sensor measurements. The speed range of the facility is 3 – 35 m/s, with turbulence intensity levels below 0.5%. A NACA-0015 airfoil with a 15.2 cm chord and a 61.0 cm span is used for all tests. The pivot location in the dynamic experiments is 25% of the chord. The experiments covered here include the two chord Reynolds numbers of 24,000 to 57,000. The associated non-dimensional pitch rate,  $\alpha^+$ , is 0.05. The model support allows constant pitching between 0° and 90°, with the mechanism being controlled using a MassComp MC 5500 microcomputer.

Since this study concentrates on the effects preceding and including the dynamic stall vortex development, the airfoil is only pitched from  $0^\circ$  to  $50^\circ$ . By an angle of attack of  $50^\circ$ , the dynamic stall vortex has formed and detached from the airfoil surface for the non-dimensional pitch rate explored.

### 3.2 Flow Visualization

A visualization investigation of all flow conditions must be made to evaluate the flow as it transitions from a separating shear layer to a dynamic stall vortex. To accomplish the visualization, smoke is injected into the flow, and illuminated such that the smoke scatters a greater amount of light than that scattered by the background. For this experimental effort, smoke is introduced using a smoke wire. This creates a discrete plane of smoke tubes, yielding a two-dimensional view of the flow. The smoke wire technique developed by **Helin and Walker (1985)** is employed. Theatrical fog fluid is applied to a horizontal 0.127 mm tungsten wire, leaving fine droplets almost uniformly along the wire. The smoke wire is located at mid-span, 30 cm upstream of the airfoil. A current applied to the wire evaporates the oil, producing fine streaklines across the test section. This method results in a clear smoke outline of the unsteady separation region and the dynamic stall vortex as it forms on the airfoil surface. A schematic of the flow visualization design is shown in Figure 3-1.

The visibility of the smoke depends upon the amount of light being scattered by the smoke particles themselves. Maximum efficiency results when the smoke is illuminated by direct light. If other parts of the test section are illuminated with too great a level, the background reflections may overpower the reflections from the

smoke. To accomplish the right balance, the lighting for the wind tunnel is provided by EG&G Strobebrite strobe lights. These high-intensity arc-lamp strobe lights are synchronized with a 35 mm still camera to illuminate the streakline flow at the desired point in the pitching cycle or at the appropriate static angle of attack. The strobe lights have an average 7  $\mu$ s flash duration, which freezes the flow.

Visual records of the flow are obtained using still photography, accomplished with a Nikon FE-II camera and a Micro Nikkor 105 mm lens. A trigger box allows synchronization of the camera with the strobe lights, smoke wire, and the pitching mechanism to yield photographs at a given desired instant in the flow.

### 3.3 Hot-film Anemometry

A key element in this study is the determination of the shear layer structure behavior in both the controlled and natural flows. Before active control can be applied to the flow, the fundamental forcing frequency of the separated static airfoil shear layer must be determined.

The flow under both natural and forced conditions was analyzed using a single hot-film probe placed at the 5.0% chord location and at different distances from the airfoil surface. A flow chart in Figure 3-2 outlines the data acquisition process. The signal from the probe is passed through a TSI Model 1054A anemometer, with the probe frequency response set at 1000 Hz. A Tektronix 7A22 differential amplifier allows amplification of the probe signal. The signal from the probe is then passed through a Kronhite 3103 variable electronic filter to attenuate frequencies above 500 Hz. The filtered signal is transmitted both to the MassComp data acquisition card for storage and an HP signal analyzer for real time

observation. The flow is sampled at a frame frequency of 1000 Hz for use in spectral calculations and 15,000 for direct time trace observation. Hot-film measurements for the dynamic case of  $\alpha^+ = 0.05$  are taken at a frame frequency of 2,000 and ensemble averaged over five data runs to increase repeatability. Error bars are indicated where appropriate.

### 3.4 Flow Modification

Flow modification is accomplished by two means, external acoustic forcing and internal tangential-pulsed air blowing. The flow is forced at the fundamental forcing frequency and the corresponding subharmonics. The external acoustic control, shown in Figure 3-3, is supplied externally to the airfoil by a speaker. A 220 Watt woofer, mounted as shown, is controlled with a sine wave generator at frequencies between 10 HZ and 300 HZ. The signal is amplified by a Crown PS-400 Dual Channel power amplifier, with the sound being transmitted through a ducting system to a location over the leading edge region of the airfoil. Five centimeter diameter PVC pipe is used to conduct the acoustic control, supplying the signal with minimum distortion. Forcing amplitude, measured by a microphone placed at the pipe exit, is kept at a constant 0.05 rms volts.

Internal tangential-pulsed air control is accomplished through three downstream facing slots located on the upper surface of the airfoil. The slots are 1.6 mm. wide and cover 47.7 cm., or 75%, of the span. Shown in Figure 3-4, the system employs six solenoid valves capable of pulsing between zero and 45 HZ. The valves are controlled through a timing circuit by a square wave generator. Compressed air is supplied at 30 psi through the valves using tygon tubing, resulting



in a peak injection velocity of 8.5 m/s. A sample velocity time trace of the air exiting the slot is shown in Figure 3-5. The multiple signal exiting the slot could be due at least in part to the fact that the air is injected into both ends of the airfoil simultaneously, and may be interacting before reaching the slot exit. The blowing momentum coefficient,  $C_{\mu}$ , is 0.01 for a chord Reynolds number of 57,000 and 0.07 for a chord Reynolds number of 24,000.

### 3.5 Pressure Measurements

Information concerning airfoil lift and drag under natural and forced conditions is necessary to evaluate the practical effectiveness of the active control methods being analyzed. Instantaneous surface pressure measurements are obtained using an Endevco 8507-2 miniature pressure transducer mounted to a connector. This connector can be attached to tubes running from pressure taps on the airfoil surface. Each tap location is measured individually, with the results being ensemble averaged over twenty data runs to ensure accuracy. Fourteen ports are located on the airfoil surface at locations shown in Figure 3-6. Lower surface measurements are obtained by pitching the airfoil in the opposite direction. The instantaneous pressure information from the sensor output is acquired in a digital format and is then processed and displayed using computerized data analysis techniques. The MassComp MC-5500 microcomputer is used for both the data collection and the data reduction. Error bars are indicated where appropriate.

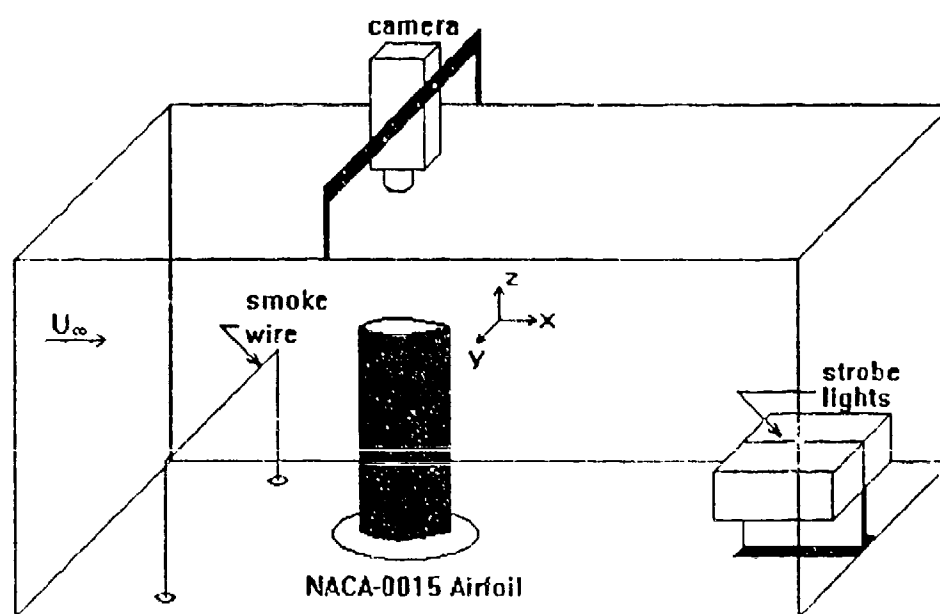
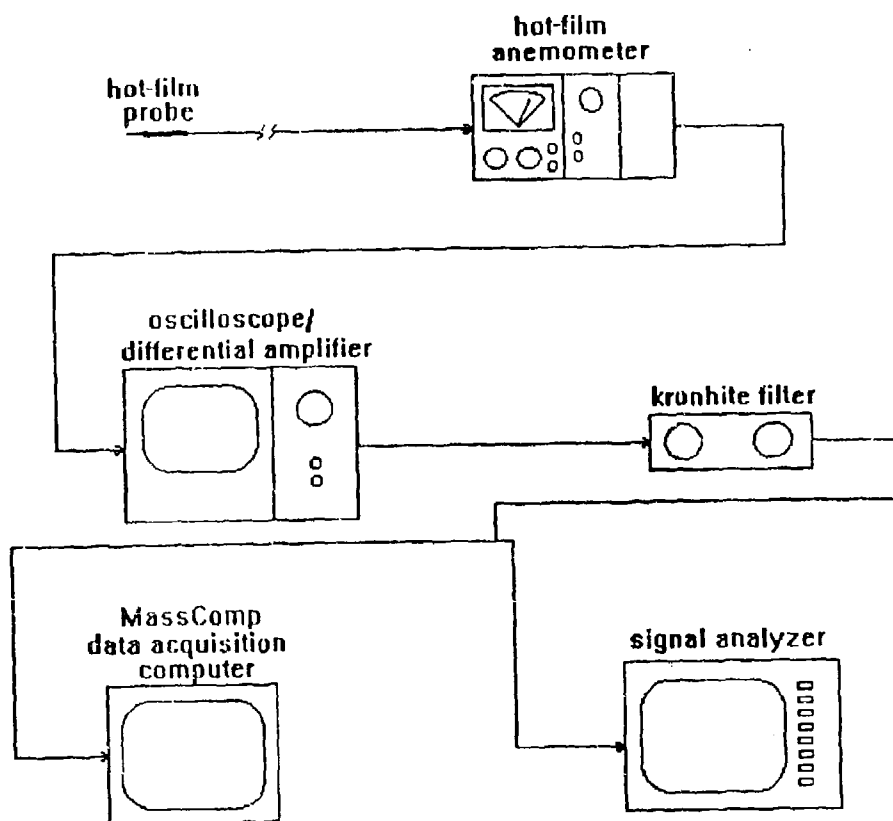


FIGURE 3-1. Flow visualization schematic.



**FIGURE 3-2.** Hot-film anemometry data acquisition process.

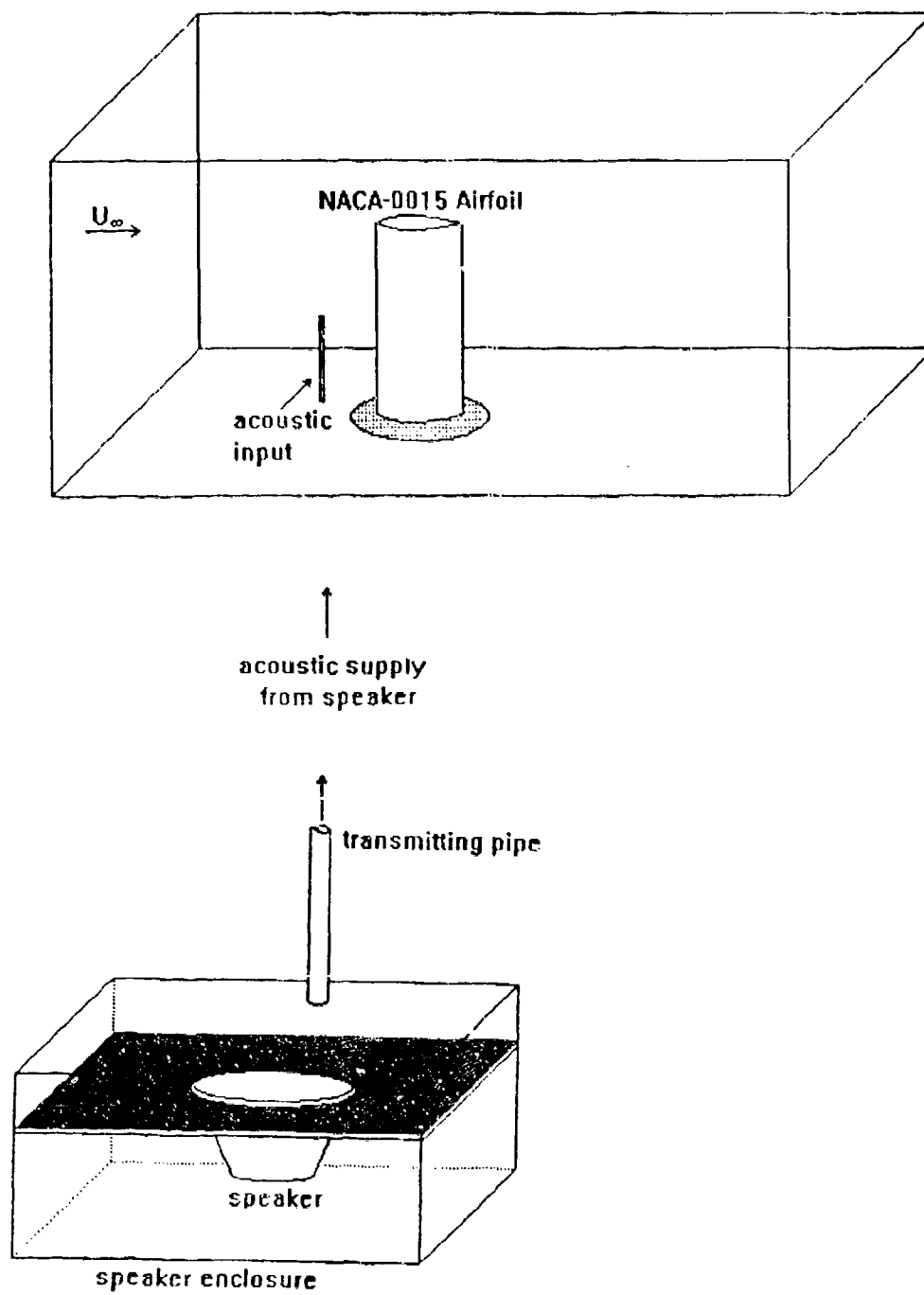


FIGURE 3-3. Acoustic Control Schematic.

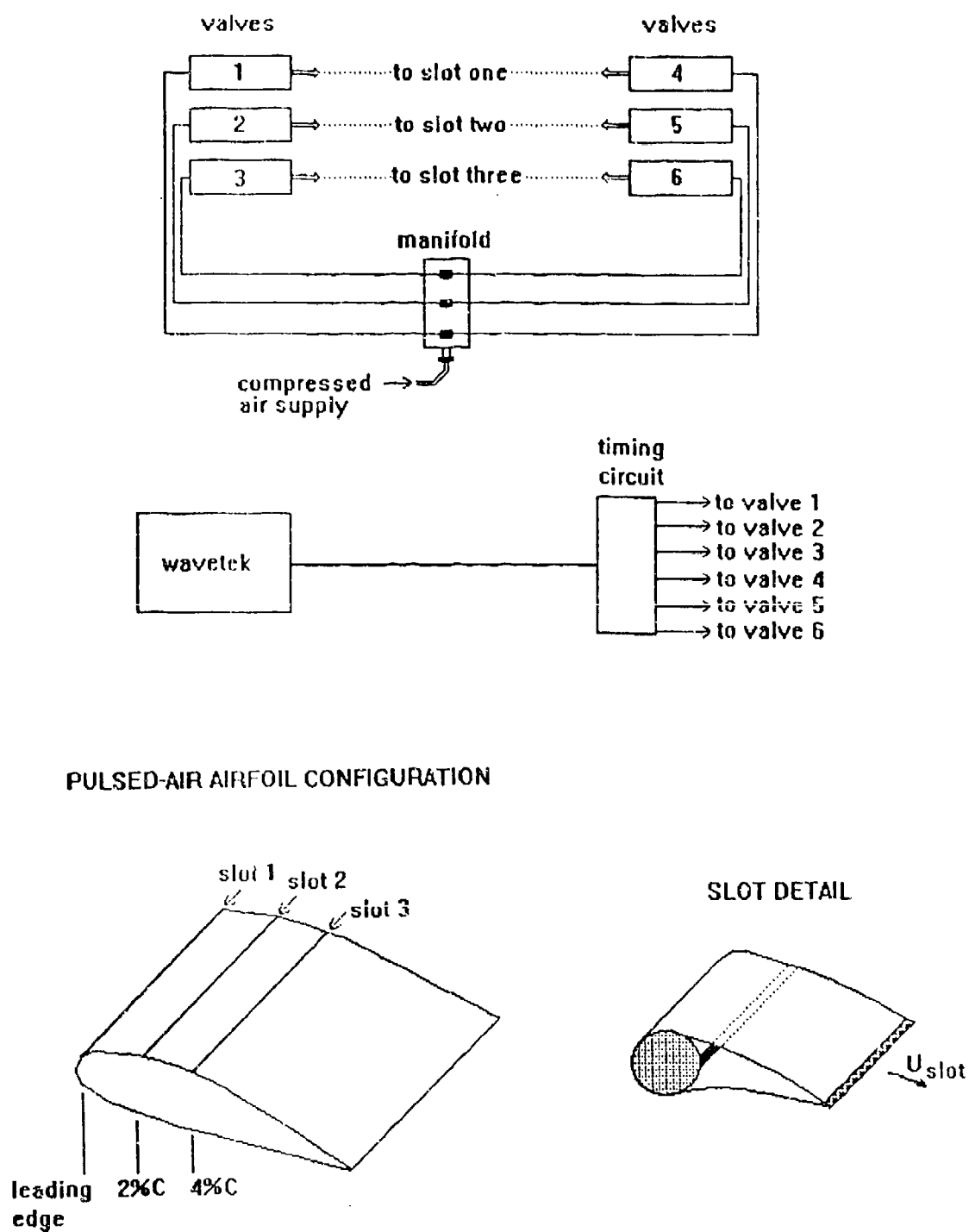


FIGURE 3-4. Tangential-pulsed air control schematic.

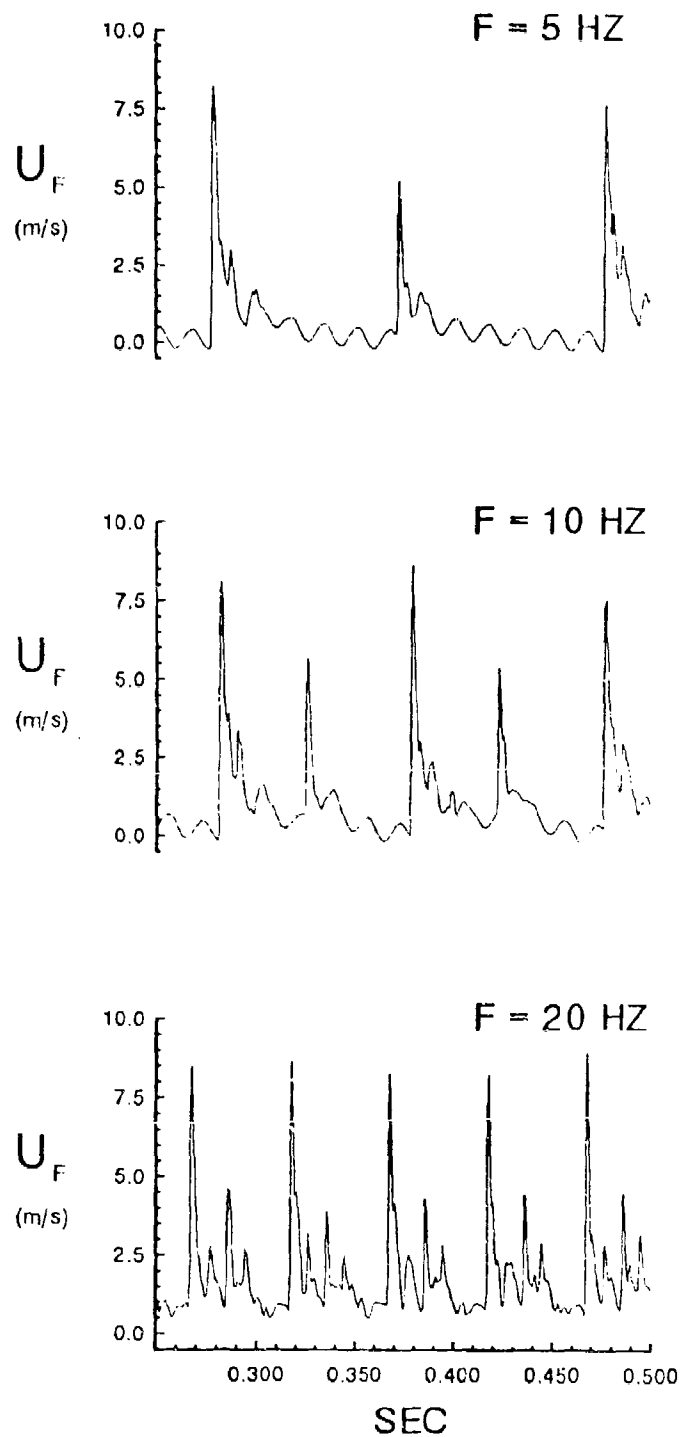


Figure 3-5.

Velocity profile of tangential-pulsed air control at the slot exit.

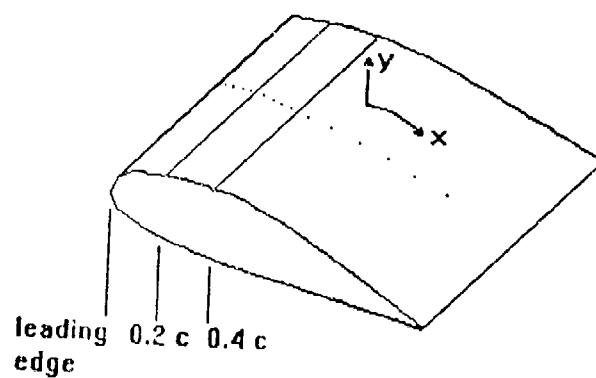


FIGURE 3-6. Pressure airfoil configuration

## CHAPTER FOUR

### ACOUSTIC CONTROL RESULTS – STEADY

#### 4.1 Determination of Fundamental Frequency

The fundamental frequency discussed here is defined as the frequency at which the flow is most receptive to forcing. Specifically, it is that control frequency which imparts the maximum amplification on the free shear layer power spectra (Crighton, D. G., 1981). The first step in determination of the fundamental frequency is identifying the edge of the separating boundary layer. Since the objective of this step is to determine the frequency at which the large-scale structures in the free shear layer are most susceptible to the forcing, it is necessary to evaluate the flow at the spatial location exhibiting the clearest structure representation (Browand and Troutt, 1980 and 1985).

The relationship of the unforced flow characteristics with distance from the airfoil surface is shown in Figure 4-1 for a chord Reynolds number of 57,000 and an angle of attack of  $20^\circ$ . The velocity traces cover a one second time period, and are measured on the upper airfoil surface at the 5% chord location. At locations close to the airfoil, both  $Y/C = 0.003$  and  $Y/C = 0.006$ , the turbulent nature of the flow indicates that the hot-film probe tip is inside the free shear layer and is experiencing the increased circulation from vortical structures. At  $Y/C = 0.010$  from the airfoil, the turbulent nature has diminished somewhat, allowing a clearer distinction between individual structures. The increase in average velocity magnitude also suggests that the probe tip is nearer to the edge of the free-shear



layer influence. It is at this location where measurements of the natural and forced flow are obtained. Further away from the airfoil, the average velocity magnitude is still higher than the freestream, but virtually all definition of the large scale nature of the flow has been lost.

The next step in the process is to ascertain the value of the most receptive forcing frequency. As determined by Crow and Champagne (1971) and Kibens (1979), when forcing is tuned to the initial shear layer's frequency for maximum amplification and the corresponding subharmonics, tones are produced in the power spectra at the forcing frequencies. All other broadband levels are suppressed by the excitation. This principle is affirmed in the power spectra shown in Figure 4-2. The flow at a chord Reynolds number of 57,000 and a static angle of attack of  $20^\circ$  is acoustically forced at frequency increments of 15 Hz. A broad spectral peak is apparent in the flow forced at 20 Hz, with the power concentrated at the forcing frequency of 20 Hz. Increasing the forcing frequency to 35 Hz results in a lower spectral peak. By 50 Hz, the forcing has virtually no effect on the flow. Forcing the flow at 65 Hz has a drastically different effect on the flow. It is clear that this band produces a significant power amplification, and in addition suppresses the majority of the spectral peaks elsewhere in the range shown. Forcing at 80 Hz and above has little effect on the flow. This information is summarized in Figure 4-3, which shows the peak power values corresponding to the forcing frequencies. Local maxima at frequencies of 20 Hz and 30 Hz and the spectral maximum at 65 Hz indicate that the most receptive forcing frequency is indeed 65 Hz. As indicated by Crighton (1981), spectral tones occur at the excitation frequency corresponding to maximum free shear layer spectral amplification, 65 Hz, and at the corresponding subharmonics of approximately  $1/2$  and  $1/4$  that

frequency. Deviation in the exact value of the subharmonics could possibly be due to experimental error.

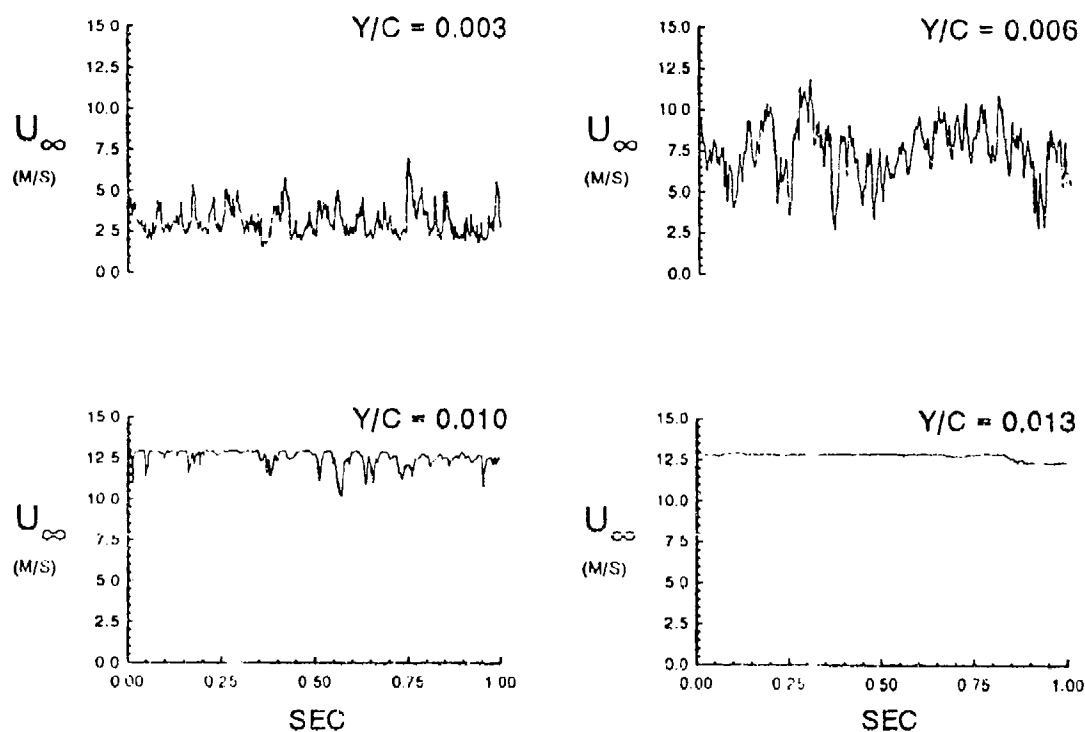


Figure 4-1. Velocity fluctuations in the separating boundary layer on a static airfoil with respect from distance from the airfoil surface.  $\alpha=20^\circ$ ,  $R_c=57,000$ .

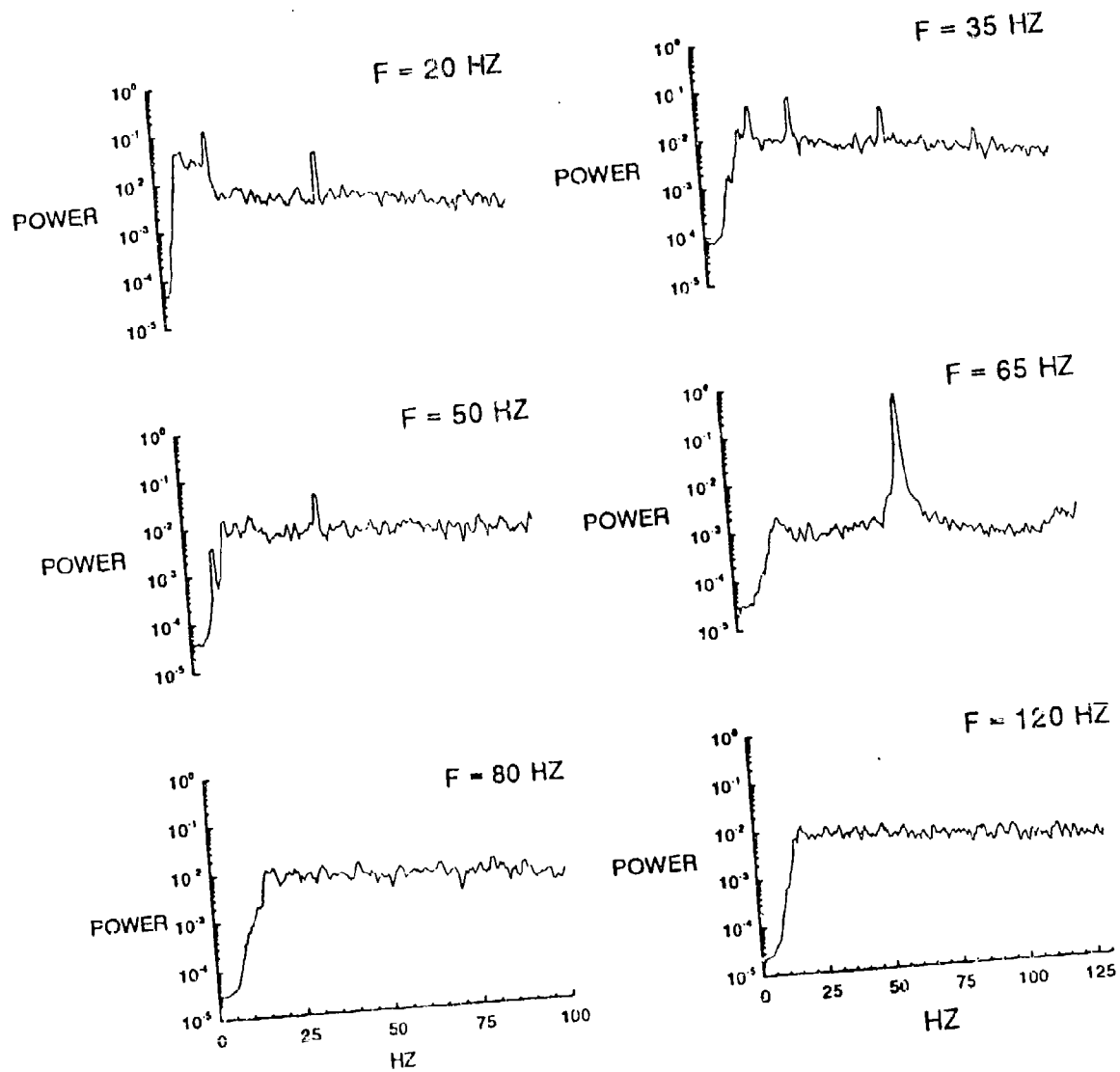


Figure 4-2.

Power spectra at varying control frequencies.  $\alpha=20^\circ$ ,

$R_c=57,000$ .

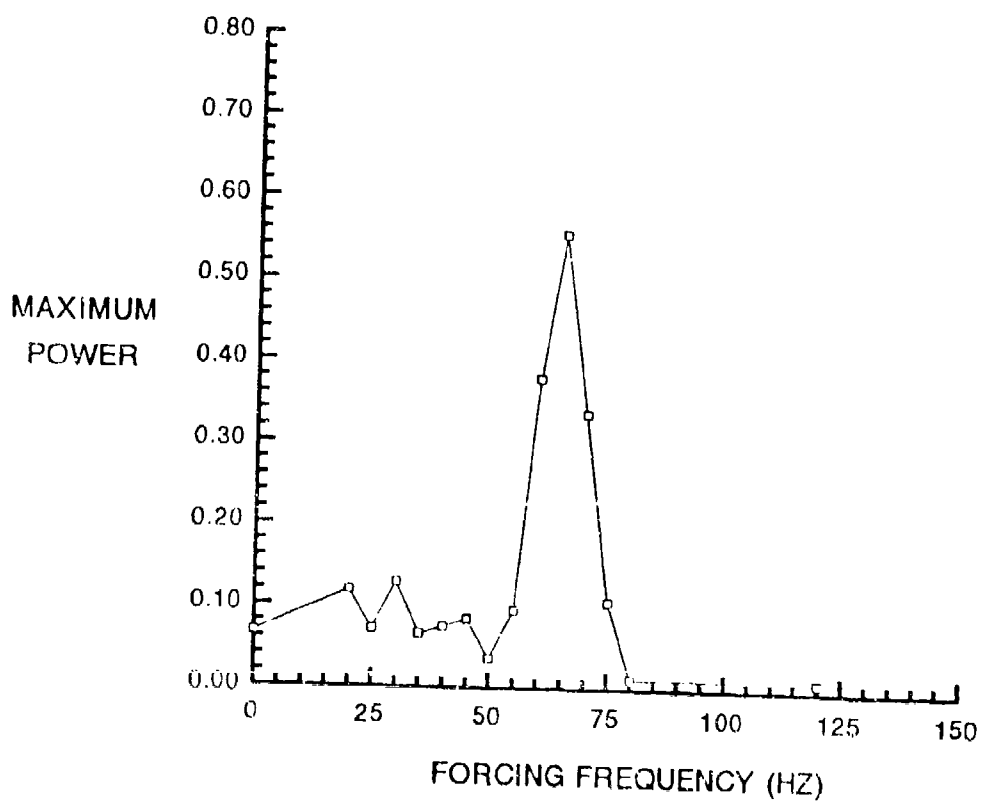


Figure 4-3. Maximum spectral values at varying control frequencies.  $\alpha=20$ ,  $R_c=57,000$ .

## 4.2 Acoustic Manipulation of the Separating Boundary Layer

The acoustically forced flow on a static airfoil at  $10^\circ$  angle of attack and a chord Reynolds number of 24,000 is shown in Figure 4-4. At this pre-stall angle of attack, it is difficult to discern large-scale structures in the velocity fluctuations for the natural case. The corresponding power spectra exhibit peaks corresponding primarily to electronic noise. When the flow is forced at the most receptive frequency of 90 Hz, the velocity fluctuations are forced to conform to that frequency. The power spectra shows the flow receptiveness to that forcing value, with the primary peak occurring at 90 Hz. Reducing the control frequency to the first subharmonic of 45 Hz increases velocity fluctuations in the free shear layer, but a clear pattern cannot be determined.

When the angle of attack is increased to  $15^\circ$ , there is a slight peak near 60 Hz, which upon further analysis is determined to be the maximum amplification frequency. Forcing at this frequency of 60 Hz results in a regular velocity fluctuation at the control band, as shown in Figure 4-5. The normalized power spectra exhibits a significant peak at 60 Hz, confirming flow response. Past studies of controlled free shear layers have shown that when the forcing frequency corresponds to the natural shear layer vortex passage frequency, defined herein as the most receptive flow frequency, the shear layer time trace takes on a regular form corresponding to that control frequency (Oster and Wygnanski, 1982). Forcing the flow at the first subharmonic of 30 Hz results in velocity fluctuations of a greater magnitude than the fluctuations at 60 Hz, and a slight conformation of the flow frequency to the control frequency. It should be noted at this juncture that a slight spectral peak appears at angles above  $10^\circ$  at 15 Hz, and does not change with airfoil

orientation. Although this bears further analysis, it is beyond the scope of this investigation.

The controlled flow at angles of attack of  $20^\circ$ ,  $25^\circ$ , and  $30^\circ$  are shown in Figures 4-6, 4-7, and 4-8 respectively. In each case, there is a broad spectral peak around 20 Hz present in the natural flow. This peak increases in magnitude with angle of attack. Forcing the flow at the determined fundamental frequency of 20 Hz results in regular, amplified velocity fluctuations at that value. Correspondingly, forcing at the first subharmonic of 10 Hz leads to bimodal velocity fluctuations, exhibited by a smooth sub-peak preceding a greater sharp peak, and a dominant spectral peak at the forcing frequency. Kamalu, (1989), stated that the characteristic velocity time trace of a free shear layer forced at the first subharmonic of the fundamental frequency manifests itself in a bimodal form. According to Ho and Huang (1982), subharmonic flow amplification causes free shear layer vortex pairing. The noticeable peaks at 30 Hz and 60 Hz are believed due to electronic noise.

The fundamental frequency for a static airfoil decreases with increasing angle of attack, as summarized in Figure 4-9. The static flow at a chord Reynolds number of 24,000 is forced at the fundamental frequency over attack angles ranging from  $10^\circ$  to  $30^\circ$ . The amplitude of the controlled velocity fluctuations increases with angle of attack, indicating an enhanced flow receptiveness to the forcing. The fundamental frequency does not change past an angle of attack of  $20^\circ$ , and control at higher angles of attack results in the same regular signal corresponding to the fundamental frequency. Since the airfoil reaches its stall angle at approximately  $17^\circ$  for this Reynolds number, it is reasonable to assume that the nature of the separated free shear layer does not alter appreciably

at greater angles. The boundary layer separation point has reached the leading edge, and the entire airfoil is stalled.

Additional acoustic control experiments at a chord Reynolds number of 57,000 demonstrate the same trend in the relationship between fundamental frequency and airfoil angle of attack. At this Reynolds number however, the most receptive control frequencies are greater than those determined at  $Re_c = 24,000$ . The fundamental frequency associated with the large-scale free shear layer structures in a static airfoil separation region is thus dependent both on angle of attack and freestream velocity prior to aerodynamic stall. Katz (1981) determined that the frequency of the large scale wake structures of a NACA-0012 airfoil could be represented by a Strouhal number of 0.18 – 0.19, with the Strouhal number being calculated using the equation  $St = f(\sin\alpha)c/U_\infty$ . In this case,  $f$  is the instability, or vortex passage, frequency,  $\alpha$  is the angle of attack,  $c$  is the chord length, and  $U_\infty$  is the freestream velocity. Figure 4-10 summarizes the fundamental forcing frequencies for the two freestream velocities determined in this analysis. In comparison with Katz' wake results, the fundamental frequencies found at the 5% chord location are four times that of the wake prior to airfoil stall. Above the stall angle of attack, the frequency becomes constant, dependent only on the freestream velocity.



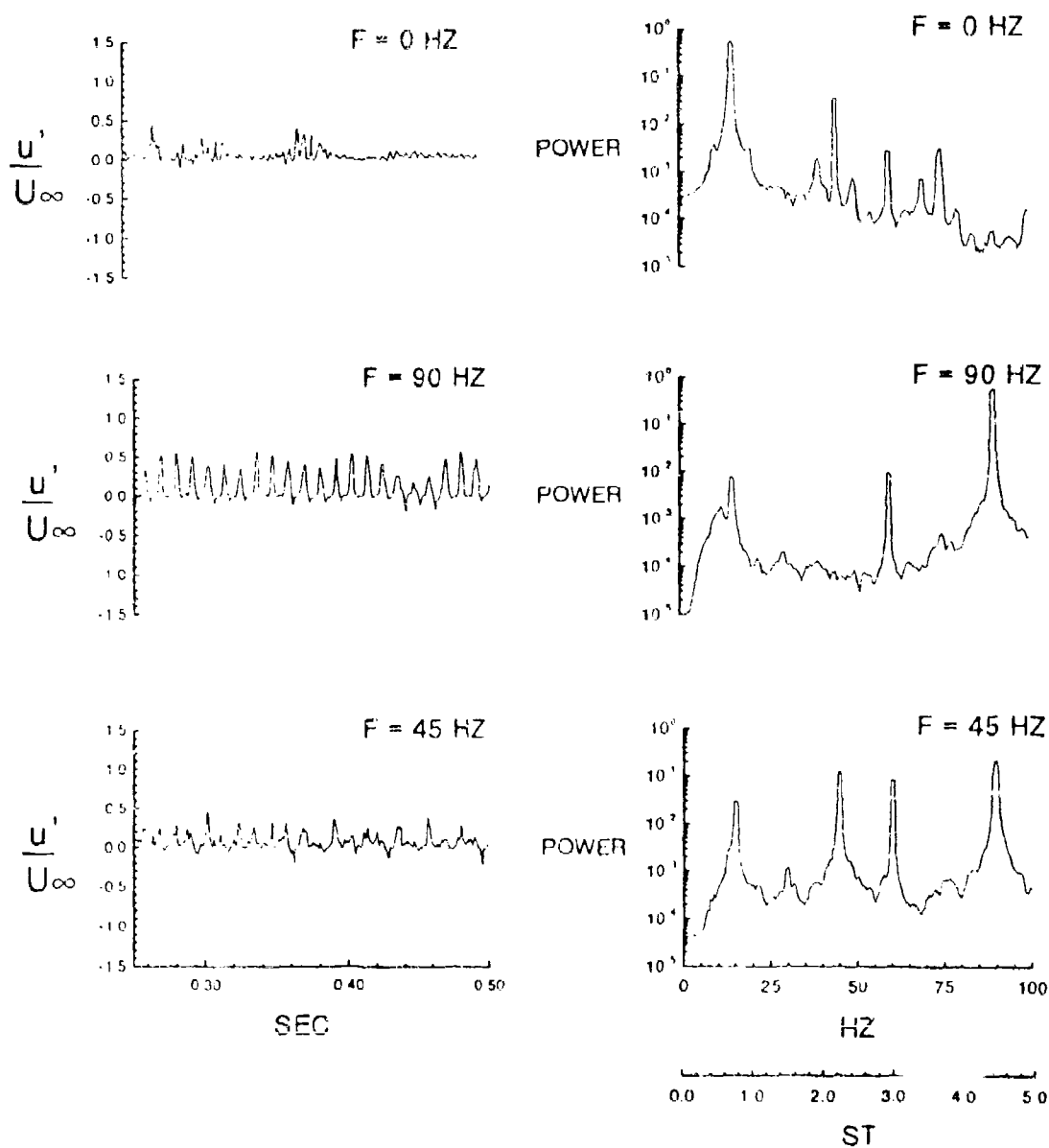


Figure 4-4.

Velocity fluctuations with respect to time and the corresponding power spectra. Acoustic control.  $\alpha=10^\circ$ ,  $R_c=24,000$ .

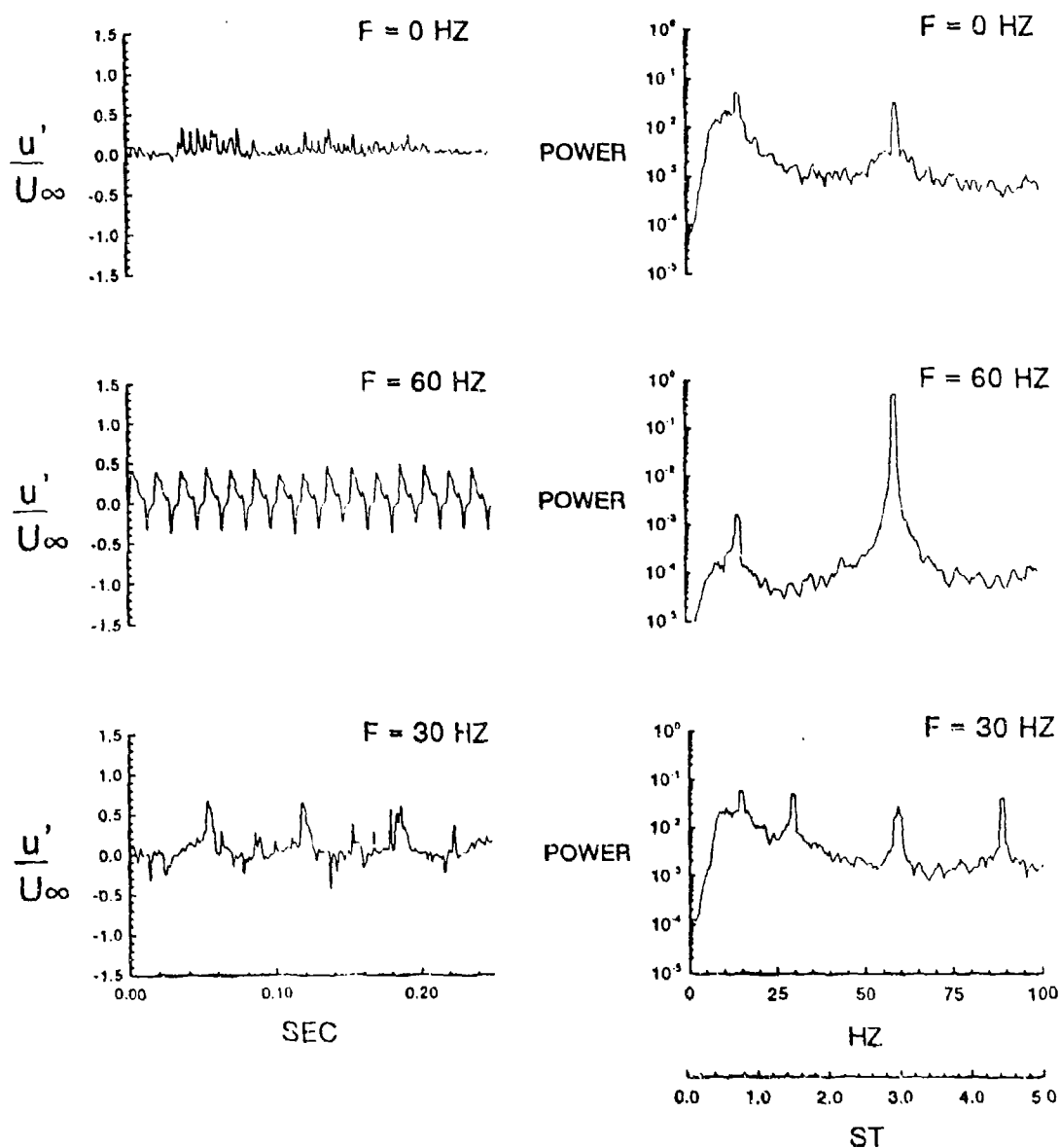


Figure 4-5. Velocity fluctuations with respect to time and the corresponding power spectra. Acoustic control.  $\alpha=15^\circ$ ,  $R_c=24,000$ .

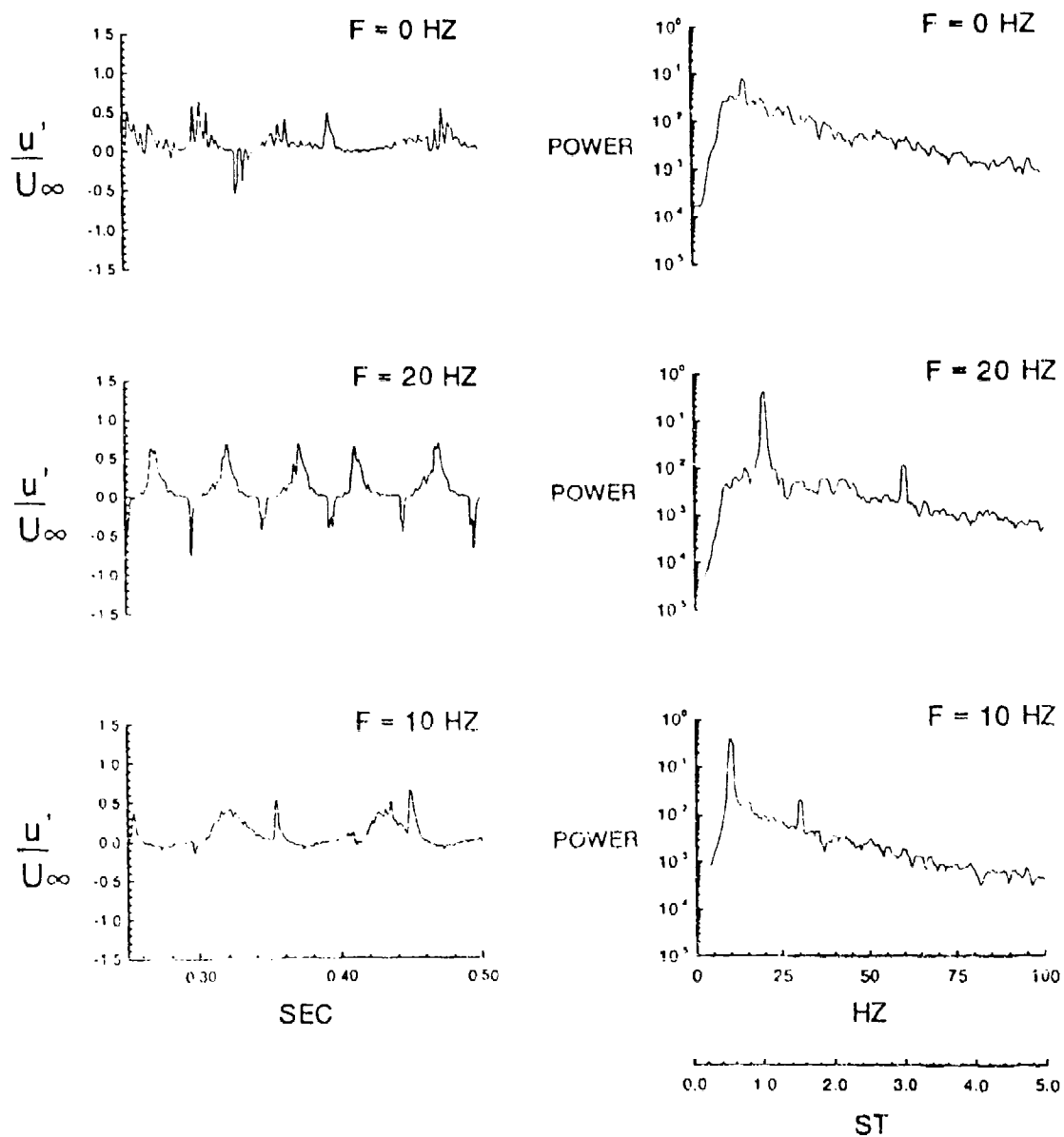


Figure 4-6. Velocity fluctuations with respect to time and the corresponding power spectra. Acoustic control.  $\alpha=20^\circ$ ,  $R_c=24,000$ .

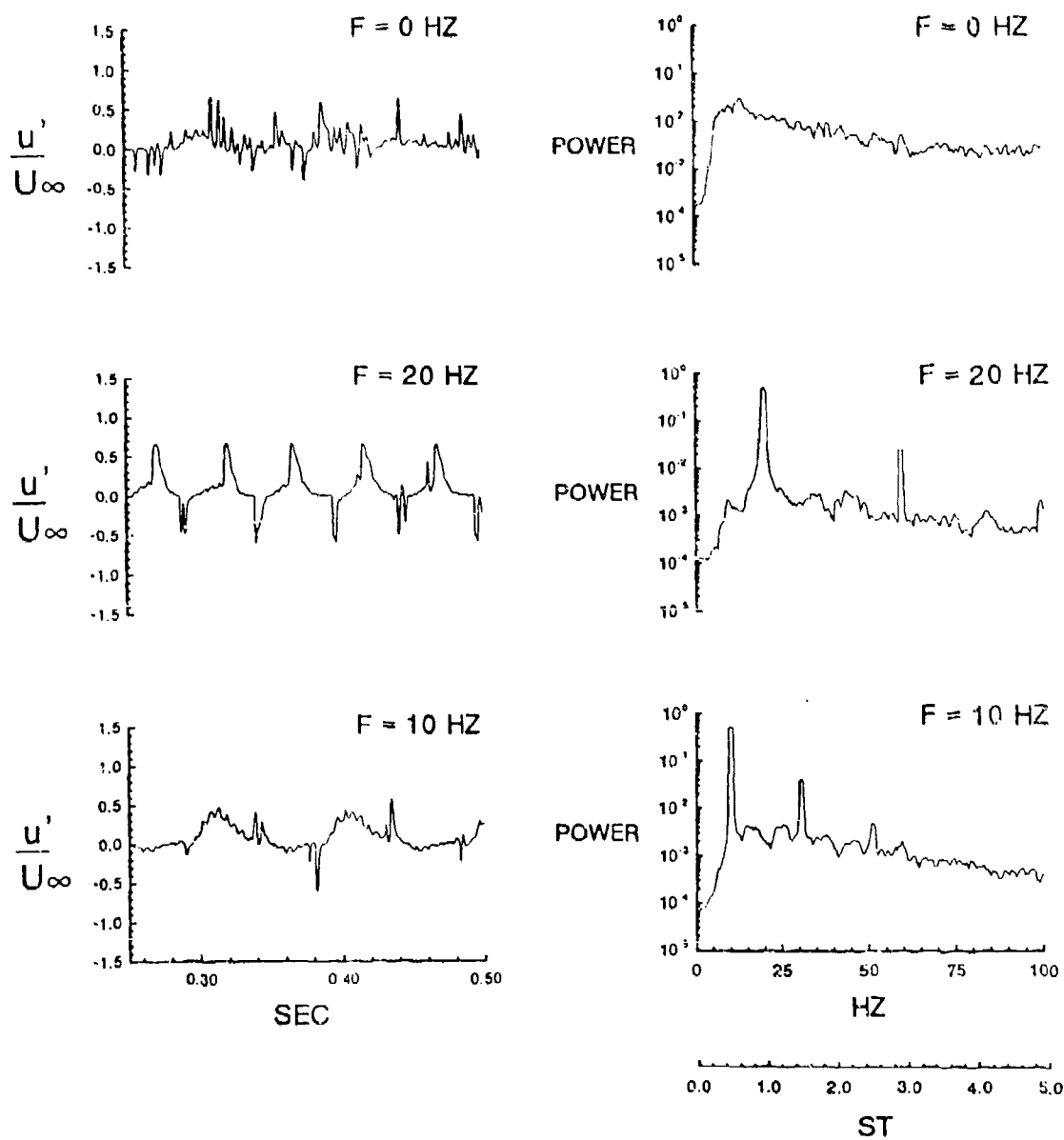


Figure 4-7.

Velocity fluctuations with respect to time and the corresponding power spectra. Acoustic control.  $\alpha=25^\circ$ ,  $R_c=24,000$ .

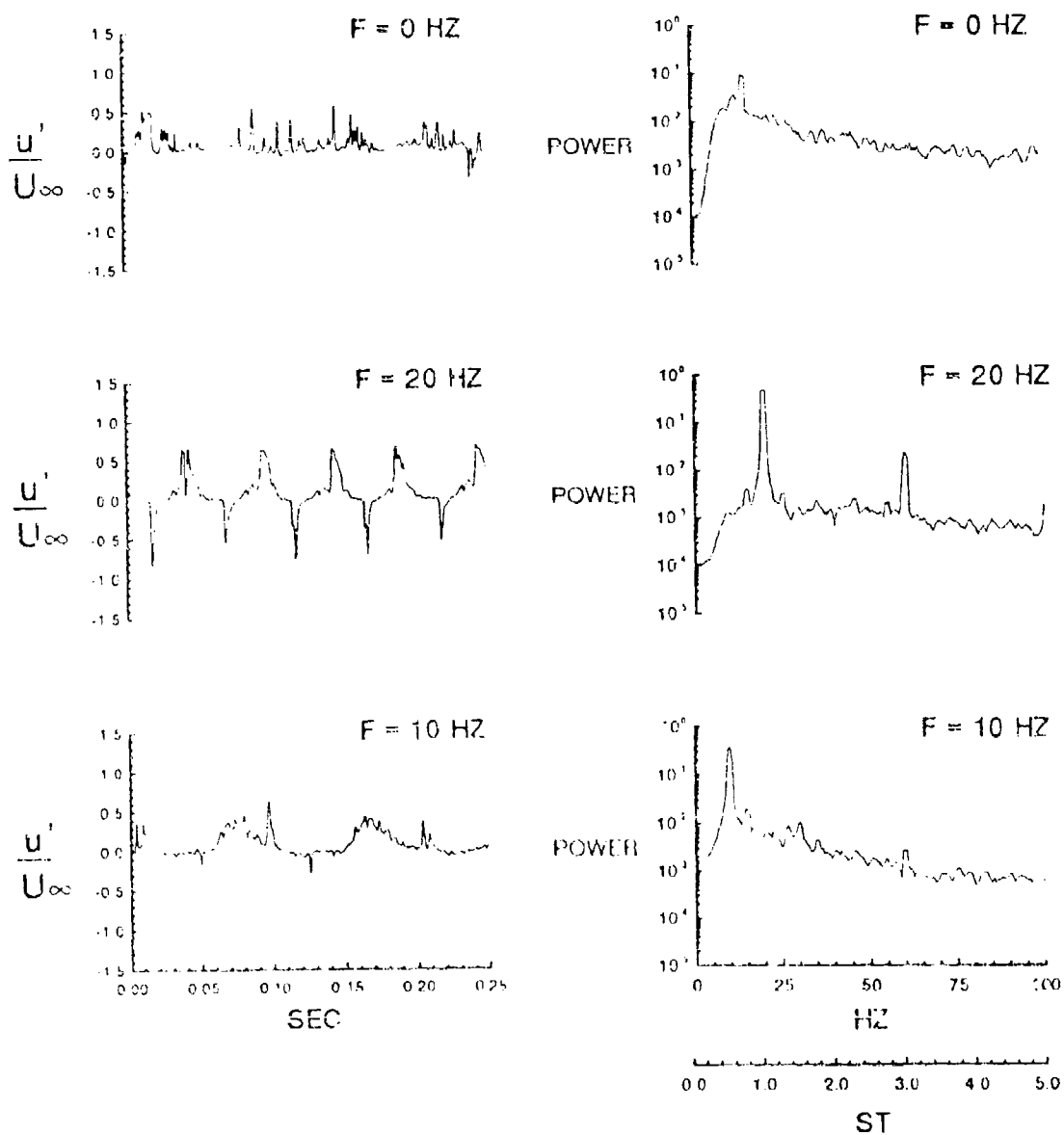


Figure 4-8

Velocity fluctuations with respect to time and the corresponding power spectra. Acoustic control,  $\alpha = 30^\circ$ ,  $R_c = 24,000$ .

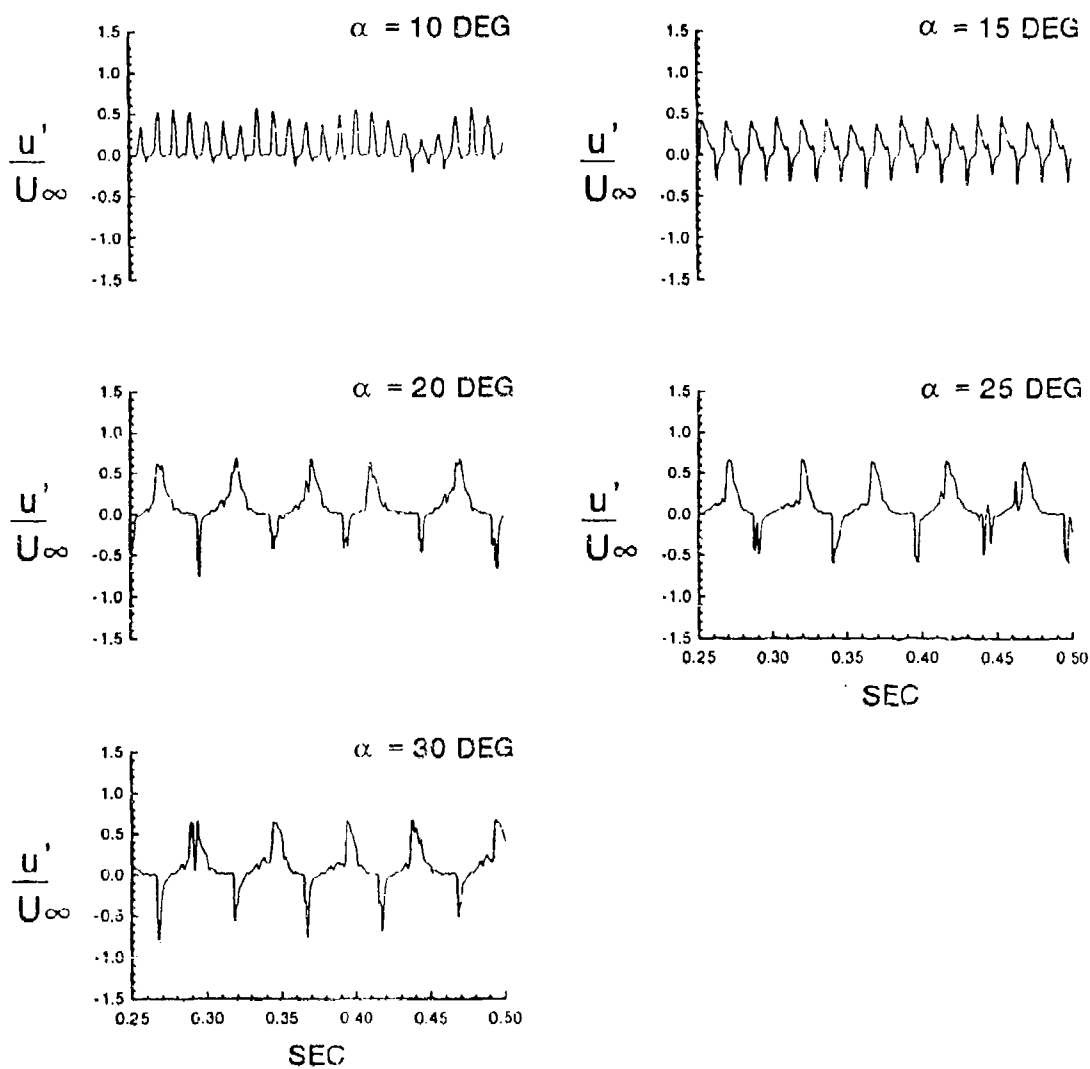


Figure 4-9. Change in free shear layer velocity fluctuations at increasing angles of attack . Acoustic control,  $R_c=24,000$ .

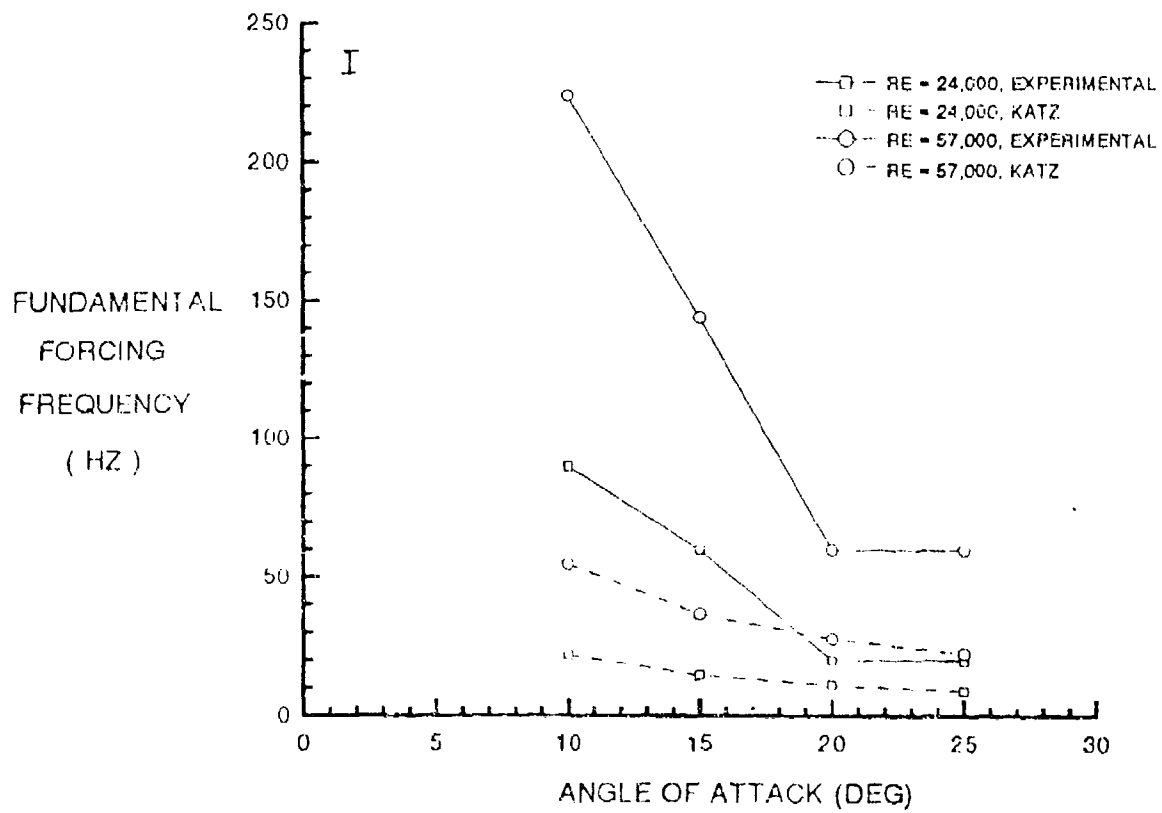


Figure 4-10. Comparison of experimental and theoretical fundamental frequencies with respect to angle of attack.  
 $R_c = 24,000$ .

## CHAPTER FIVE

### INTERNAL TANGENTIAL PULSED AIR CONTROL RESULTS – STEADY

#### 5.1 Pulsed Air Manipulation of the Separating Boundary Layer

Having determined the fundamental forcing frequencies using acoustic manipulation, the flow is then modified using internal tangential pulsed air control. The rationale for using this forcing methodology lies both in its greater potential for practical application as well as a wider range of forcing input choices. Figure 5-1 shows the flow at a static angle of attack of  $10^\circ$ , forced at the first subharmonic of 45 Hz, the second subharmonic of 22 Hz, and the third subharmonic of 11 Hz. For each case, the forced flow exhibits increased velocity fluctuations over the natural case (refer to Figure 4-4). There is a noted enhanced regularity in the flow forced at the first subharmonic, but not at the lower frequencies. Characteristic of the tangential-pulsed air control are the harmonics of the fundamental frequency evident in both the velocity time trace and the associated power spectra. This is due to the nature of the pulses exiting the spanwise slot, as shown in Figure 3-5.

Forcing the flow at the first, second, and third subharmonics at an angle of attack of  $15^\circ$ , presented in Figure 5-2, results in greater flow receptivity in all three cases, with receptivity being defined in part by the conforming nature of the velocity fluctuations to the active control. The power spectra at control frequency exhibit regular, repetitive peaks at the forcing band and subsequent harmonics, with bandwidths elsewhere being damped out by the control.



The design constraints of the pulsed air control system do not allow forcing at the most receptive frequencies for the above mentioned attack angles of  $10^\circ$  and  $15^\circ$ . However, this was possible for angle of attack of  $20^\circ$  and  $25^\circ$ , shown in Figures 5-3 and 5-4 respectively. When the control frequency corresponds to the previously determined fundamental frequency, the velocity fluctuations take on a regular pattern which resembles the acoustically forced cases, keeping in mind the input wave-form of the pulsed air. Forcing the flow at the first and second subharmonics of 10 Hz and 5 Hz results in a regular bimodal signal, again similar to the acoustically forced case. The corresponding power spectra contain both a peak at the control frequency as well as its harmonics.

The change in forcing receptiveness with angle of attack is represented in Figure 5-5. Angles of attack ranging from  $10^\circ$  to  $25^\circ$  are shown forced at their second subharmonic. It can clearly be seen that the regularity of the controlled free shear layer, evidenced in the velocity fluctuation time traces, is enhanced as the angle of attack increases. While the flow appears more turbulent at  $10^\circ$ , in that a clear periodic nature is not that apparent in the velocity trace, by  $25^\circ$  the velocity changes have become clearly periodic. As was mentioned in Chapter 4, the boundary layer separation point moves upstream along the airfoil chord as the angle of attack is increased, until it reaches the leading edge at approximately  $17^\circ$ . Since all hot-film measurements discussed here are obtained at the 5% chord location, it is reasonable to expect that the flow receptivity would be enhanced at the higher attack angles. Since separation is necessary for control method success, enhanced separation would be expected to increase flow responsiveness to the control. This increase in flow regularity with angle of attack is also shown in Figure 5-6. The flows at attack angles of  $20^\circ$  and  $25^\circ$  are shown for a period of one-half of a second

under forcing conditions at the fundamental, first subharmonic, and second subharmonic frequencies. Although change is apparent in the flow at  $20^\circ$  under control conditions, it is clearly evident that the periodic nature of the velocity at the greater attack angle of  $25^\circ$  is significantly more defined, especially at the lower subharmonics. It should be noted that the forcing frequencies at these attack angles are the same, since the airfoil has completely stalled at this point.

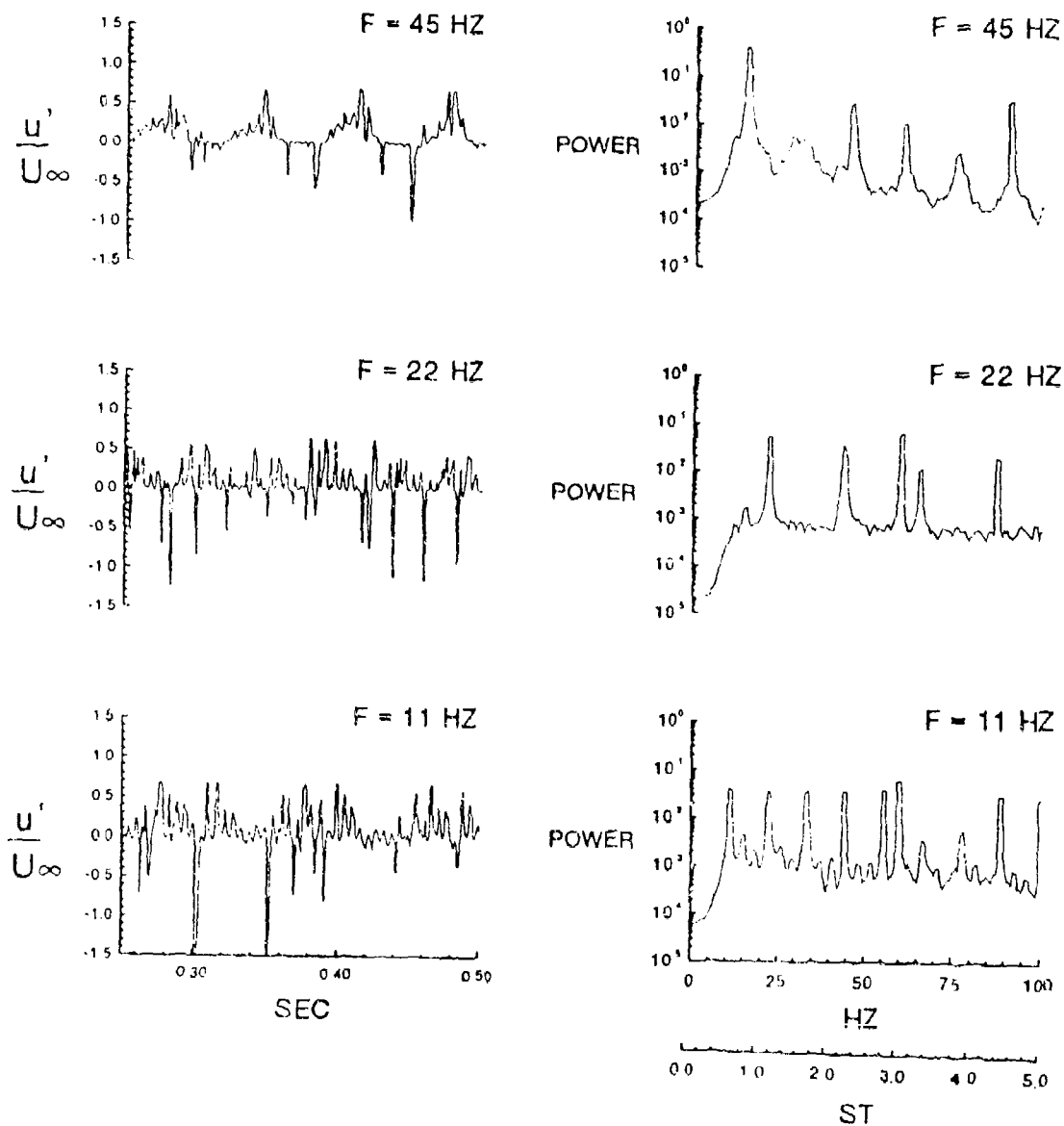


Figure 5-1. Change in velocity fluctuations with respect to time and the corresponding power spectra. Pulsed air control.  $\alpha=10^\circ$ ,  $R_c=24,000$ .

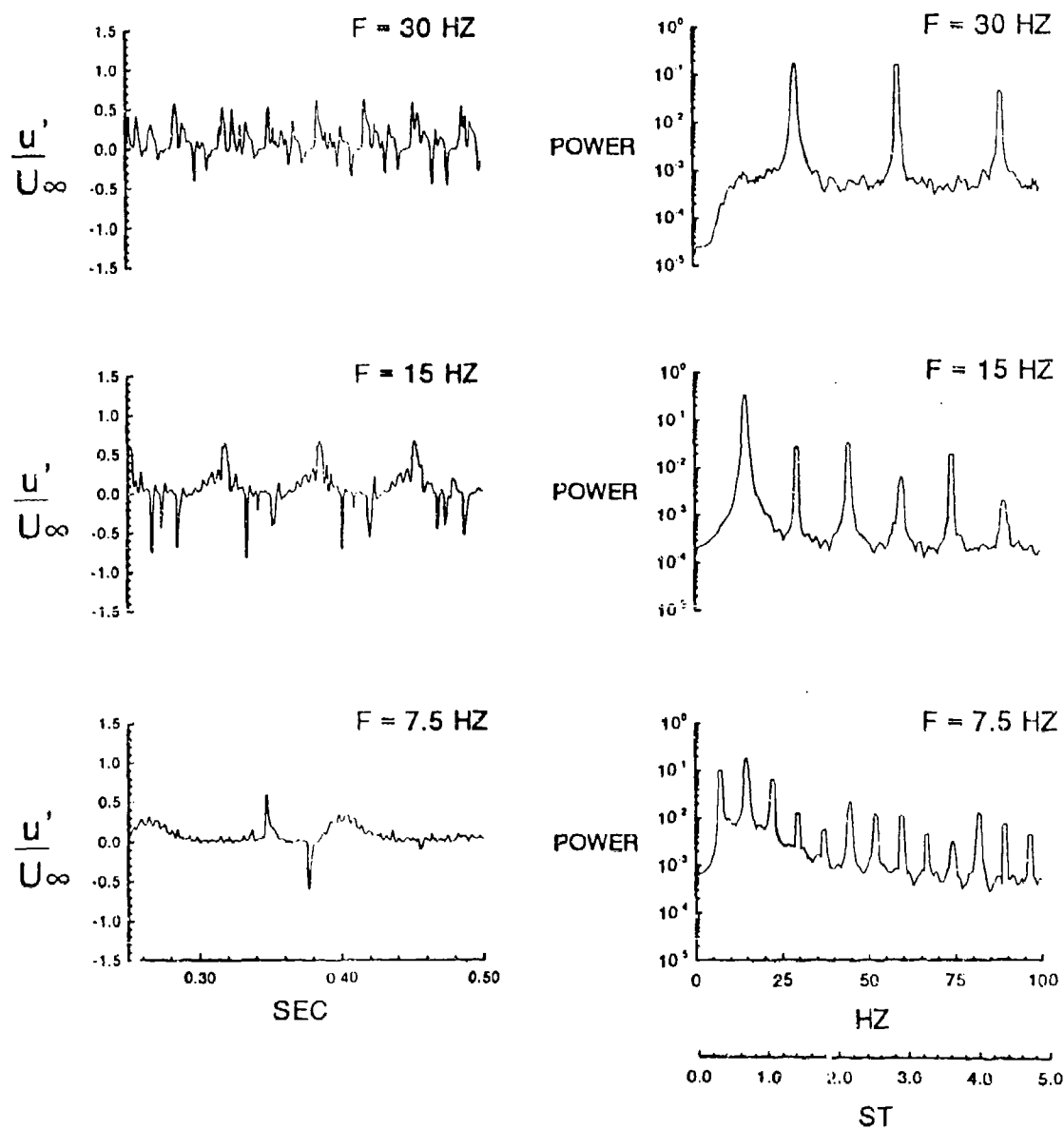


Figure 5-2. Change in velocity fluctuations with respect to time and the corresponding power spectra. Pulsed air control.  $\alpha=15^\circ$ ,  $R_c=24,000$ .

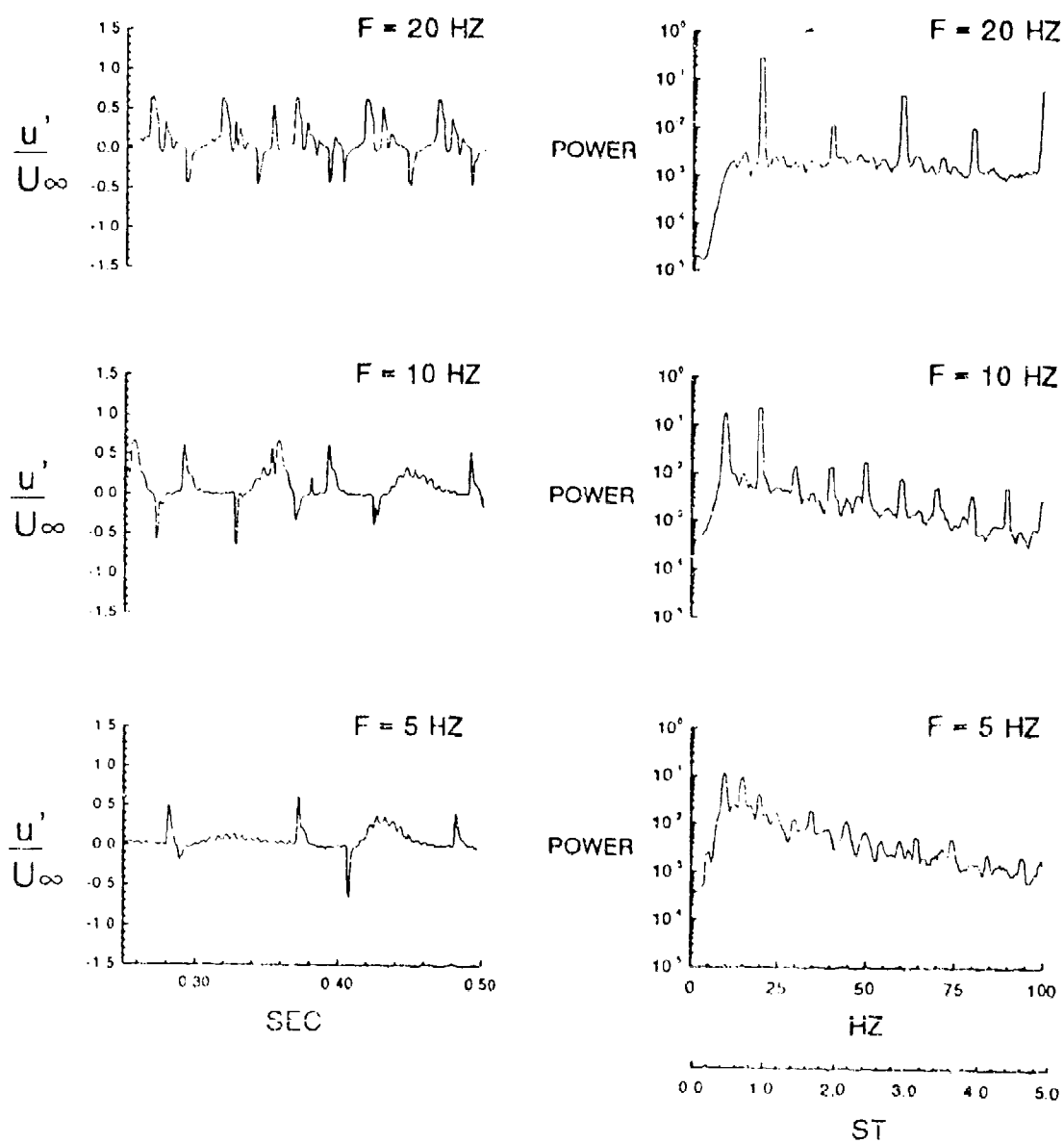


Figure 5-3. Change in velocity fluctuations with respect to time and the corresponding power spectra. Pulsed air control.  $\alpha=20^\circ$ ,  $R_c=24,000$ .

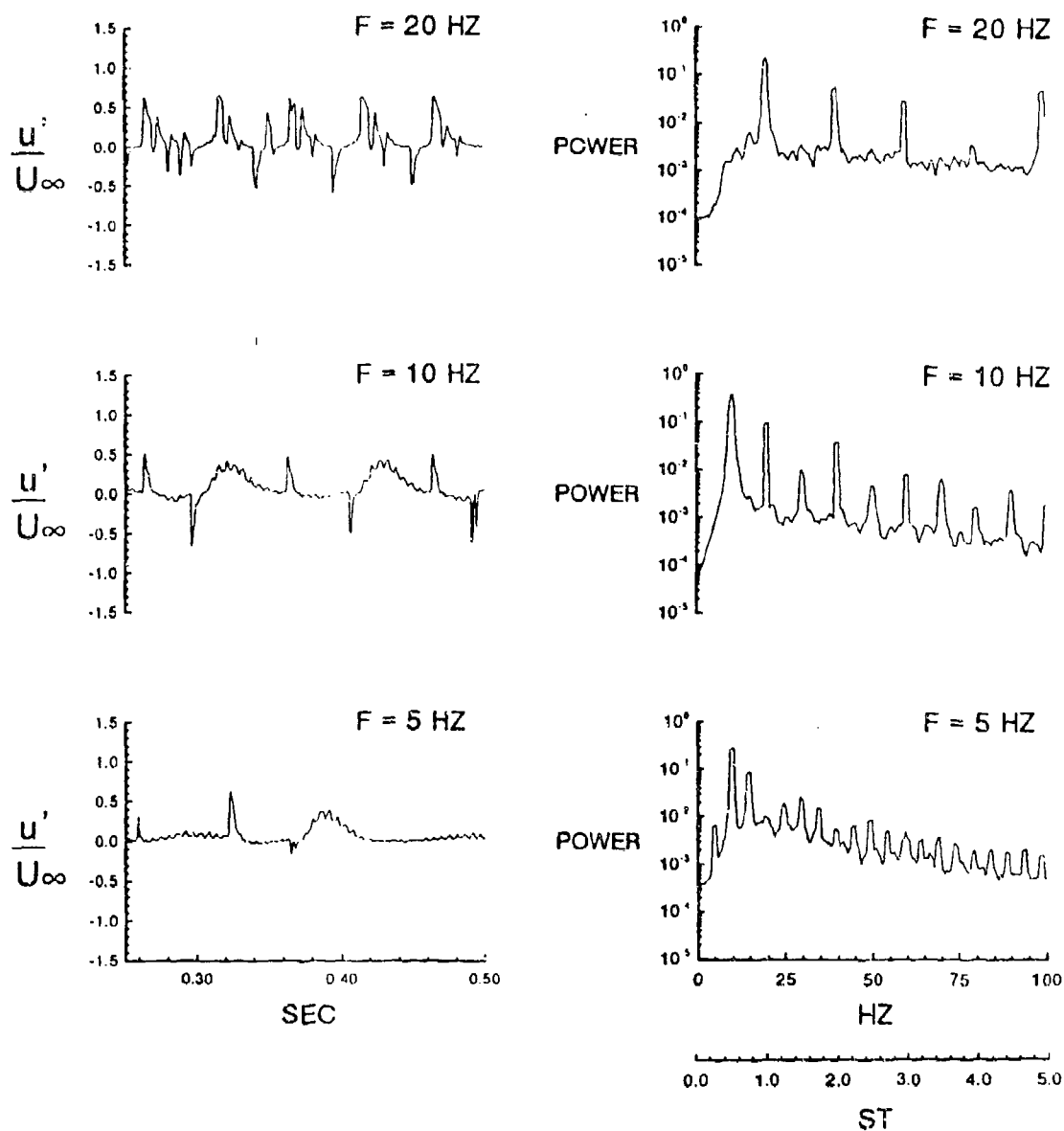


Figure 5-4.

Change in velocity fluctuations with respect to time and the corresponding power spectra. Pulsed air control.  $\alpha = 25^\circ$ ,  $R_c = 24,000$ .

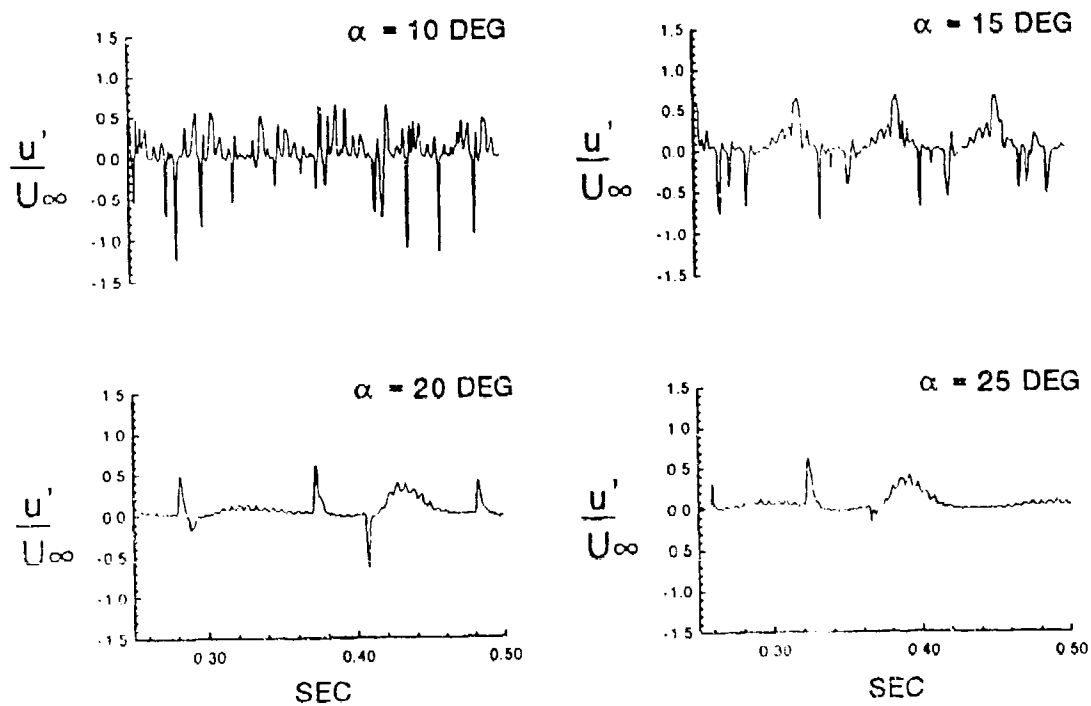


Figure 5-5. Changes free shear layer velocity fluctuations at increasing angles of attack. Pulsed air control.  $R_c = 24,000$ .

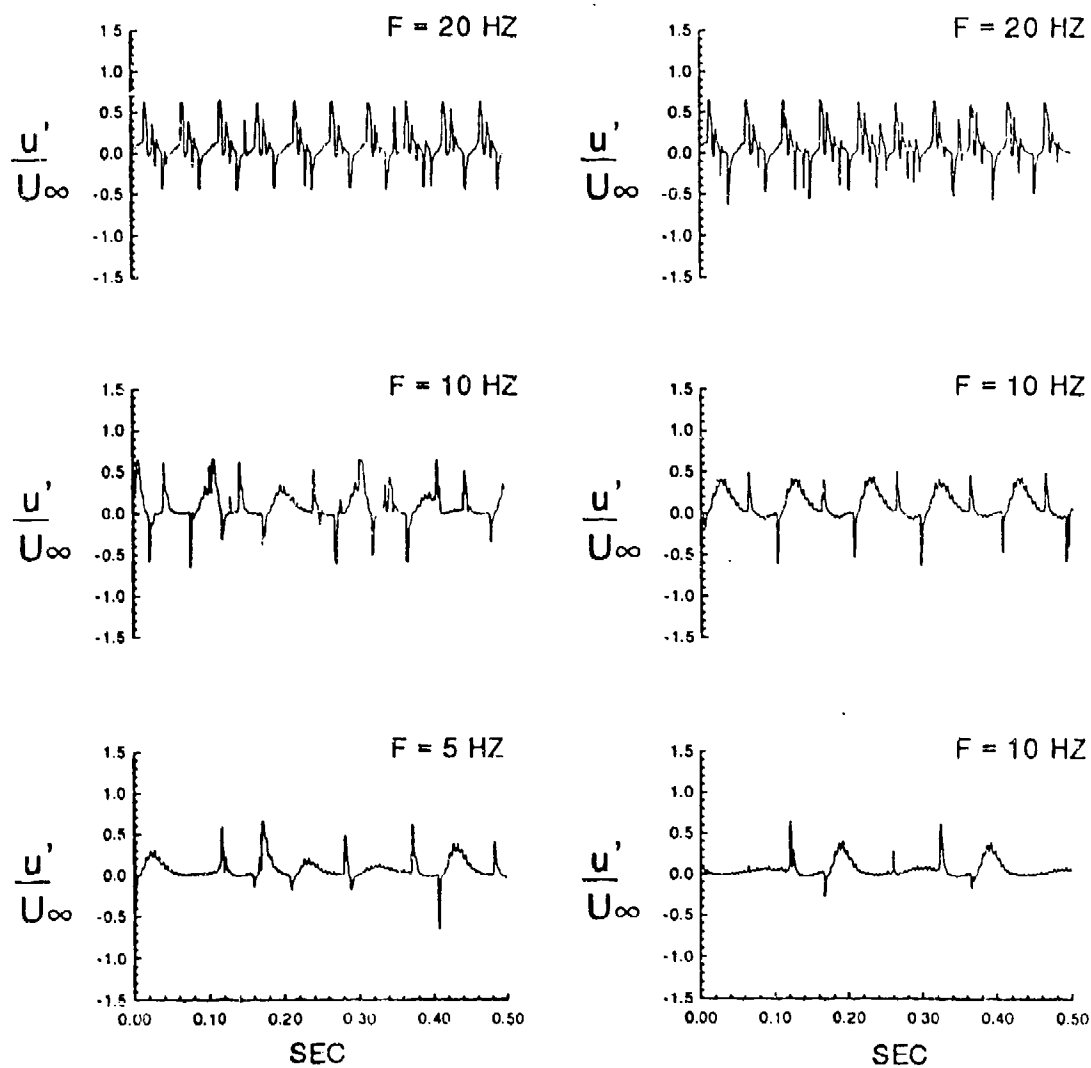


Figure 5-6. Flow receptivity to forcing with increasing angle of attack. Pulsed air control.  $R_c \approx 24,000$ .



## 5.2 Qualitative Response to Pulsed Air Control

The next step in the research study involves a flow visualization analysis of the tangential pulsed air control effects on the flow over a static airfoil. Figure 5-7 shows a detail of the flow near the airfoil leading edge forced at frequencies corresponding to the fundamental and subharmonics of the most receptive flow frequency. As mentioned in the Experimental Methods chapter, forcing at frequencies greater than 45 Hz is not possible due to the design constraints of the pulsed air system. As such, certain flow frequencies can not be applied. The angles of attack of 10°, 15°, 20°, and 25° are analyzed at a chord Reynolds number of 24,000. The natural flow, in row one, transitions from a primarily attached flow containing near surface shear layer structures at 10° to one that is clearly detaching from the airfoil surface at 15°. The flow is completely separated at an angle of attack of 20°, and the large-scale shear layer structures developing in the separating boundary layer can clearly be seen. At an attack angle of 25°, the shear layer structures are less defined, but still evident.

Controlling the flow at the fundamental frequency, shown in the second row for angles of attack at 20° and 25°, results in noticeable reattachment over the portion of the airfoil shown. Close scrutiny of the flow at 25° reveals a disruption in the large-scale shear layer structures that were apparent in the natural case. This coincides with the results of the hot-film measurements, where forcing at the fundamental flow frequency created a regular velocity fluctuation time trace. It is vortex pairing that causes the growth of the free shear layer, and in the case of flow over an airfoil the free shear layer grows as the angle of attack is increased and the ensuing separation progresses upstream along the airfoil chord. Inhibiting the free

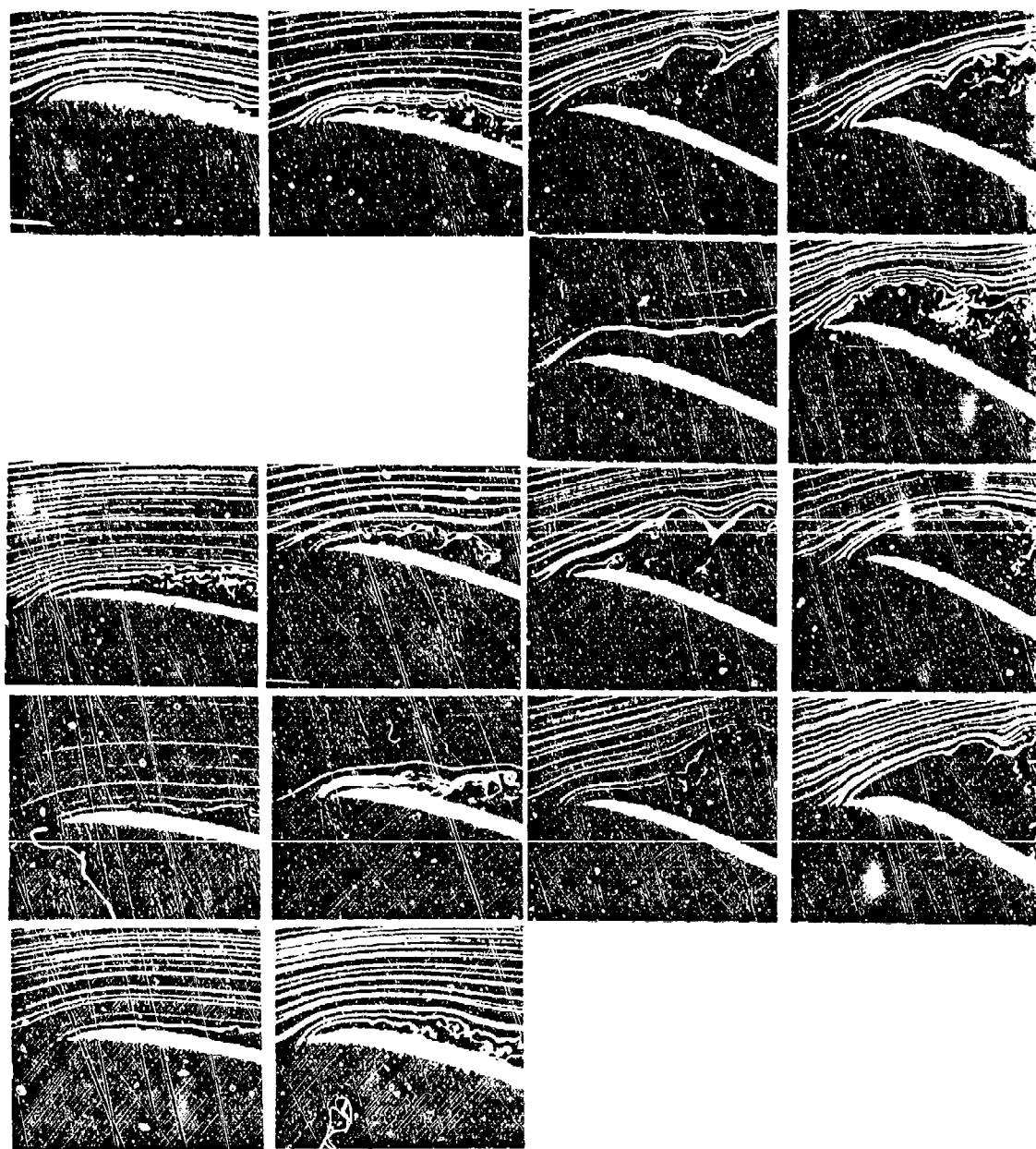
shear layer vortex pairing over the airfoil should reduce the growth of the separation region. Since the velocity fluctuations are repetitive for the fundamental frequency, and do not exhibit the bimodal signal previously associated with a free shear layer experiencing enhanced shear layer vortex pairing, the results support the results of Oster and Wygnanski (1982) that forcing at the fundamental frequency inhibits free shear layer vortex pairing.

The third, fourth, and fifth rows of Figure 5-7 correspond to control at the first, second, and third flow subharmonics, respectively. As previously shown in section 5-1, forcing the flow at these frequencies leads to a bimodal signal characteristic of enhanced free shear layer vortex pairing. Flow visualization for these cases confirms this result. Observing the flow at  $10^\circ$  and  $15^\circ$ , the overall separation region over the airfoil has grown, an expected result of enhanced shear layer vortex pairing. At an angle of attack of  $20^\circ$ , forcing at the first and second subharmonics clearly causes enhanced growth of the large scale structures. Where there were two vortices over the leading edge of the natural airfoil, there is now only one over the controlled airfoil. Although the shear layer vortices are less defined at the higher attack angle of  $25^\circ$ , the same control effect is evident.

Observing the same natural and control cases over the entire airfoil in Figure 5-8 yields an interesting result. While active control at the pre-stall attack angles of  $10^\circ$  and  $15^\circ$  actually increase the size of the separation region over the entire airfoil, the pulsed air forcing at the post-stall attack angles of  $20^\circ$  and  $25^\circ$  results in an actual reduction in the overall size of the separation region. Comparison of the natural flow at an angle of attack of  $20^\circ$  with the three controlled cases below it in Column three shows a reduction in separation near the airfoil leading edge, indicated by the slight curving of the streaklines towards the

airfoil surface at approximately 2% chord. Nearer to the trailing edge of the airfoil, the upper surface separation region height is reduced at all three control frequencies. At an angle of attack of  $25^\circ$ , forcing at the low subharmonics generates what qualitatively appears to be a separation bubble over the previously stalled airfoil, resulting possibly in flow reattachment near the airfoil trailing edge.

The dependence of static flow behavior on forcing frequency is shown for an angle of attack of  $25^\circ$  in Figure 5-9. At the higher frequencies, shown in Figure 5-9(a) at 36 Hz and Figure 5-9(b) at 31 Hz, there are few effects on the flow. There is no appreciable reduction in the separation region, and only minimal effects of the shear layer vortex development. This is as expected, since it has been previously shown that forcing at frequencies greater than the fundamental frequency fails to alter shear layer characteristics (refer to Chapter 4). Forcing at values close to the fundamental frequency, 22 Hz. in Figure 5-9(c) and 18 Hz. in Figure 5-9(d), results in enhanced flow reattachment and a noticeable increase in shear layer structure definition. Reducing the forcing frequencies into the subharmonic range, Figures 5-9(e-g), results in enhanced shear layer vortex pairing and again a significant decrease in separation region area.



10°

15°

20°

25°

Figure 5-7.

Leading edge smoke flow visualization of a static airfoil.

Pulsed air control,  $R_c = 24,000$

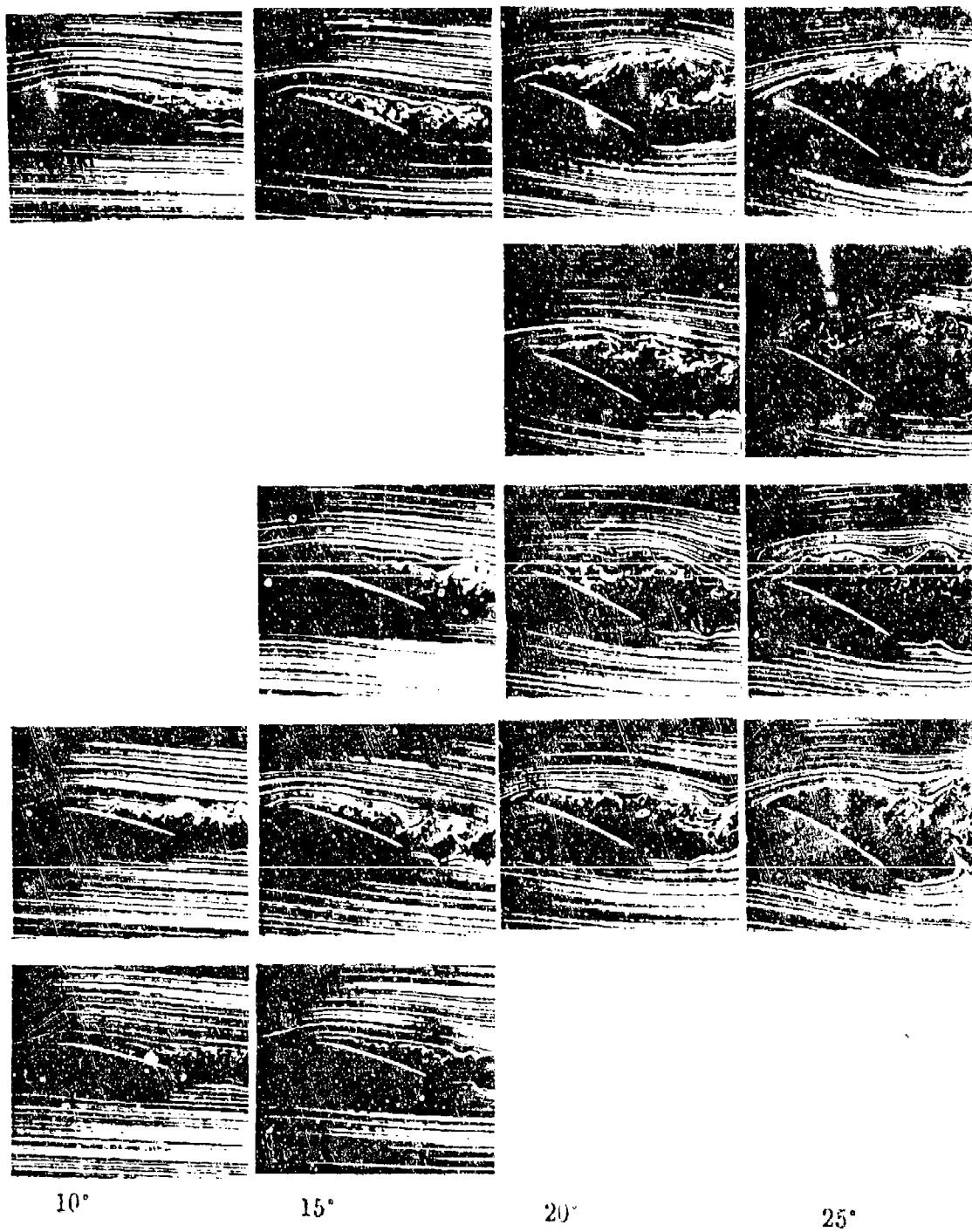


Figure 5-8.

Smoke flow visualization of the entire flowfield over a static airfoil. Pulsed air control,  $R_c = 24,600$

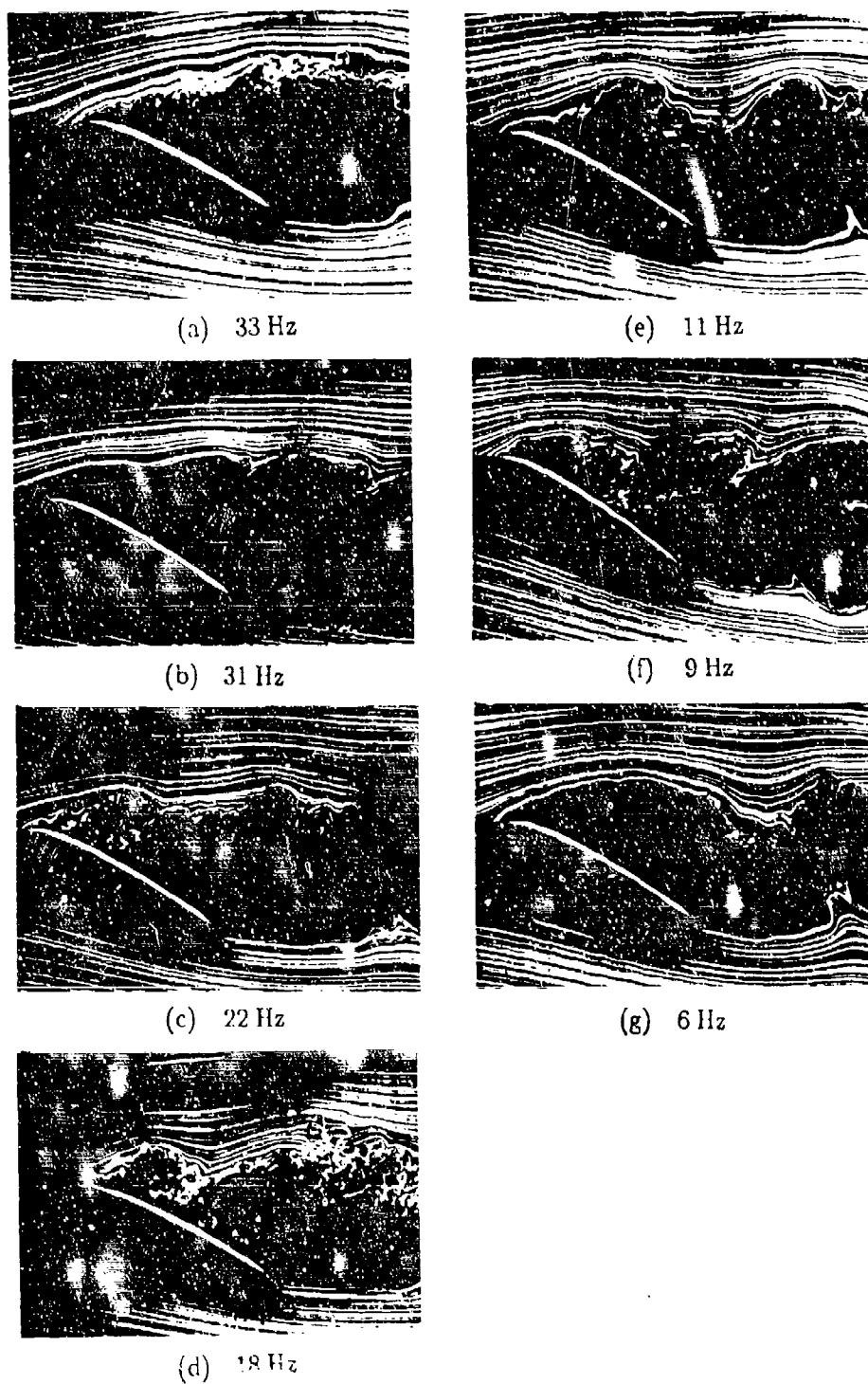


Figure 5-9. Smoke flow visualization of a static airfoil. Pulsed air control,  $\alpha=25^\circ$ ,  $R_c=24,000$ .

### 5.3 Effect of Reynolds Number on Control Response

The effect of Reynolds number on active control results is investigated for an airfoil under tangential pulsed air forcing. Figure 5-10 gives an example of a chord Reynolds number of 57,000 under forcing conditions for an angle of attack of  $20^\circ$ . Control frequencies correspond to the first, second, and third subharmonic of the fundamental forcing frequencies at this Reynolds number. The tangential pulsed air mechanism limitations do not allow control at the fundamental frequency of approximately 60 Hz. for this case. Although the flow is not as organized compared to the lower Reynolds number, similar characteristics are present. For all three forcing frequencies, the hot-film velocity trace exhibits a bimodal signal as seen previously in the acoustically controlled flow at the subharmonic frequencies. A sharp spike followed by a double smooth peak occurs at each frequency. Power spectra for these cases indicate strong spectral peaks corresponding to the forcing frequency, confirming flow receptiveness to the control.

A comparison of the controlled flow at chord Reynolds numbers of 24,000 and 57,000 is given in Figure 5-11 for an angle of attack of  $20^\circ$ . Velocity fluctuations under control frequencies corresponding to the first and second subharmonics of the flow are shown for both Reynolds numbers. At a Reynolds number of 24,000, the normalized velocity fluctuations corresponding to the flow control frequencies are noticeably larger than the case for  $R_c = 57,000$ . A noticeable difference in the time traces at the two Reynolds numbers is that, at the greater Reynolds number, the "bimodal" signal indicating vortex pairing contains a double rounded peak preceded by a spike whereas the lower Reynolds number case is characterized by a single rounded peak accompanied by a spike. It should be noted

that, for all experiments discussed in this report, the level of both acoustic and tangential-pulsed air control remained constant. It is possible that the reduced change in velocity fluctuations at the greater Reynolds number is due at least in part to a reduction in forcing strength with respect to freestream velocity, since the blowing momentum coefficient,  $C_{\mu}$ , at a Reynolds number of 57,000 is one seventh that of  $C_{\mu}$  at a Reynolds number of 24,000. While the control methodology relies on the frequency response of the flow, these results indicate a possible dependence on control amplitude of the tangential pulsed-air blowing as well.



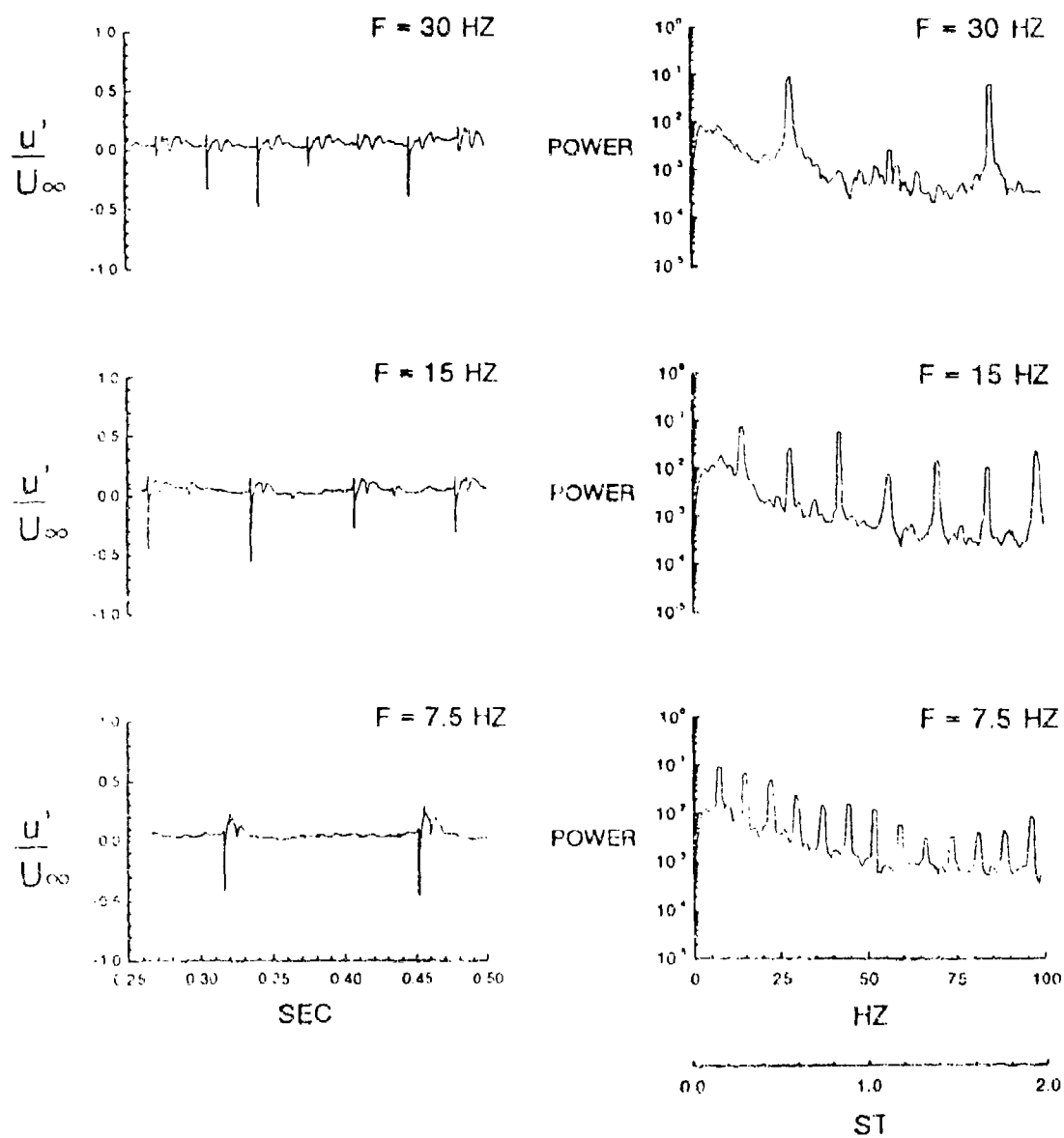


Figure 5-10. Changes in velocity fluctuations with respect to time and the corresponding power spectra. Pulsed air control.  $\alpha = 20^\circ$ ,  $Re = 57,000$ .

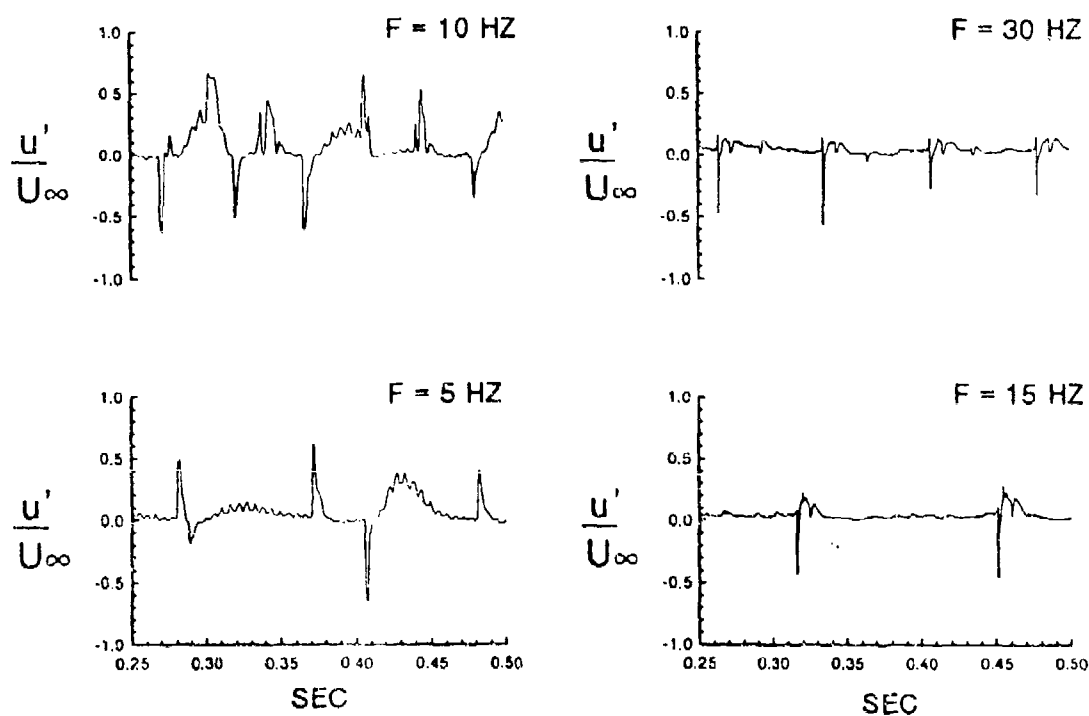


Figure 5-11.

Comparison between the velocity fluctuations with respect to time for  $R_c=24,000$  (column 1) and  $R_c=57,000$  (column 2). Pulsed air control at the first and second subharmonics.

#### 5.4 Effect of Pulsed Air Control on Surface Pressures

An essential aspect of this study is to determine control effects on static airfoil performance. Upper surface pressure coefficients are evaluated for three locations on the airfoil, just downstream of the leading edge slot,  $0.033c$  (port 1), in between the leading edge slot and the slot at 20% chord,  $0.067c$  (port 2), and downstream of the 20% chord slot,  $0.283c$  (port 3). The chord Reynolds number is 57,000. Figure 5-12 gives the pressure coefficients as a function of time for an angle of attack of  $10^\circ$  under natural and pulsed-air controlled conditions. For the natural case, the pressure coefficient decreases in magnitude in the downstream direction. Forcing the flow at the third subharmonic creates little effect on the pressure, except for an slight increase in variation with time and an increase in pressure magnitude at port 1. Figure 5-13 clearly shows this slight enhancement of surface pressure.

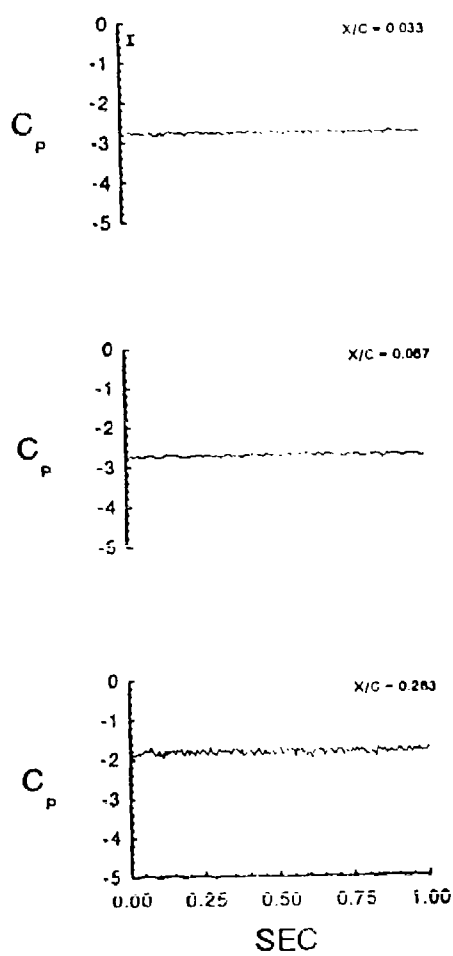
The effects of forcing are noticeably greater at an angle of attack of  $15^\circ$ , evident in Figure 5-14. Pressure fluctuations with time have increased with the higher attack angle, especially at port 1. Forcing at the second subharmonic of 34 Hz creates a pressure fluctuation at port 1 corresponding to the forcing frequency. Cherry, Hillier, and Latour (1939) determined that peaks in pressure time traces corresponded to the convection of massive "centers of vorticity" over the pressure tap, while dips in the negative pressure coincided to "troughs" in between shear layer structures. Similar pressure fluctuations are apparent at port 2, although the peak-to-peak magnitude has decreased. There are disturbances in the pressure field at port 3, although they do not appear periodic. Forcing at the third subharmonic of 17 Hz in Figure 5-15 creates greater pressure fluctuations at all

three port locations. Observance of Figure 5-16 shows that it is control at this low frequency which is most successful in increasing the pressure coefficient magnitude over the natural case. The pressure increases correspond primarily to the first port, although minimal increases are present at ports two and three.

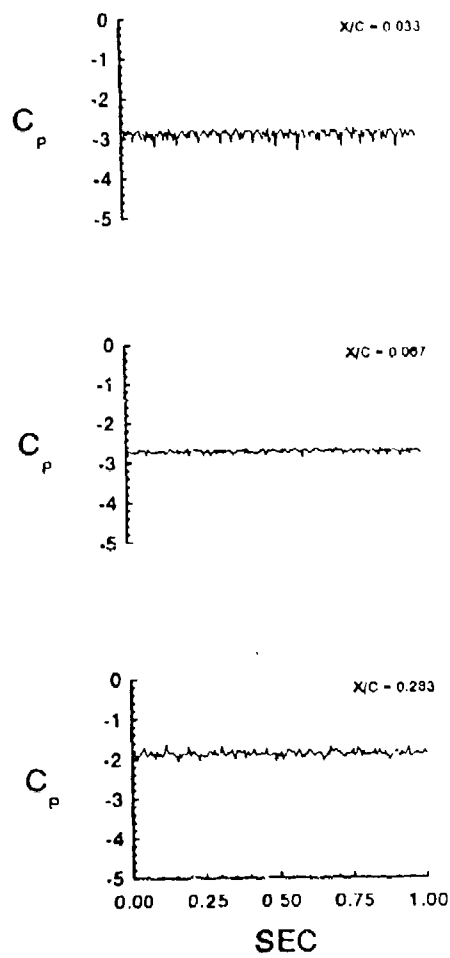
Pressure fluctuations due to pulsed air control continue to increase in amplitude when the angle of attack is increased to  $20^\circ$  in Figure 5-17. Although the natural pressure variations are only slightly greater than those at  $15^\circ$ , the pressure coefficients under control at the first, second, and third subharmonics have increased by a factor of about five. Forcing at the two lower frequencies, 15 Hz corresponding to the second subharmonic and 7.5 Hz corresponding to the third subharmonic, results in an enhanced periodicity of the pressure coefficient with respect to time, as seen in Figure 5-18. The fluctuations of the pressure approximately equal the forcing frequency in each case. The active control has a significant effect on the average pressure coefficient at each port. Referring to Figure 5-19, the natural pressure magnitudes are lower than those at  $15^\circ$ , and the minimal changes in pressure across the ports indicates that the airfoil is separated. Forcing at all three frequencies discussed increases the pressure coefficient magnitudes at all three ports, but most significantly at the two ports nearest the leading edge. This suggests that the active control has caused the separating boundary layer to reattach.

The amplitude and the periodicity of the pressure fluctuations with respect to time are greater at an angle of attack of  $20^\circ$ . While pressure variations for the natural case are actually reduced here compared to  $20^\circ$ , as seen in Figure 5-20, the case forced at the first subharmonic of 30 Hz exhibits enhanced regularity in the pressure peaks at all three port locations. When the control frequency is reduced to

the second and third subharmonics, in Figure 5-21, the forcing results in a pressure time trace fluctuating at a frequency closely corresponding to the control value. The average pressure coefficients for this angle of attack are greater in magnitude than the natural case, shown in Figure 5-22, but are slightly less than at the lower attack angle of  $20^\circ$ .



$F = 0$  HZ



$F = 27$  HZ

Figure 5-12.

Upper surface pressure coefficients for a one second period. Pulsed air control.  $\alpha = 10^\circ$ ,  $R_c = 57,000$ .

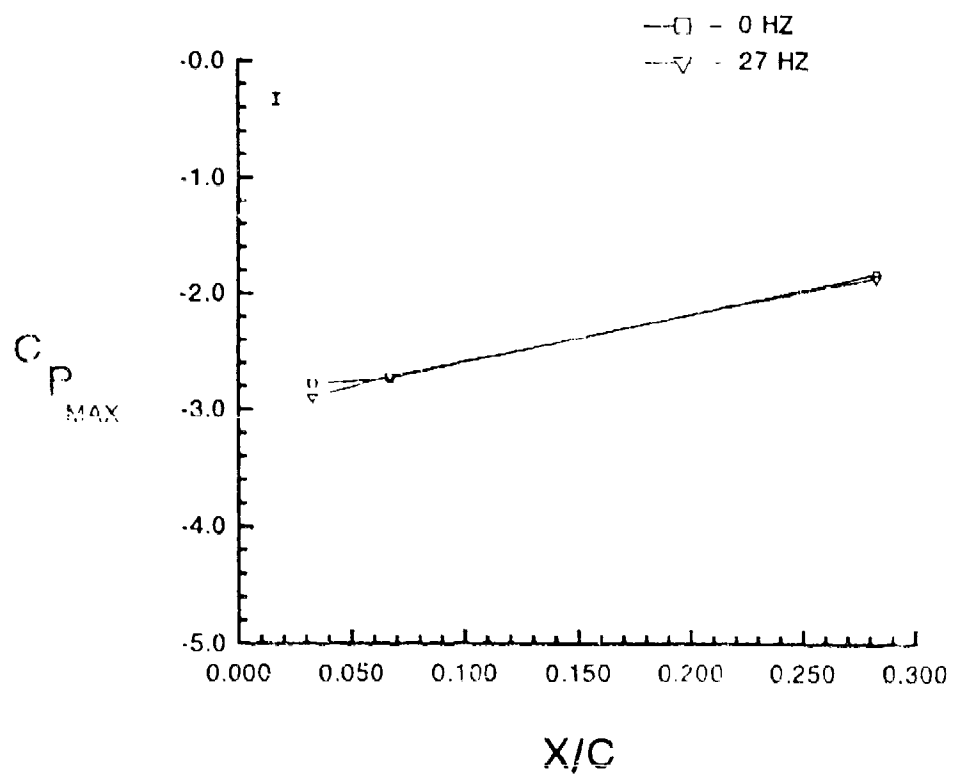


Figure 5-13.

Average pressure coefficients for a static airfoil with respect to port location. Pulsed air control.  $\alpha=10^\circ$ ,  $R_c=57,000$ .

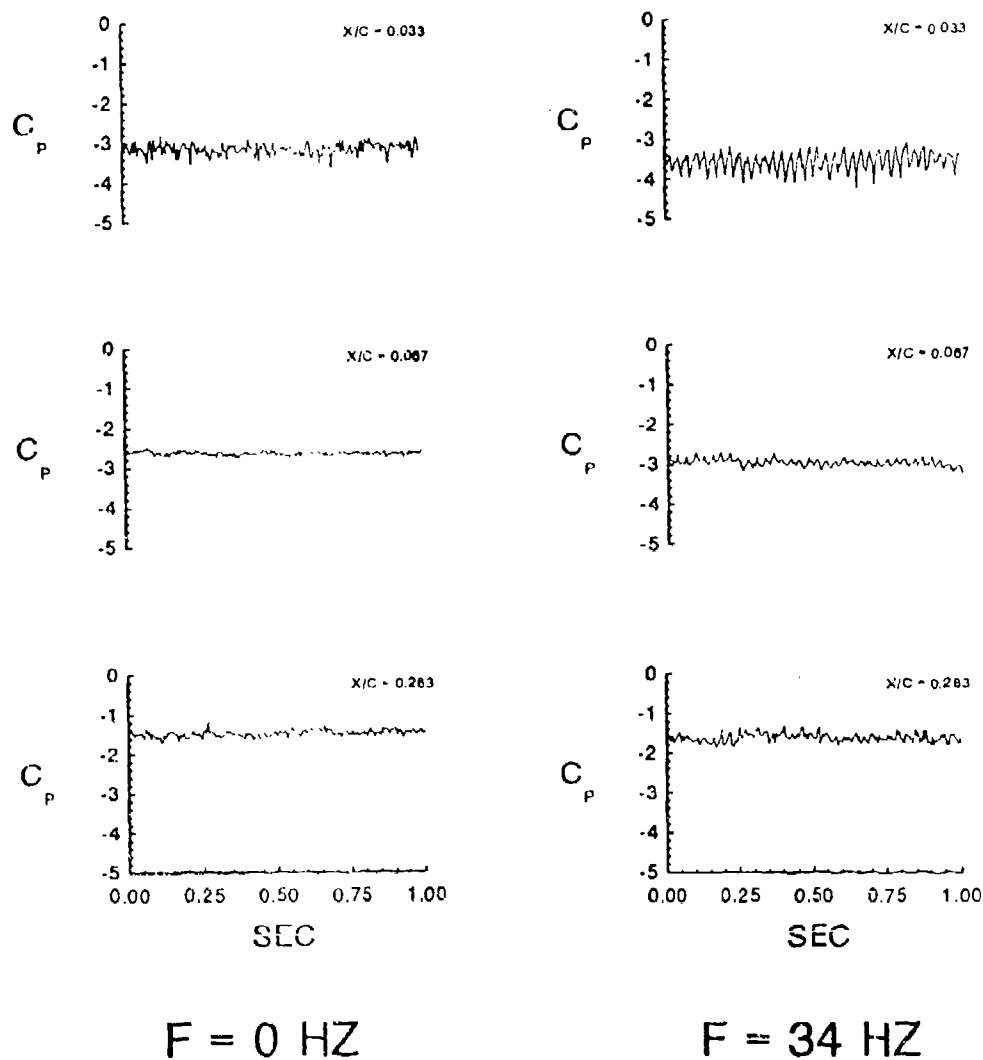
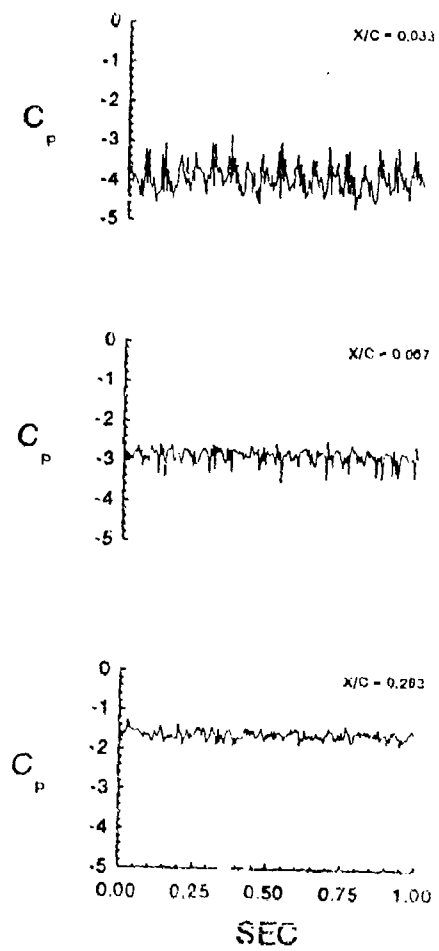


Figure 5-14. Upper surface pressure coefficients for a one second period. Pulsed air control.  $\alpha = 15^\circ$ ,  $R_c \approx 57,000$ .





$$F = 17 \text{ HZ}$$

Figure 5--15. Upper surface pressure coefficients for a one second period. Pulsed air control.  $\alpha=15^\circ$ ,  $R_c=57,000$ .

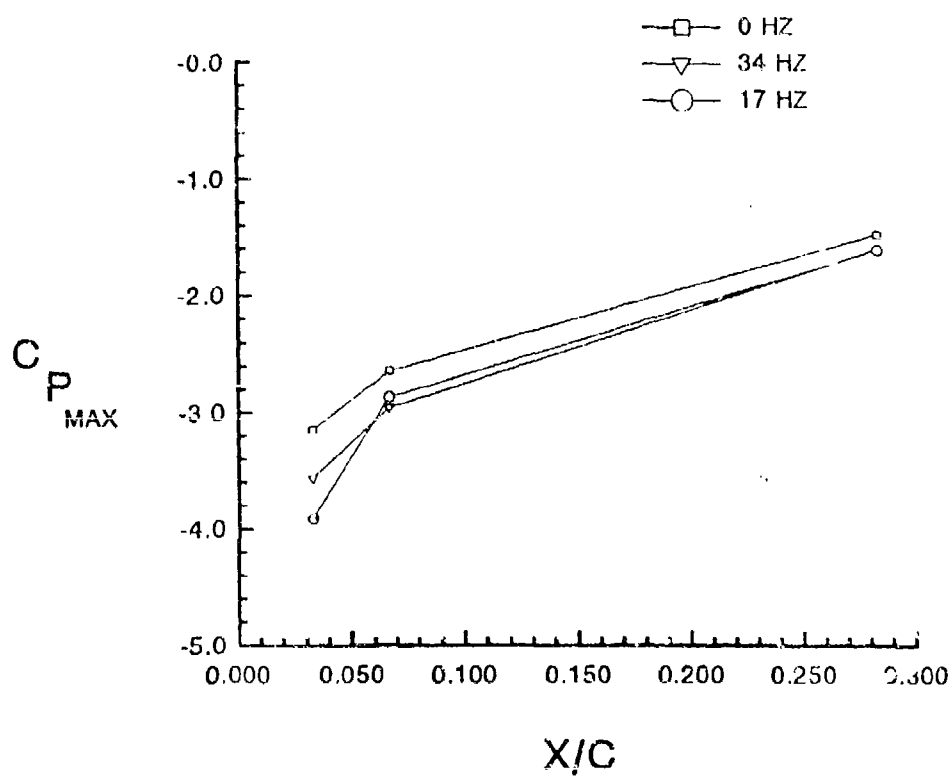


Figure 5-16.

Average pressure coefficients for a static airfoil with respect to port location. Pulsed air control.  $\alpha=15^\circ$ ,  $R_c=57,000$ .

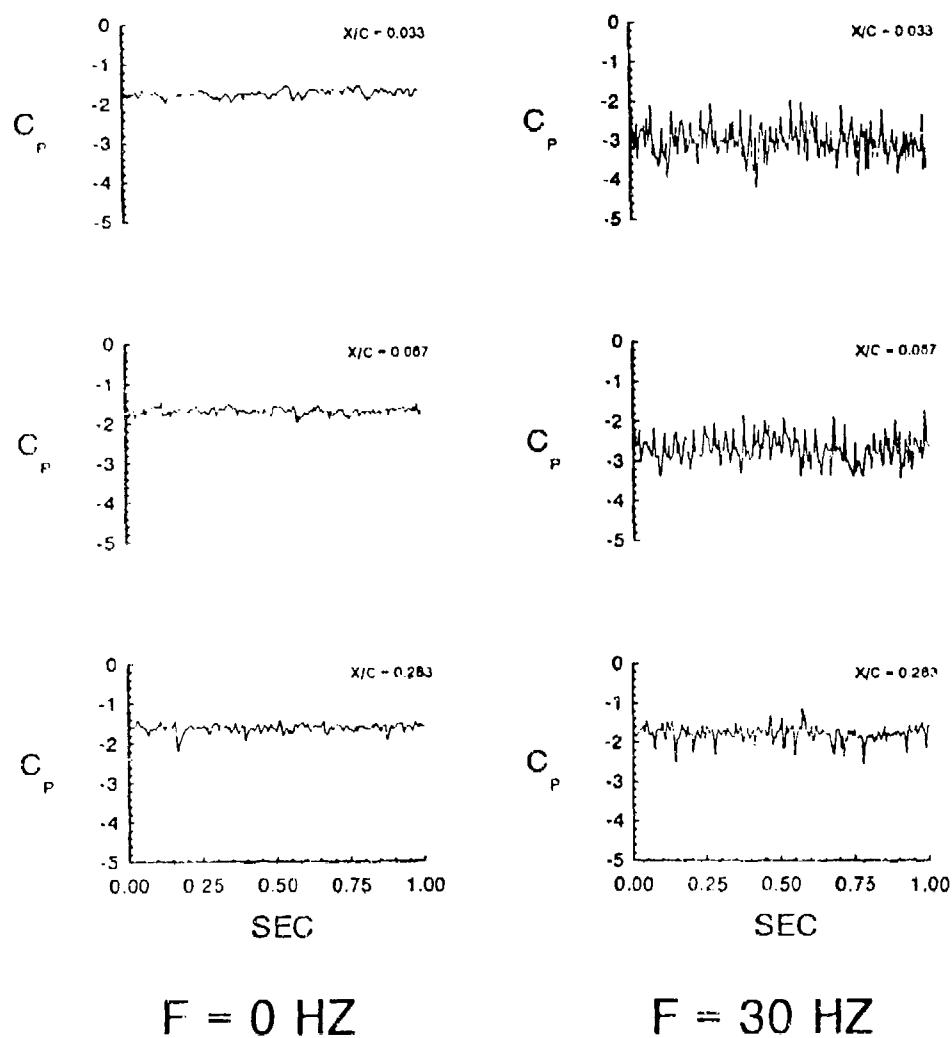


Figure 5-17. Upper surface pressure coefficients for a one second period. Pulsed air control.  $\alpha=20^\circ$ ,  $R_c=57,000$

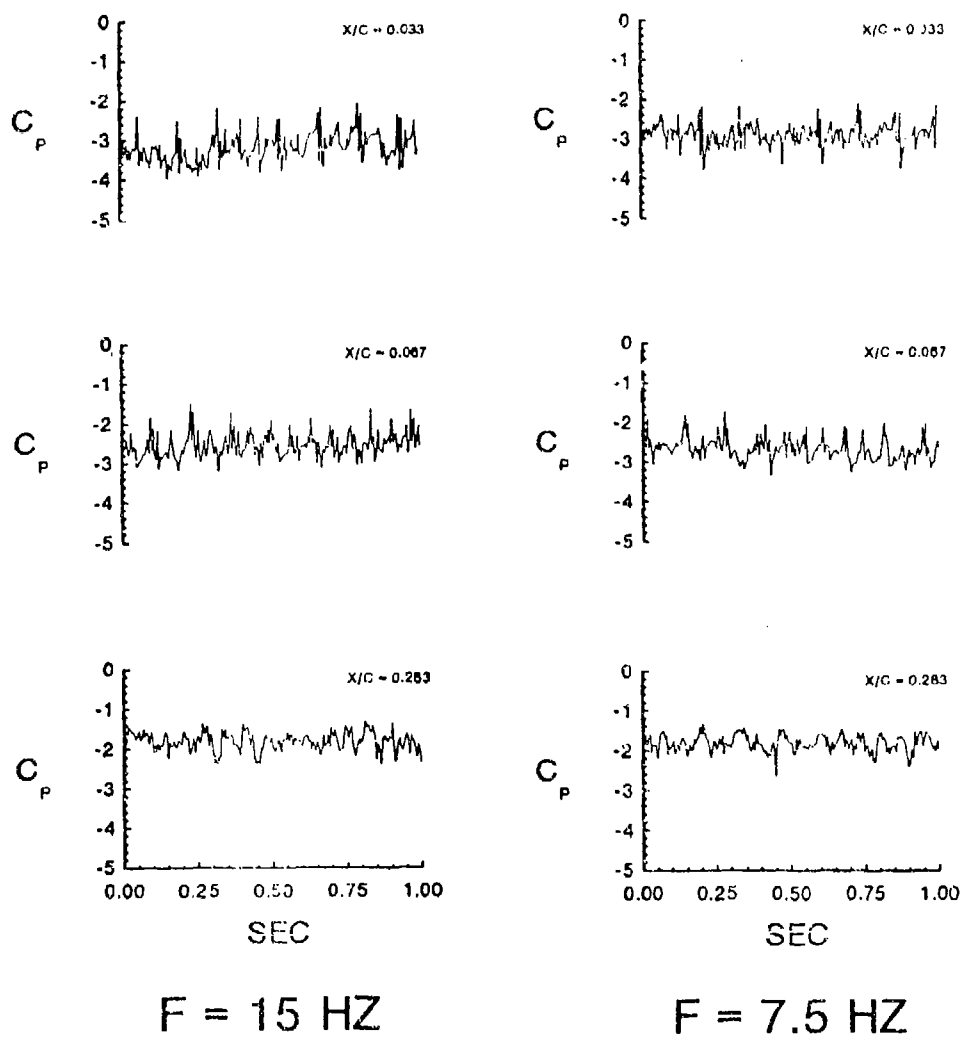


Figure 5-18.

Upper surface pressure coefficients over a one second period. Pulsed air control.  $\alpha = 20^\circ$ ,  $R_c = 57,000$ .

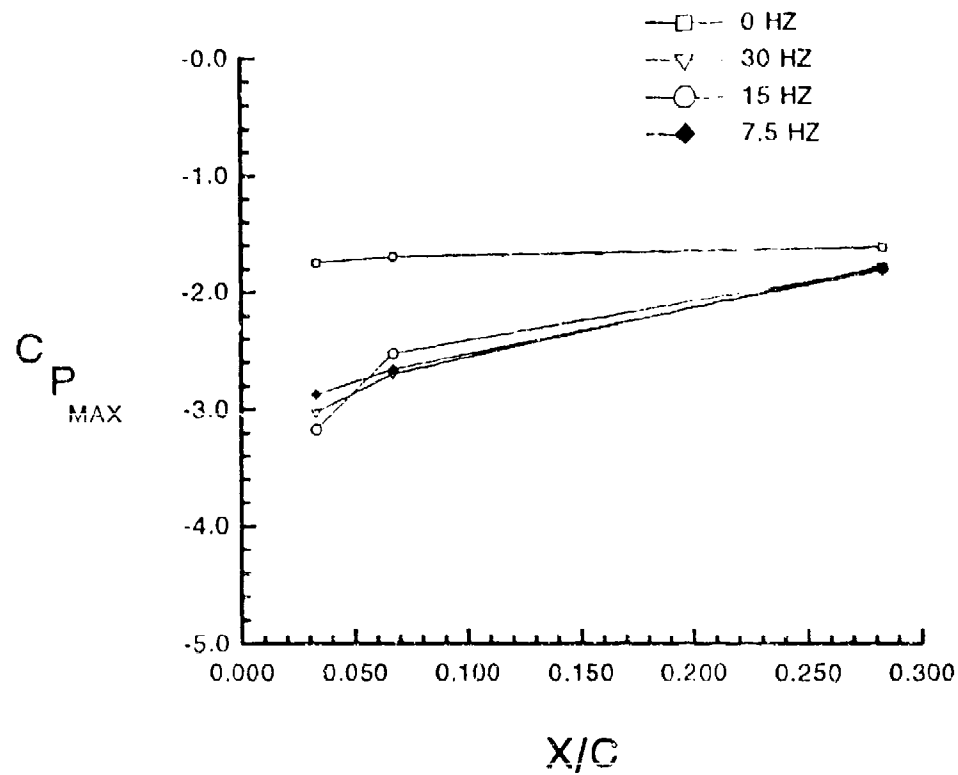


Figure 5-19.

Average pressure coefficients for a static airfoil with respect to port location. Pulsed air control.  $\alpha=20^\circ$ ,  $R_c=57,000$ .

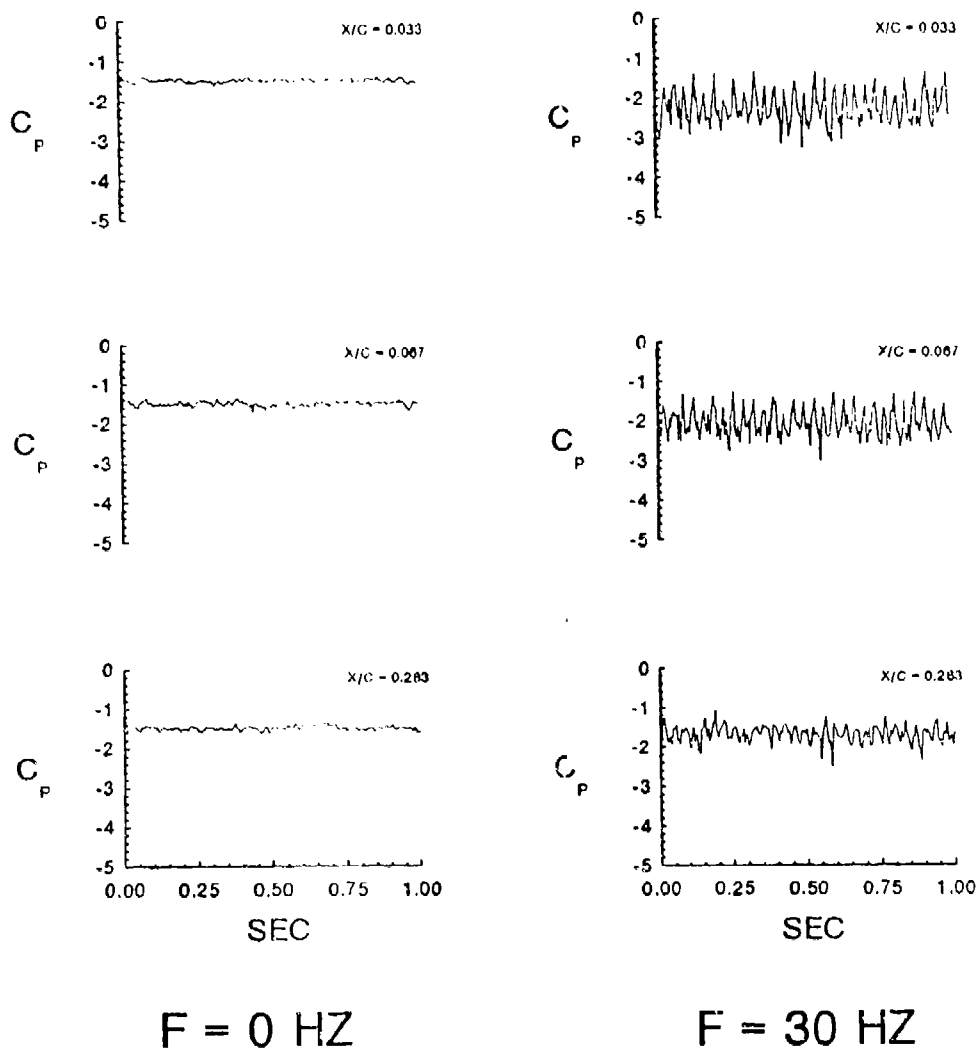
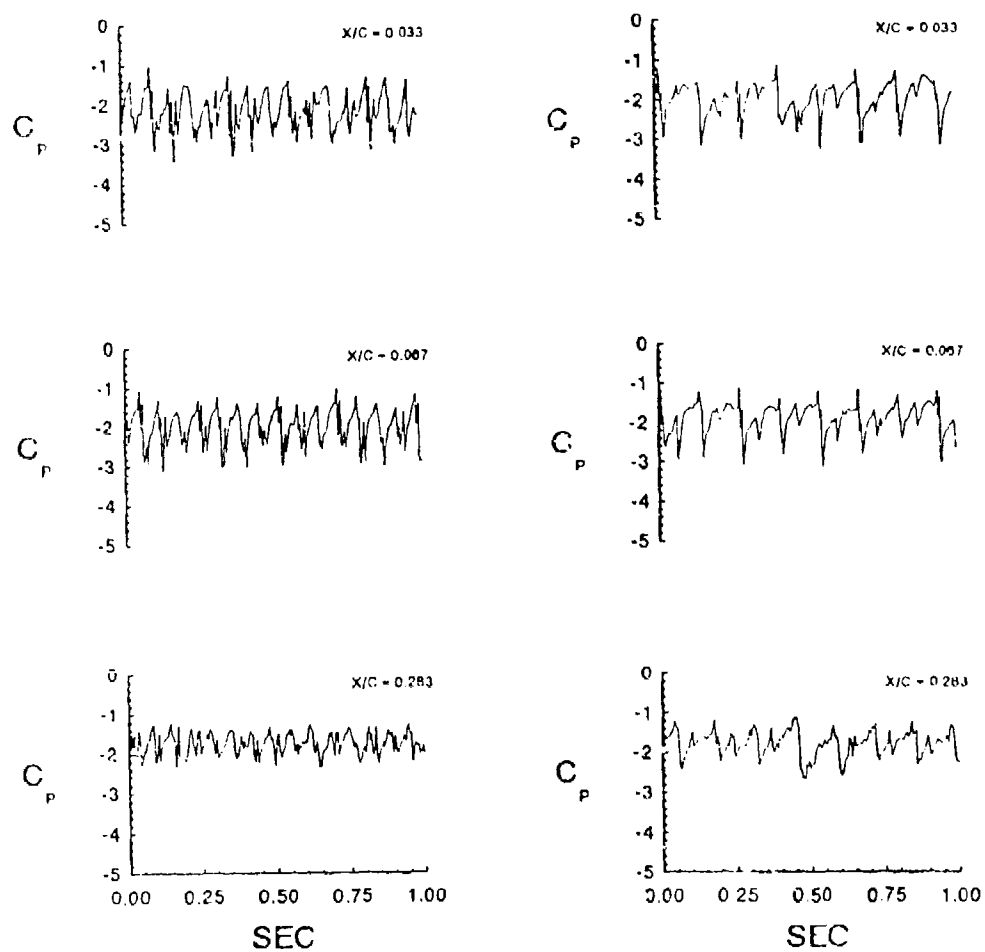


Figure 5-20.

Upper surface pressure coefficients over a one second time period. Pulsed air control.  $\alpha = 25^\circ$ ,  $R_c = 57,000$ .



$F = 15 \text{ HZ}$

$F = 7.5 \text{ HZ}$

Figure 5-21. Upper surface pressure coefficients over a one second period. Pulsed air control.  $\alpha=25^\circ$ ,  $R_c=57,000$ .

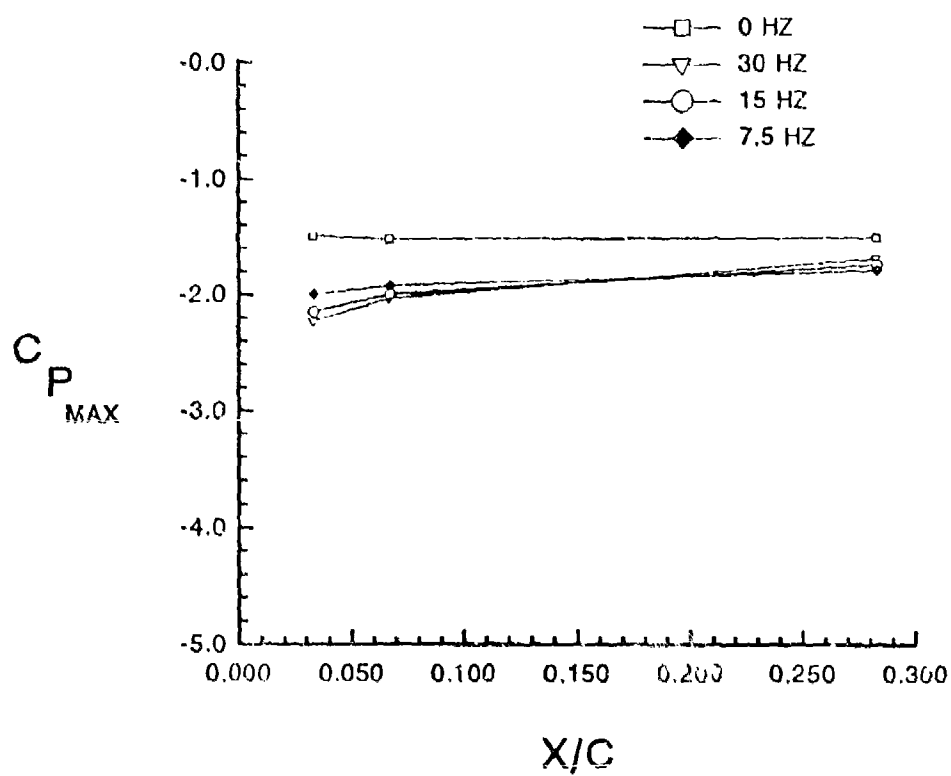


Figure 5-22.

Average pressure coefficients for a static airfoil with respect to port location. Pulsed air control.  $\alpha=25^\circ$ ,  $R_c=57,000$ .



## CHAPTER SIX

### DYNAMIC FLOW CONTROL

#### 6.1 Pulsed-Air Control of an Unsteady Separating Boundary Layer

The final part of this experimental investigation is to force an unsteady separating boundary layer using the determined static post-stall fundamental frequencies. Since we now have a detailed picture of the actively controlled static airfoil, the first step in the development of a dynamic control methodology must be to ascertain how the determined post-stall fundamental forcing frequencies affect the dynamic airfoil flow. A proposal for the remainder of the study is outlined in detail in Chapter Eight.

To observe control effects on the unsteady flow, a hot-film probe was placed at the 1% chord location at various distances from the airfoil surface. The chord Reynolds number is 24,000. Figure 6-1 presents the natural unsteady flow at an  $\alpha^+$  of 9.05. The velocity  $V$  represents the total velocity measured by the hot-film probe as the airfoil is pitched, including instantaneous, angular, and average velocity components in the  $x$  and  $y$  directions. Close to the airfoil, the reduced velocity exhibits a sharp decrease near an angle of attack of  $18^\circ$ . The velocity decreases to a minimum at an attack angle of approximately  $22^\circ$ . As the distance from the airfoil is increased, the peak in the velocity becomes sharper at first, and then gradually smooths out over a greater range of attack angle, until the broad peak extends from about  $22^\circ$  to about  $40^\circ$ . This large decrease in velocity, from the

velocity peak to the minimum, has been shown to correspond to the presence of the dynamic stall vortex on the airfoil (Luttges, Robinson, and Kennedy, 1985).

Active control by tangential-pulsed air forcing has a noticeable effect on the flow, with the flow response depending upon forcing frequency and distance from the airfoil. When the flow is forced at the fundamental frequency of the corresponding post-stall static flow, 20 Hz, two changes are apparent, as shown in Figure 6-2. The first occurs at the four closest points to the airfoil surface, appearing as a slight reduction in peak velocity. For the first six positions from the airfoil, there is also a delay in velocity reduction by about  $10^\circ$ . Regular fluctuations occur most noticeably at  $Y/C=0.131$  and  $Y/C=0.262$  at a slightly lower frequency than the control value.

The broadening of the velocity peak and the delay of velocity decay do not occur when the flow is forced at the first and second subharmonics corresponding to the static post-stall values of 10 Hz and 5 Hz. Shown in Figures 6-3 and 6-4 respectively, the velocity traces appear similar to the non-forced case. At a forcing frequency of 10 Hz, a secondary peak is evident at both  $Y/C=0.052$  and  $Y/C=0.066$ . There are also increased velocity fluctuations at those and greater distances from the surface. The secondary peak is on slightly visible at  $Y/C=0.052$  in the flow forced at 5 Hz. In fact, this sub-peak takes on the appearance of yet another velocity fluctuation, rather than a separate occurrence.

These results are summarized in Figure 6-5, which gives the average percentage velocity changes over the free-stream. For all three controlled cases, there is an apparent increase in velocity magnitude over the natural case. Values at the location farthest from the airfoil surface do no change appreciably, but closer to

the airfoil the change is appreciable. This is most evident for the case forced at 20 Hz.

Identical measurements were also obtained at the 30% chord location. Shown in Figure 6-6 for the natural flow, the significant occurrence in the flow is a secondary peak centered around approximately  $25^\circ$ . This sub-peak is not present at locations farther than  $Y/C=0.098$ , and the broad velocity peak that was present at 10% chord is replaced by a sharp peak that moves from about  $23^\circ$  at  $Y/C=0.098$  to about  $26^\circ$  at  $Y/C=0.262$ .

Forcing the flow at the post-stall fundamental frequency of 20 Hz significantly delays the secondary-peak that was present in the natural flow, as presented in Figure 6-7. While the secondary peak was centered around about  $24^\circ$  in the natural flow, it does not appear until approximately  $27^\circ$  in the forced case. In addition, this peak is reduced in magnitude by about 20%. The sharp peak appearing at  $Y/C=0.098$  in the natural flow does not clearly manifest itself until  $Y/C=0.262$  in the controlled flow. Overall velocity peaks are reduced by the forcing, and the velocity decay is delayed by an average of  $4^\circ$ .

The greatest effect of forcing at the static post-stall first subharmonic of 10 Hz, shown in Figure 6-8, is an increase in velocity oscillations at the location closest to the airfoil,  $Y/C=0.026$ . Velocity fluctuations diminish with increasing distance from the airfoil surface. It is only at the two farthest points from the airfoil,  $Y/C=0.197$  and  $0.262$ , that the velocity peak is reduced and delayed with respect to angle of attack due to the forcing. Forcing at the static post-stall second subharmonic of 5 Hz, given in Figure 6-9, has effects similar to forcing at the first subharmonic.

The nature of the velocity at the 30% chord location is summarized in Figure 6-10. It is clear that the overall velocity magnitudes for the case forced at the static post-stall fundamental frequency are significantly greater than the natural flow. Velocity magnitudes are only slightly lower than this for the flow forced at the static post-stall first subharmonic. This minimal decreasing trend continues to the static post-stall second subharmonic frequency, but it should be noted that the forced velocity is still greater than the natural flow, especially at points farthest from the airfoil surface.

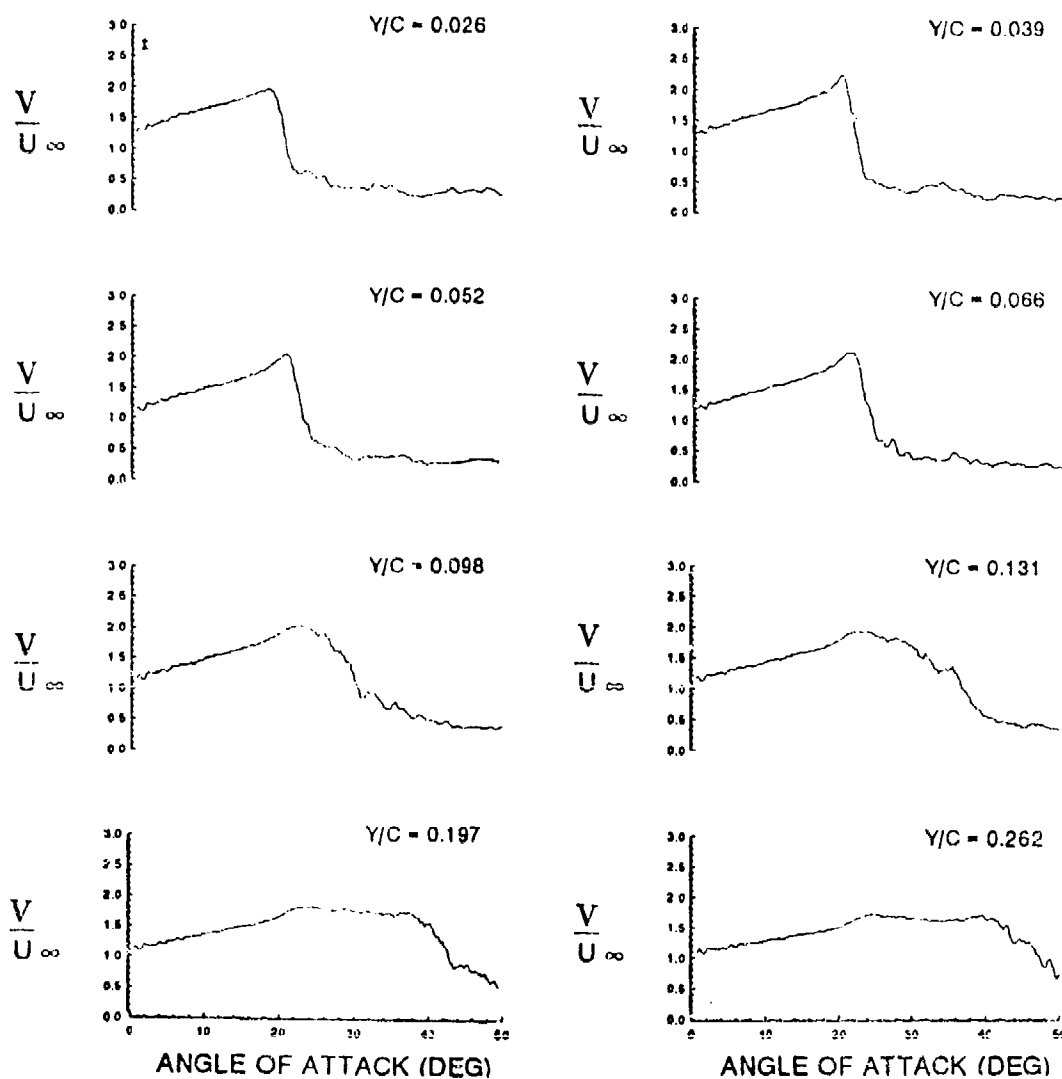


Figure 6-1.

Instantaneous velocity trace over a dynamic airfoil with respect to angle of attack. Natural flow.  $\alpha^+ = 0.05$ ,  $R_c = 24,000$ .  $X/C = 0.10$ .

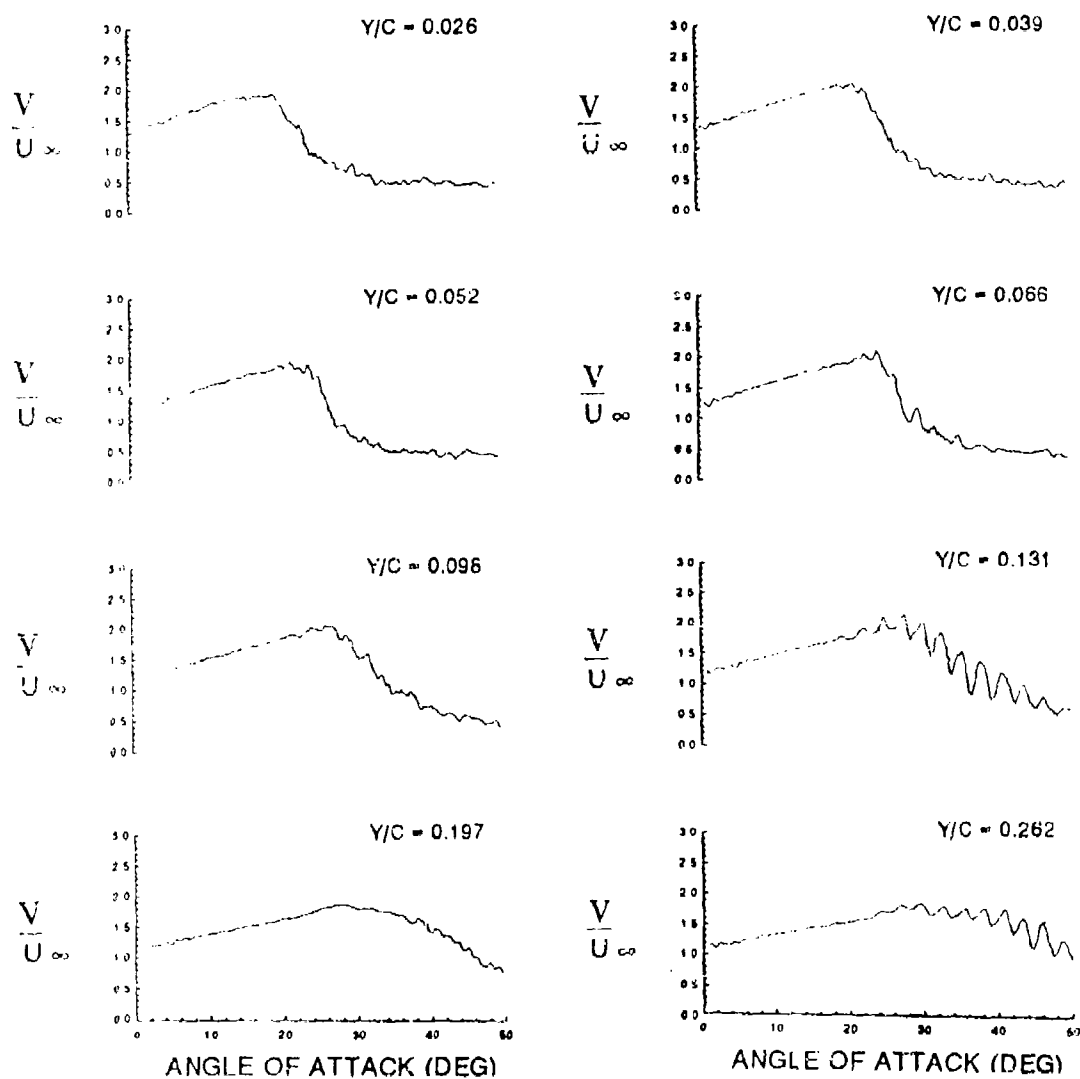


Figure 6-2.

Instantaneous velocity trace over a dynamic airfoil with respect to angle of attack. Pulsed air control at 20 Hz.  $\alpha^+ = 0.05$ ,  $R_c = 24,000$ .  $X/C = 0.10$ .

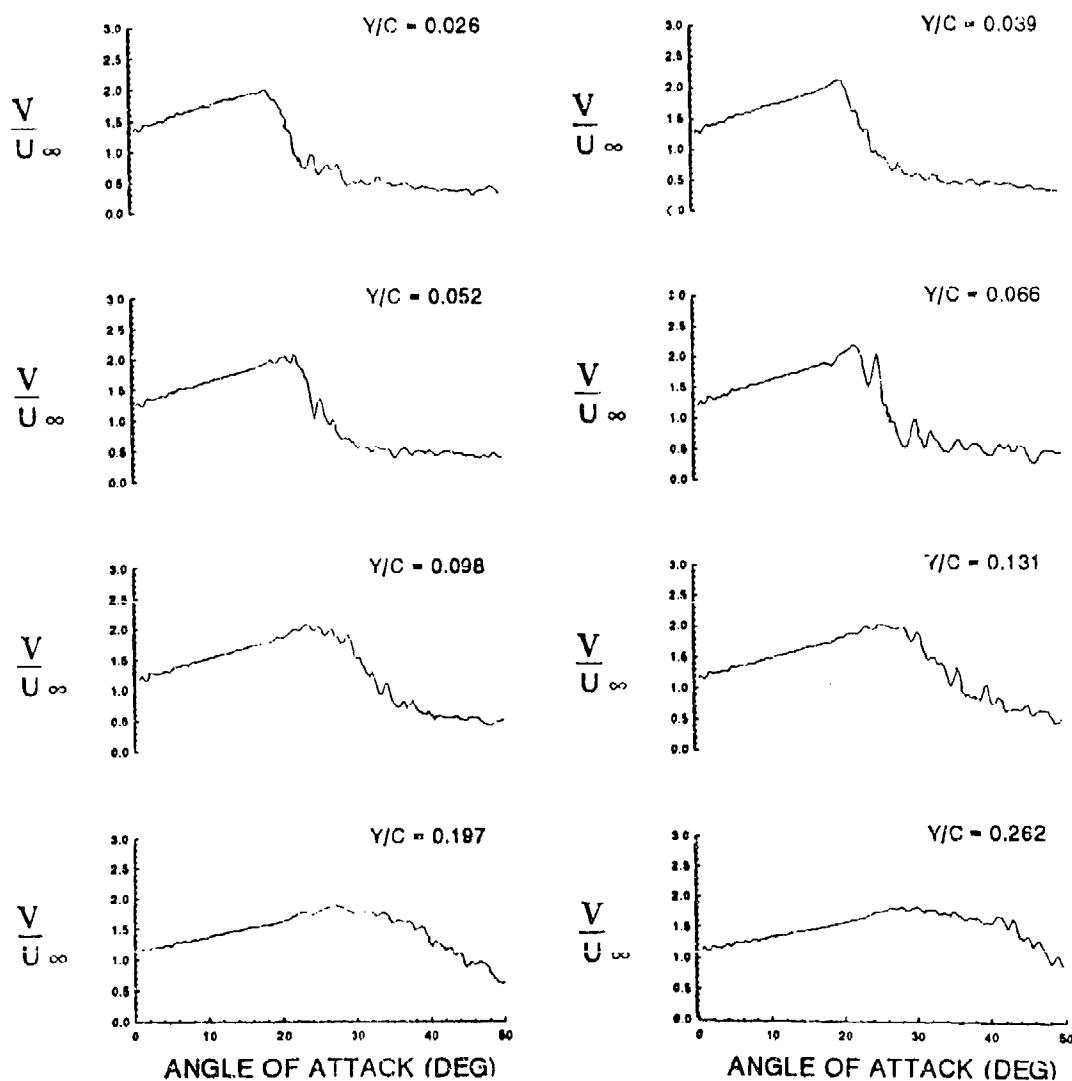


Figure 6-3.

Instantaneous velocity trace over a dynamic airfoil with respect to angle of attack. Pulsed air control at 10 Hz.  $\alpha^+ = 0.05$ ,  $R_c = 24,000$ .  $X/C = 0.10$ .

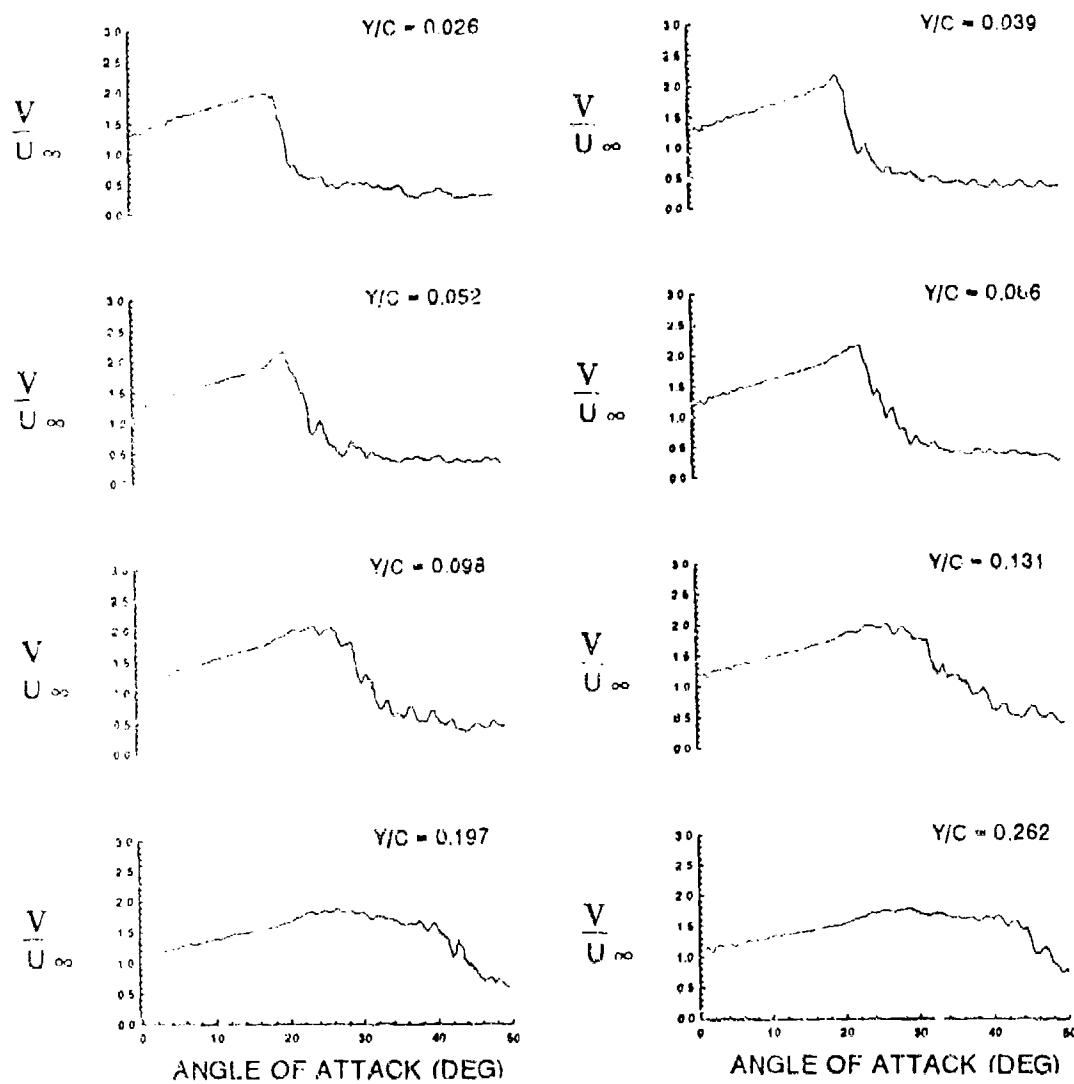


Figure 6-4.

Instantaneous velocity trace over a dynamic airfoil with respect to angle of attack. Pulsed air control at 5 Hz.  $\alpha^+ = 0.05$ ,  $R_c = 24,000$ .  $X/C = 0.10$ .



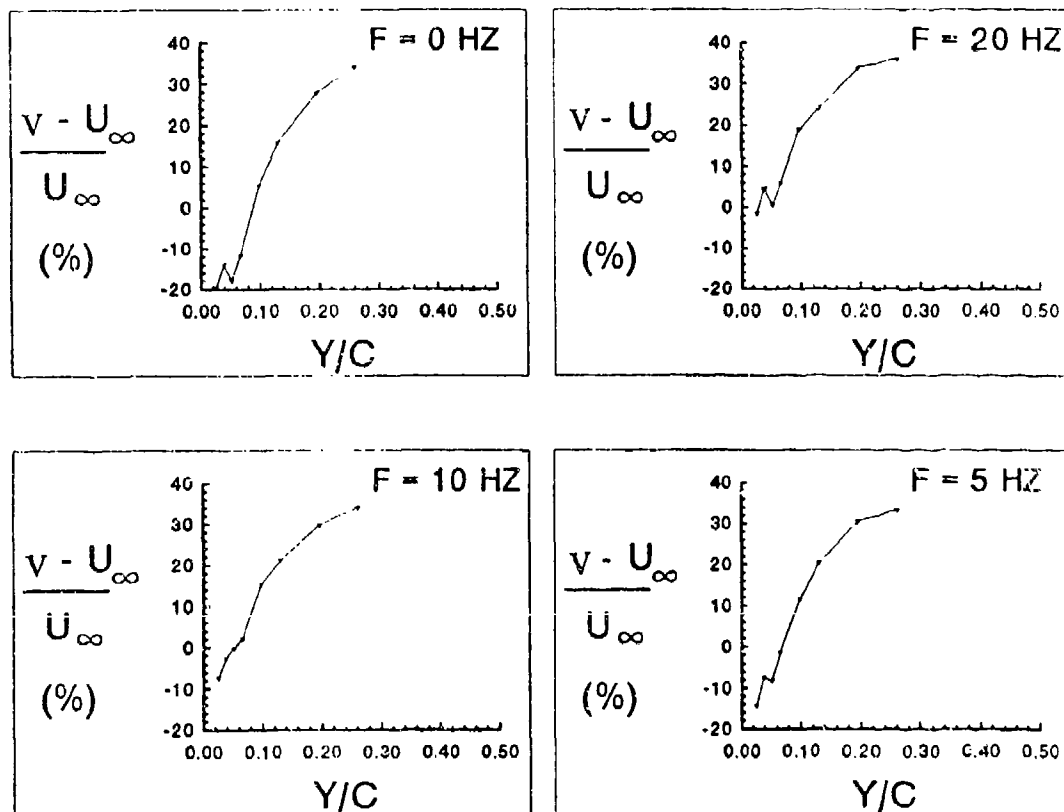


Figure 6-5.

Instantaneous velocity increases with respect to distance from the airfoil surface. Pulsed air control.  $\alpha^+ = 0.05$ ,  $R_c = 24,000$ .  $X/C = 0.10$ .

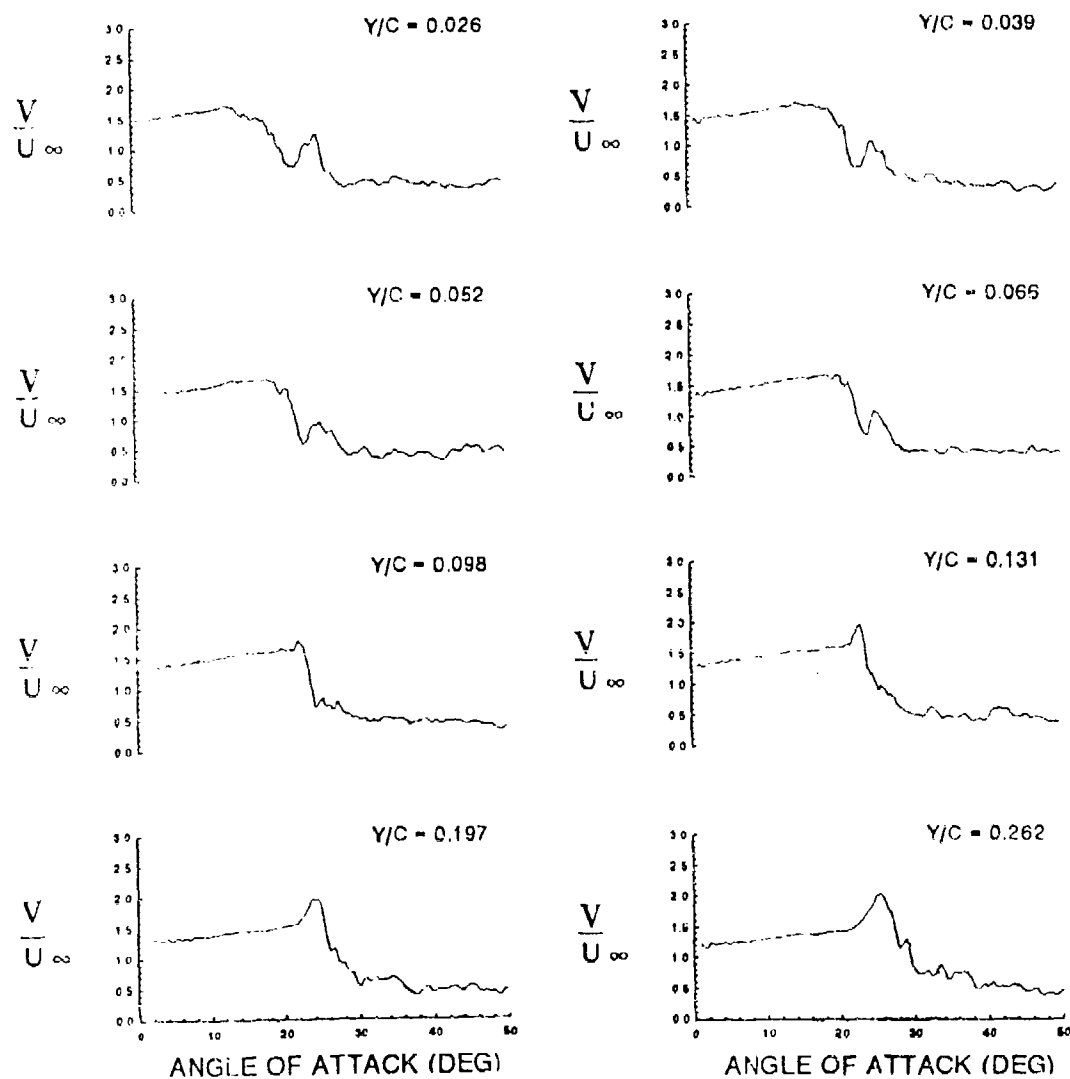


Figure 6-6.

Instantaneous velocity trace over a dynamic airfoil with respect to angle of attack. Natural flow.  $\alpha^+ = 0.05$ ,  $R_c = 24,000$ .  $X/C = 0.30$ .

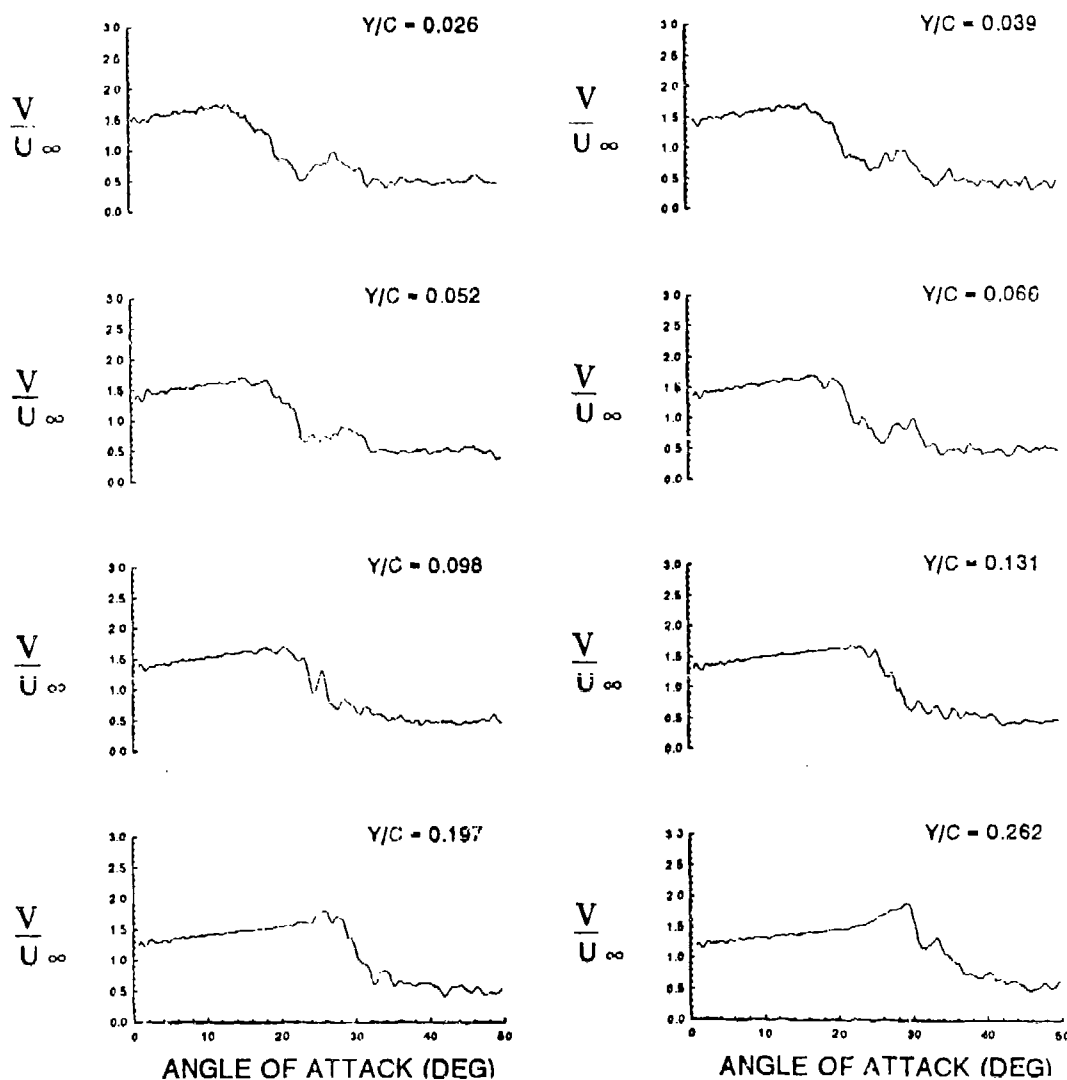


Figure 6-7.

Instantaneous velocity trace over a dynamic airfoil with respect to angle of attack. Pulsed air control at 20 Hz.  $\alpha^+ = 0.05$ ,  $R_c = 24,000$ .  $X/C = 0.30$ .

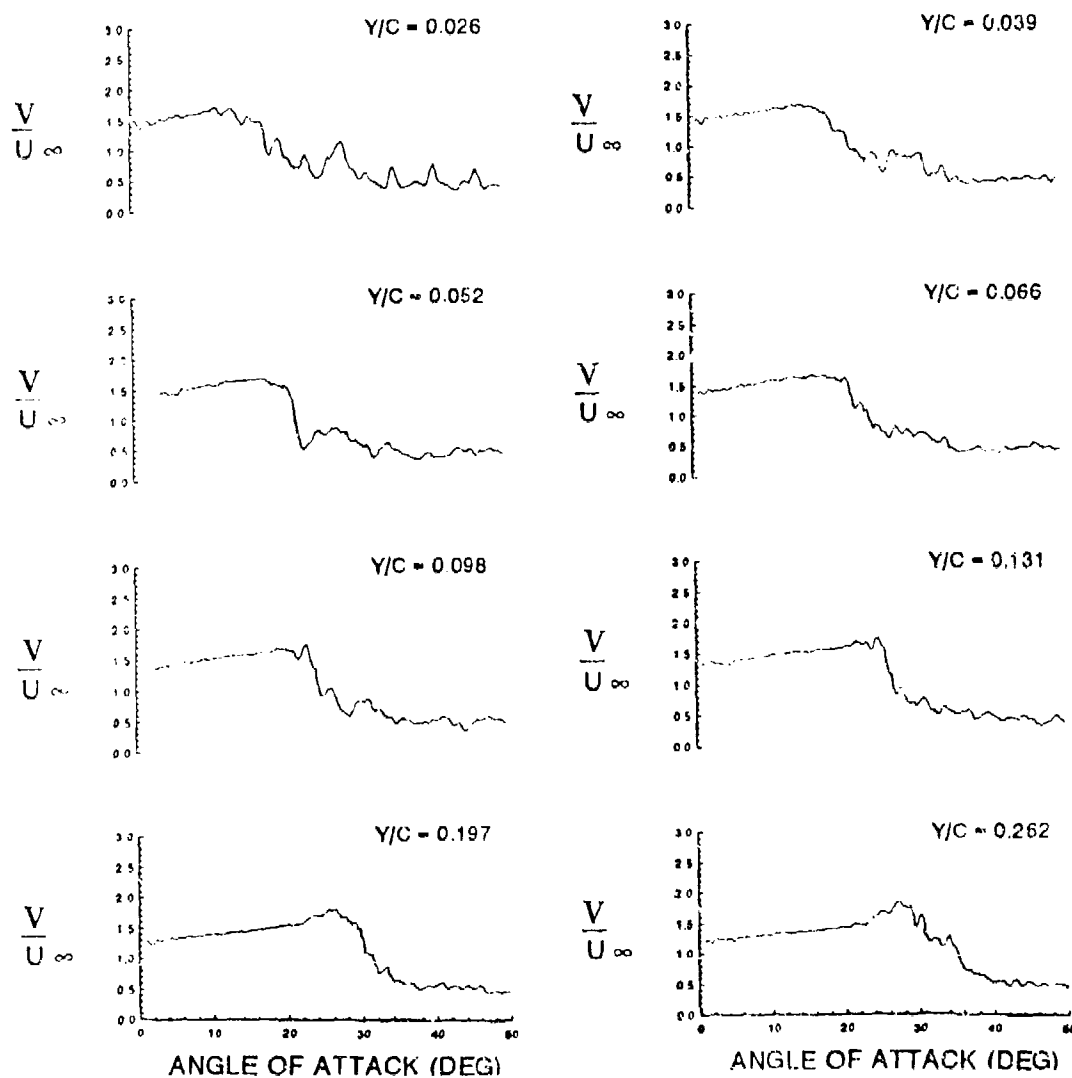


Figure 6-8.

Instantaneous velocity trace over a dynamic airfoil with respect to angle of attack. Pulsed air control at 10 Hz.  $\alpha^+ = 0.05$ ,  $R_c = 24,000$ .  $X/C = 0.30$ .

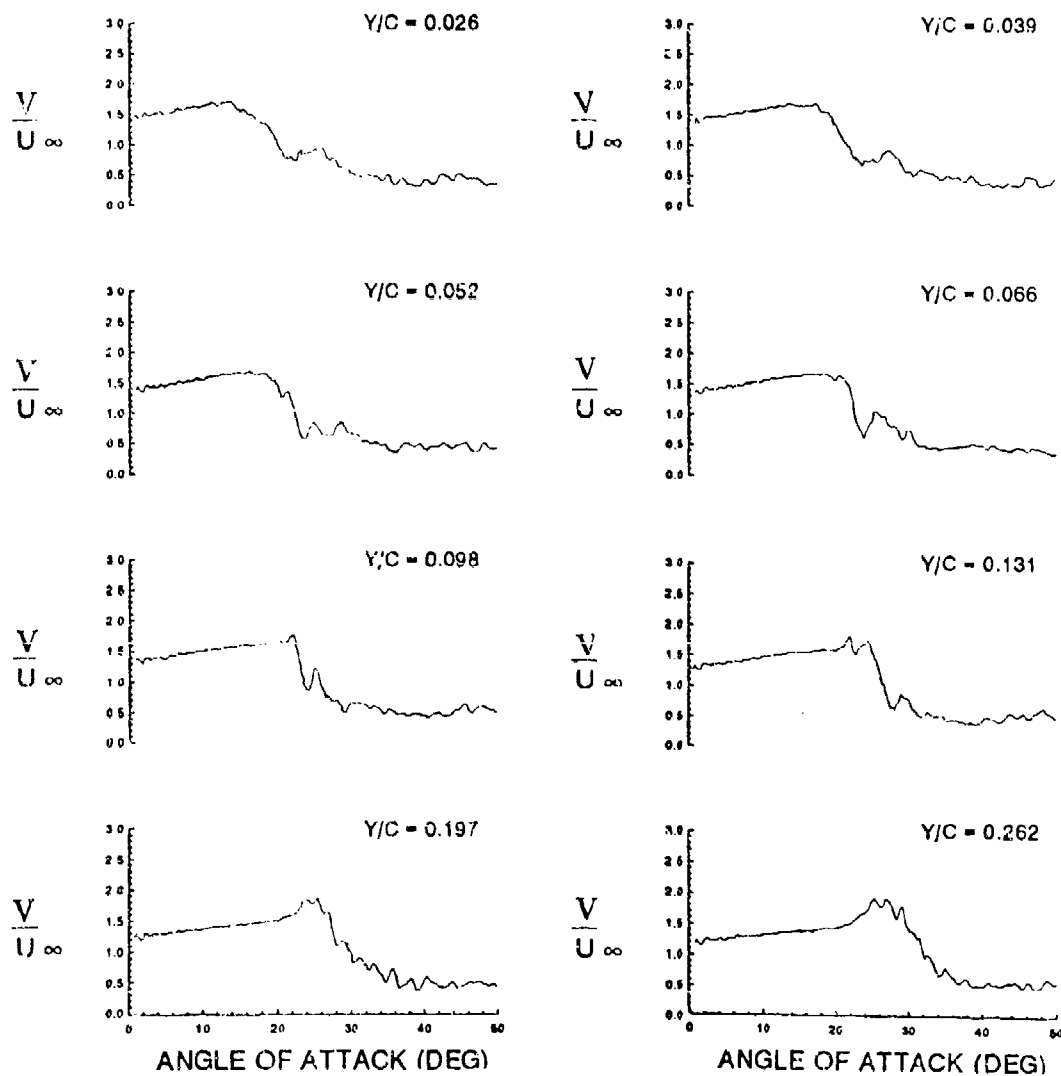


Figure 6-9.

Instantaneous velocity trace over a dynamic airfoil with respect to angle of attack. Pulsed air control at 5 Hz.

$\alpha^+ = 0.05$ ,  $R_c = 24,000$ .  $X/C = 0.30$ .

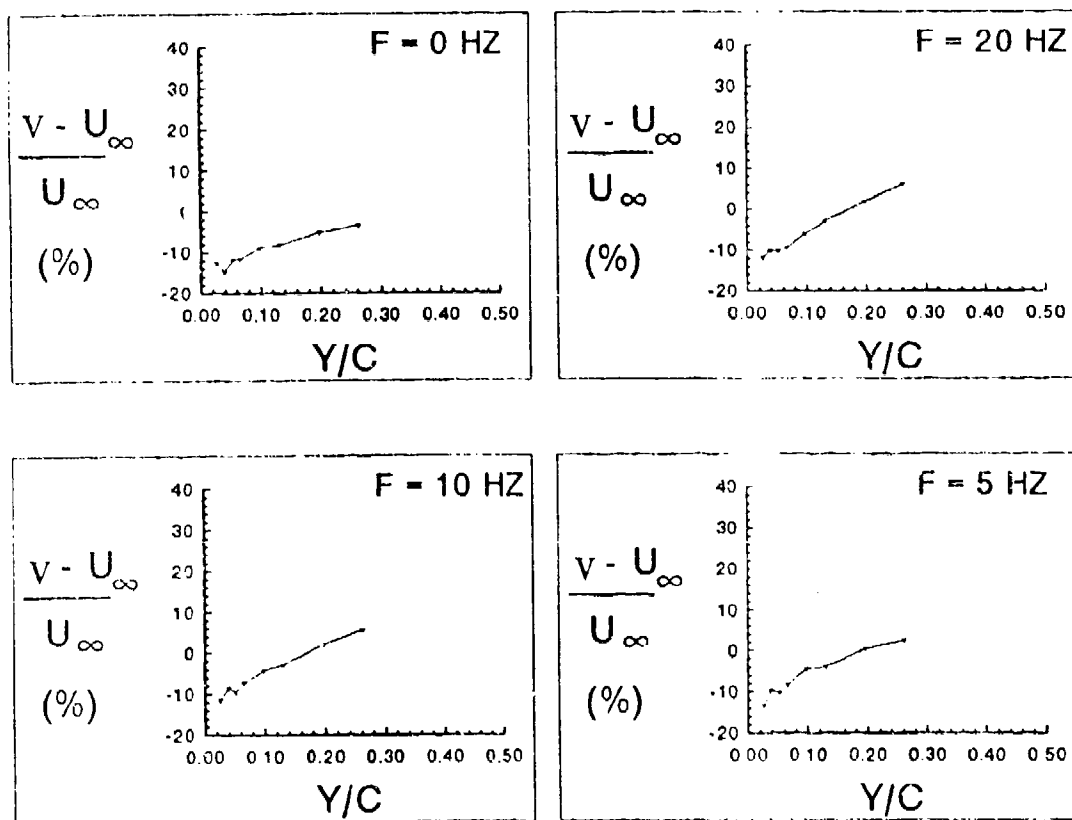


Figure 6-10.

Instantaneous velocity increases with respect to distance from the airfoil surface. Pulsed air control.  $\alpha^+ = 0.05$ ,  $R_c = 24,000$ .  $X/C = 0.30$ .

## 6.2 Qualitative Control Response of the Unsteady Separating Boundary Layer

The effect of internal tangential pulsing on a dynamic flow at a non-dimensional frequency of  $\alpha^+ = 0.05$  depends on forcing frequency, as shown in Figure 6-11 for a chord Reynolds number of 24,000. Flow visualization of the flow forced at frequencies near the fundamental forcing frequency of 20 Hz shows a marked reattachment of the flow over the leading one-third of the airfoil for all three attack angles shown. This enhanced reattachment could be correlated with the reduction in the velocity peak that was noted in the hot-film measurements. There is a significant attenuation of the dynamic stall vortex at an angle of attack of 25° for both forcing frequencies of 22 Hz and 18 Hz. By 30°, the dynamic stall vortex has manifested itself visually over the airfoil, but is preceded upstream by a smaller leading edge structure.

Forcing at frequencies near the first subharmonic of 10 Hz, shown in rows four and five, results in a notable reduction in the overall separation region size at the 20° attack angle. The vortex attenuation that occurred at an attack angle of 25° for the greater control frequencies continues at the lower forcing frequencies, and is still apparent at an angle of attack of 30° for the flow forced at 9 Hz. This example is notable because the flow qualitatively resembles the development of a large periodic free shear layer. This confirms the hot-film measurements at a 10 Hz forcing frequency, which exhibited the greatest enhancement in periodic shedding of the large scale free shear layer structures. Forcing the flow near the static second subharmonic of 5 Hz also appears to visibly enhance free shear layer vortex development, especially at an angle of attack of 25°. The presence of numerous structures on the airfoil is clearly evident for this case.

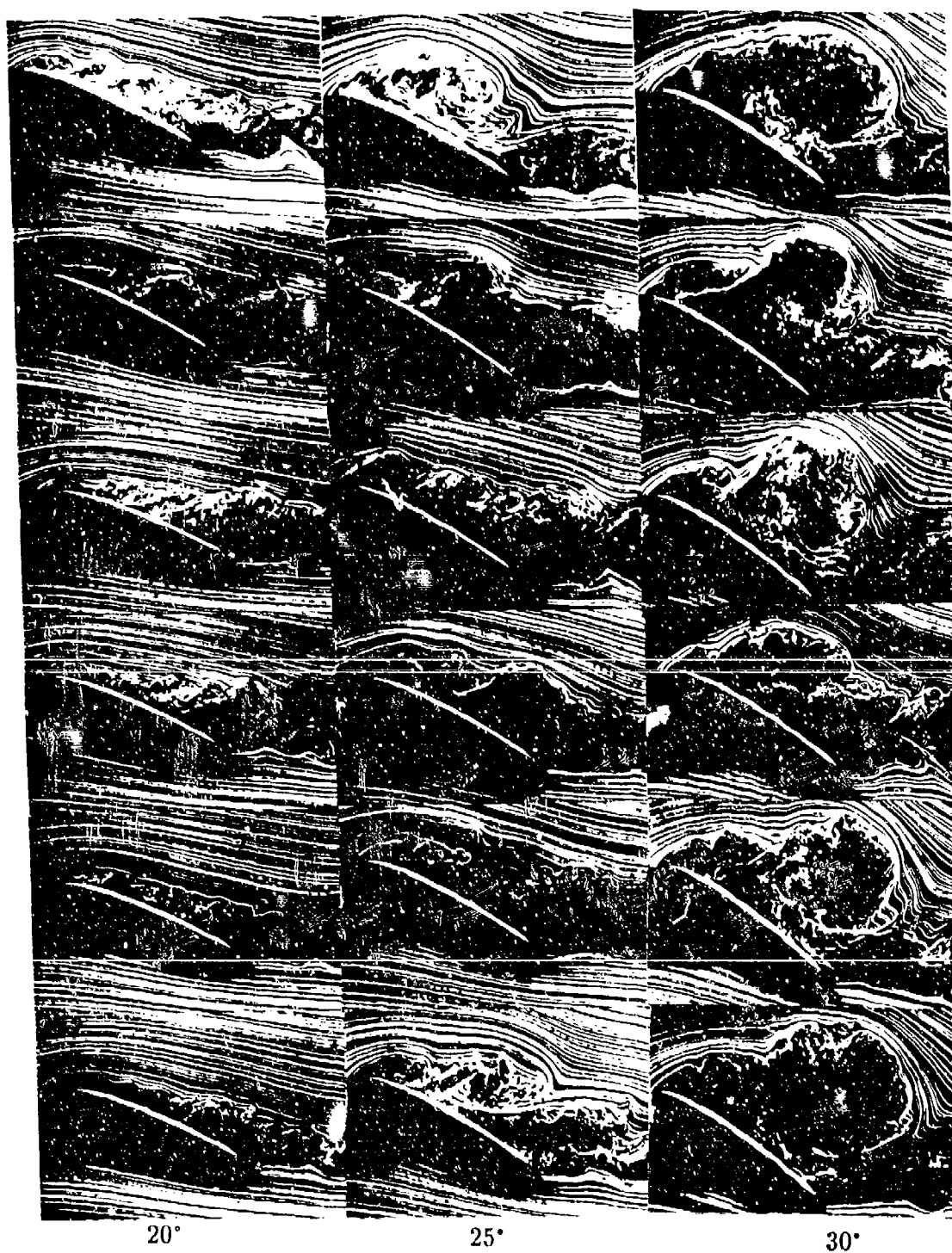


Figure 6-11. Smoke flow visualization of a dynamic airfoil under natural and pulsed air forcing conditions.



### 6.3 Control Effects on Unsteady Airfoil Performance

An evaluation of the aerodynamic benefits of tangential pulsed air control is conducted to judge practical applicability of the forcing. Upper surface pressure coefficients are shown in Figure 6-12 for a chord Reynolds number of 57,000. The first column exhibits the pressure coefficients over the airfoil chord for angles of attack of  $20^\circ$ ,  $25^\circ$ , and  $30^\circ$  for the natural flow. The presence of the dynamic stall vortex, exhibited by the rise in pressure coefficient, can be tracked moving along the surface of the airfoil as the angle of attack is increased. Forcing at the static post-stall first subharmonic frequency creates a significant change in the pressure field over the airfoil at an angle of attack of  $25^\circ$ . Whereas the pressure signature of the dynamic stall vortex is over the trailing edge half of the airfoil for the natural flow, there is a vortical pressure signature over the latter three quarters of the airfoil. It should be noted at this point that there is an apparent bias in the dynamic pressure measurements discussed in this report, resulting in a variation of the lift coefficient magnitudes by a different constant for each of the forcing frequencies. This phenomena could be due to the pulsed air forcing input or to the lack of a pressure tap at the leading edge of the airfoil, or to an undetermined experimental source.

Forcing at the static post-stall subharmonics of 15 Hz and 7.5 Hz, shown in Figure 6-13, yields a reduction in pressure near the leading edge of the airfoil at an angle of attack of  $20^\circ$ . At an attack angle of  $25^\circ$ , there is a smoother transition in the pressure field from the leading edge to the trailing edge. Correlating these results with the flow visualization taken at  $R_c=24,000$  might indicate that this smooth pressure coefficient trace is due to the attenuation of the dynamic stall

vortex. By an angle of attack of  $30^\circ$ , there is little effect on the pressure field due to active control.

Lift coefficients are shown in Figure 6-14 for a non-dimensional pitch rate of 0.05 and a chord Reynolds number of 57,000. The natural flow exhibits a characteristic plateau followed by a peak at approximately  $26^\circ$ . This peak coincides with the presence of the dynamic stall vortex on the airfoil surface. A second peak near an angle of attack of  $40^\circ$  is caused by the formation of a counter-rotating trailing edge vortex (Panda, 1991)

Forcing the flow at the static post-stall first subharmonic forcing frequency, 30 Hz, corresponding to a chord Reynolds number of 57,000 results in a noted shift in lift coefficient peaks to an earlier angle of attack, indicating that the control is enhancing dynamic stall, or at least free shear layer vortex formation. There is also a lessening in appearance of the pre-stall plateau in the lift curve. Reducing the forcing frequency to 15 Hz does not alter the flow as significantly as the greater forcing frequency. The greatest effect due to flow control occurs at the third subharmonic of 7.5 Hz. The plateau which consistently forms prior to the lift coefficient peak in an unforced flow has manifested itself into an actual sub-peak prior to the primary lift peak associated with dynamic stall. The change in lift coefficient magnitude with respect to control frequency cannot be considered at this point. Although the natural lift measurements agree closely with those of Jumper, Schreck, and Dimmick (1987), there appears to be a bias in the lift measurements, shifting the entire plot up or down with respect to lift coefficient magnitude. Considerable alterations in the drag curve shape at control frequencies of 15 and 30 Hz, shown in Figure 6-15, indicates the lift bias may be flow related, but it is the opinion of the author that these results need further analysis. The events such as

peak lift and lift curve shape are not under scrutiny and thus are the only information considered at this time.

Corresponding drag coefficients under natural and actively controlled conditions are shown in Figure 6-15. As expected, the drag curves follow the same trends that as the lift coefficients. The earlier appearance of the dynamic stall vortex at the 30 Hz control frequency is confirmed in the early peak in the drag curve. In addition, the drag peak at the low forcing frequency of 7.5 Hz is delayed by approximately one degree. Since the peak drag corresponds to dynamic stall vortex detachment from the airfoil surface in an unforced flow, it is reasonable to assume that active control has delayed vortex departure.

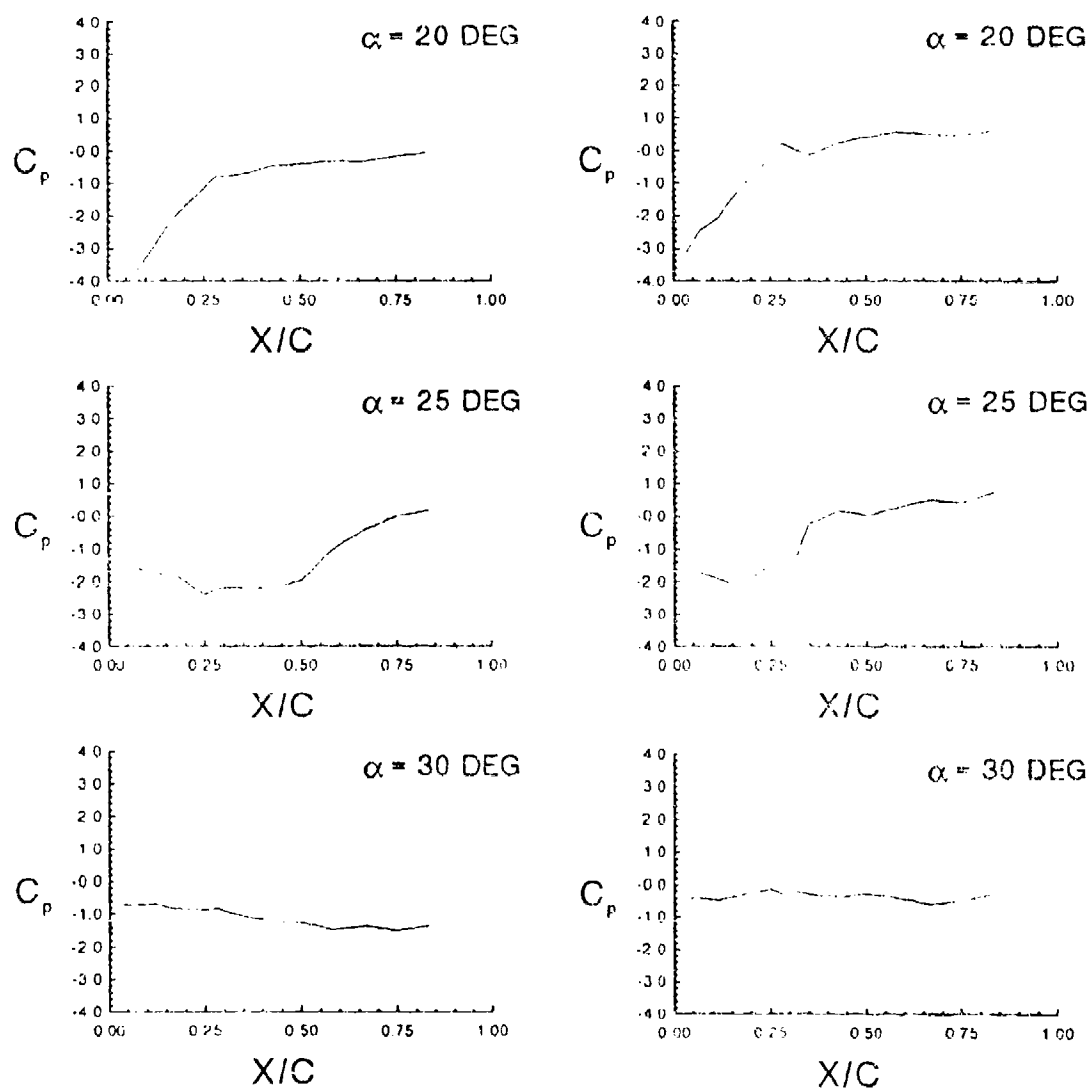


Figure 6 -12.

Instantaneous surface pressure coefficients on a dynamic airfoil under natural conditions (column 1) and pulsed air forced conditions at 30 Hz.  $\alpha^+ = 0.05$ ,  $R_c = 57,000$ .

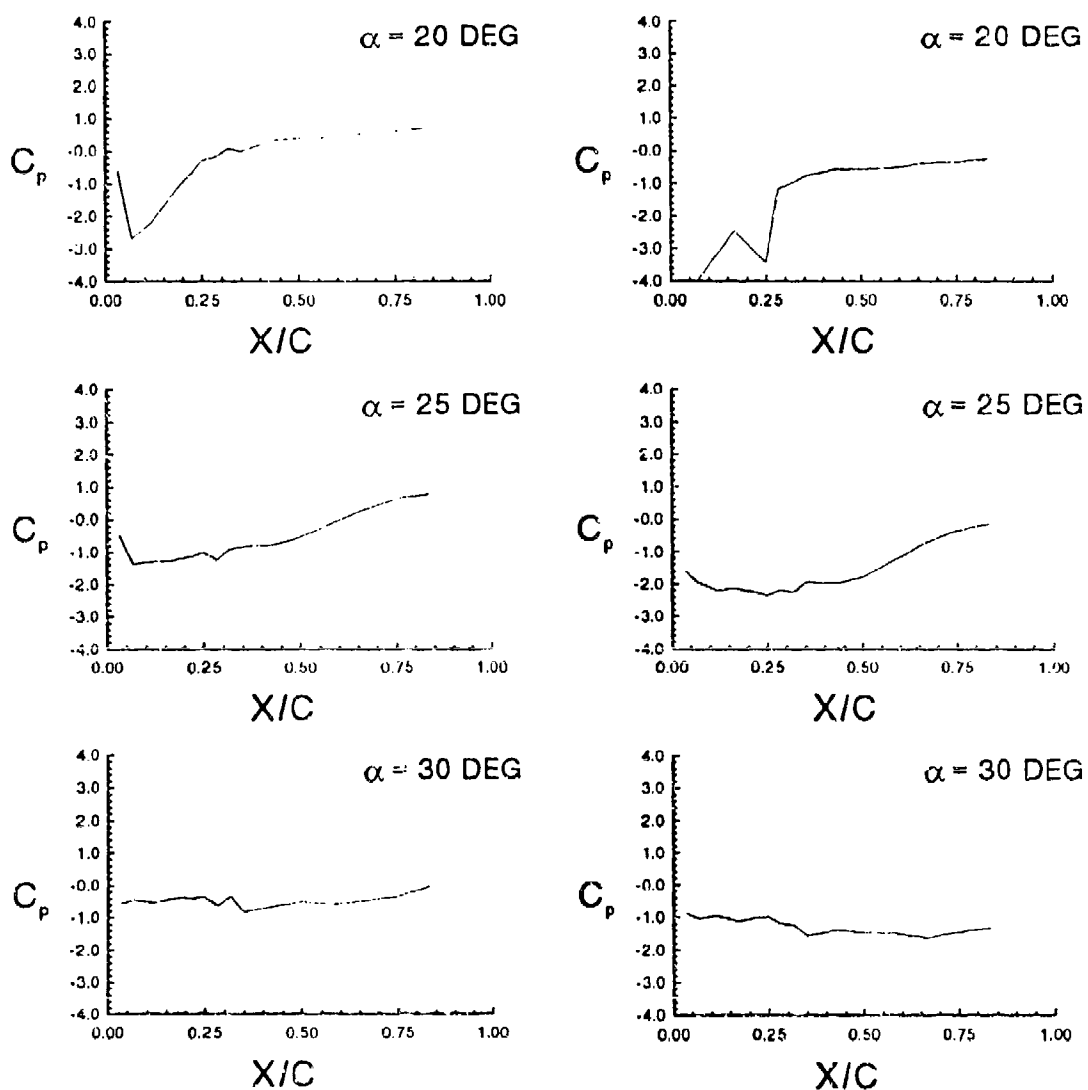


Figure 6-13.

Instantaneous surface pressure coefficients on a dynamic airfoil under pulsed air forcing. Column 1 = 15 Hz and Column 2 = 7.5 Hz.  $\alpha^+ = 0.05$ ,  $R_c = 57,000$ .

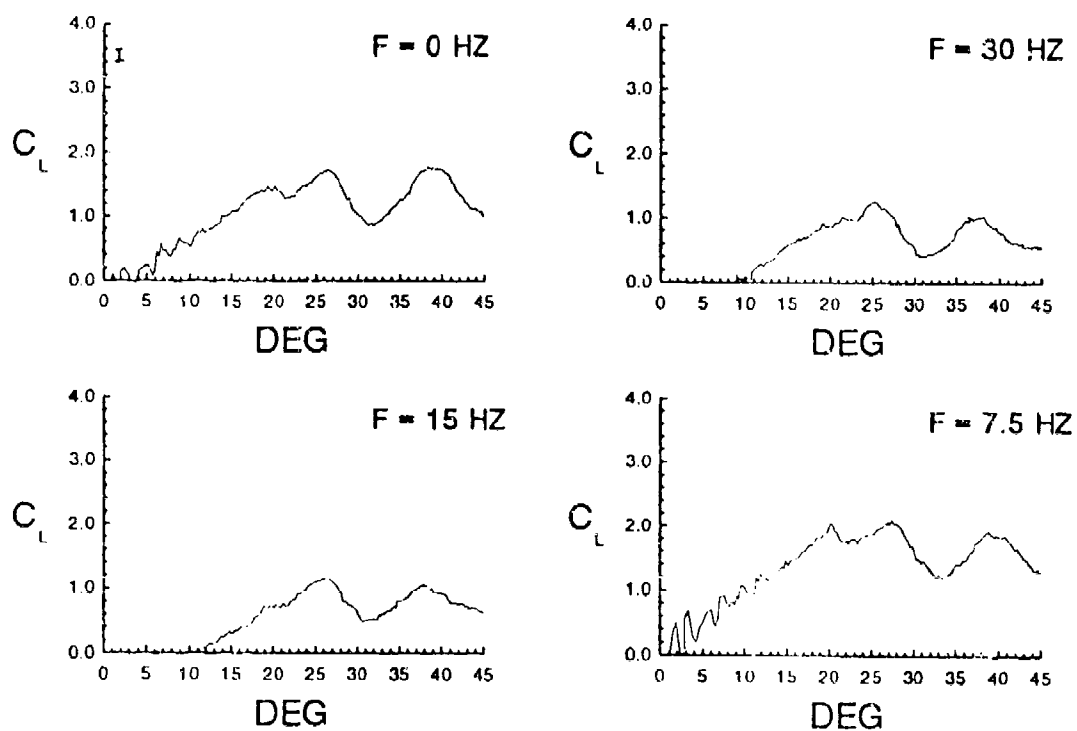


Figure 6-14.

Lift coefficients with respect to angle of attack on a dynamic airfoil. Pulsed air control.  $\alpha^+ = 0.05$ ,  $R_c = 57,000$ .

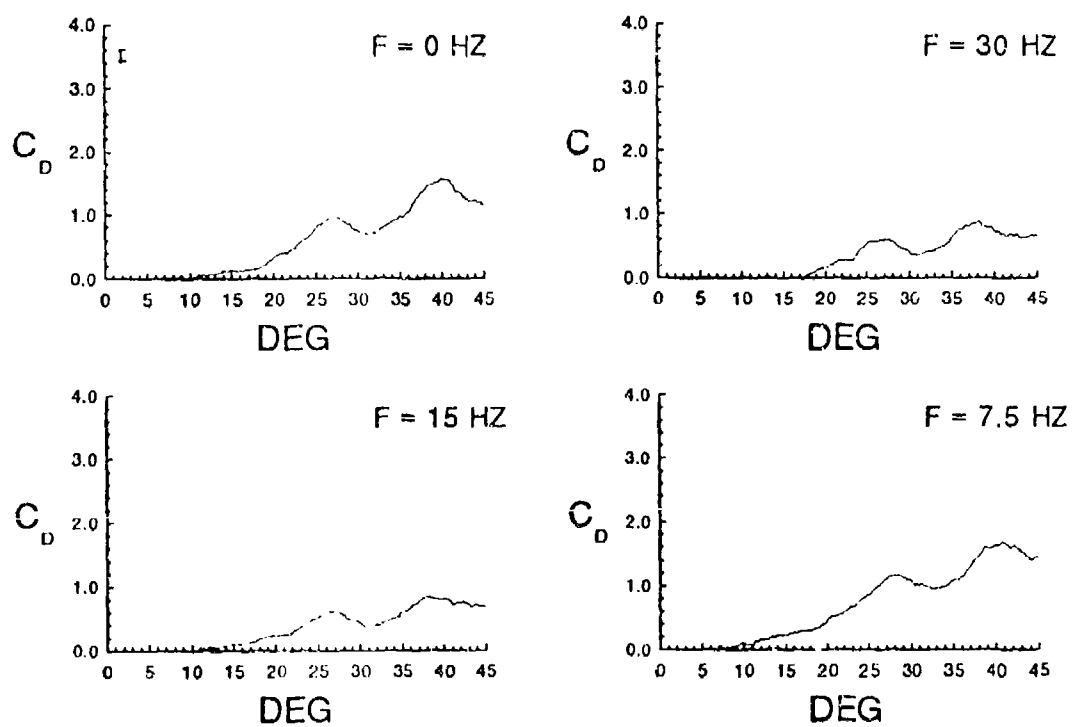


Figure 6-15.

Drag coefficients with respect to angle of attack on a dynamic airfoil. Pulsed air control.  $\alpha^+ = 0.05$ ,  $R_c = 57,000$ .

## CHAPTER SEVEN

### DISCUSSION AND CONCLUSIONS

The overall objective of this research project was to develop and evaluate a control methodology for separation control on a two-dimensional NACA-0015 airfoil. This control process is based on two important criteria. The first is that the separating boundary layer on a static airfoil can be considered a free shear layer. The second is that this free shear layer is susceptible to control via shear layer vortex manipulation. The final part of the study extrapolates to the assumption that the separating unsteady boundary layer prior to dynamic stall vortex formation on a dynamic airfoil is analogous to the free shear layer on a static airfoil. There is a distinct difference between steady and unsteady separation. Static airfoil flow is characterized by leading edge separation, where the flow initially separates from the airfoil leading edge, reattaches into the long separation bubble in some flows, but eventually separates over the entire airfoil, resulting in stall. If the assumption that pre-vortex separated dynamic flow is indeed accurate, then the pre-stall unsteady separation should be sensitive to the developed static airfoil free shear layer control methods.

#### 7.1 Discussion — Static Airfoil

The fundamental frequency, or that frequency at which the free shear layer is most receptive to active control, is equal to four times the calculated airfoil wake frequency for the NACA-0015 airfoil studied. The fundamental frequency reaches a



constant after the separation point reaches the leading edge and the airfoil has stalled. It follows reason that the fundamental frequency measured at the 5% chord location in this experiment would be greater than the calculated wake frequency, since the unforced free shear layer structures pair as the distance along the airfoil increases. By the time the wake is reached, the vortices have paired sufficiently to reduce the frequency associated with vortex passage by a factor of four.

Both external acoustic and internal tangential-pulsed air control successfully manipulate the growth and development of the large-scale layer structures in the airfoil separating boundary layer. Forcing at the fundamental frequency inhibits vortex pairing, while forcing at the corresponding subharmonics enhances vortex pairing. This effect is visible in both the near-surface hot-film velocity traces and in the surface pressure time traces. The nature of the near-surface hot-film velocity traces closely resembles that of a similarly controlled mixing layer, indicating that the static separating boundary layer can indeed be considered a free shear layer.

The overall size of the separation region is reduced for a post-stall airfoil under tangential-pulsed air forcing at both the fundamental frequencies and the subharmonic frequencies. Control at the fundamental frequencies prevents shear layer vortex pairing and thus inhibits shear layer growth, reducing the separation region. Control at the subharmonic frequencies actually enhances free shear layer vortex pairing, causing the free shear layer to grow. The resultant controlled separation region size is actually reduced, however. It is speculated that the enhanced free shear layer vortices offer a mechanism for the separating boundary layer to dissipate more energy into the freestream thus inhibiting separation progression and enhancing flow reattachment.

Internal-tangential pulsed air control at free shear layer subharmonic frequencies enhances the aerodynamic performance of the static airfoil, resulting in as much as a 36% increase in pressure coefficient magnitude over the airfoil upper surface under forced conditions. Since the input velocity of the forcing is on the order of actual bleed air available on aircraft engines (Stermer, 1991), the augmented airfoil upper surface pressure magnitudes indicate a promising future practical application.

## 7.2 Discussion — Dynamic Airfoil

Imparting tangential-pulsed air control into the flow over a dynamic airfoil at frequencies associated with a post-stall static flow alters the development of the unsteady separating boundary layer. Both static fundamental and subharmonic frequency control enhance velocity oscillations at locations above the upper airfoil surface, and in some cases smooth out the velocity reductions indicating vortex passage past the airfoil. Comparing these results with the dynamic flow visualization, it is apparent that the smoother transition is accompanied by dynamic stall vortex attenuation at an angle of attack of  $25^\circ$ . This indicates that the broadening of the velocity peak represents a reduction in the vortex strength on the upper airfoil surface. These events also coincide with a slight increase in the average total velocities measure by the hot-film probe.

### 7.3 Conclusions – Static and Dynamic Airfoil

The following conclusions can be drawn from the experimental results:

#### Static Airfoil:

- The fundamental frequency for a two-dimensional NACA-0015 airfoil is a function of angle of attack and freestream velocity prior to airfoil stall. This frequency is an integral multiple of the wake frequency. After stall, the frequency remains constant as the angle of attack increases, being a function of freestream velocity only.
- Acoustic and pulsed air active control at the airfoil fundamental frequencies are successful in inhibiting pairing of the structures in the separating boundary layer. Active control at subharmonics of the fundamental frequency enhances structure pairing.
- The response of the airfoil separating boundary layer to active control indicates that it can be considered a boundary layer in transition to a free shear layer.
- Active control at frequencies corresponding to the fundamental frequencies of the NACA-0015 airfoil and its subharmonics reduces the size of the post-stall separation region over the airfoil and results in significantly

increased surface pressure coefficient magnitudes. This result shows promise for future practical applications.

### Dynamic Airfoil

- Active control at static post-stall fundamental frequencies on a dynamic NACA-0015 airfoil attenuates the dynamic stall vortex and reduces the size of the overall separation region.
- Active control at these frequencies also results in a slight delay in dynamic stall.
- Both surface pressure coefficient magnitudes and airfoil lift and drag values are significantly altered by the active control.

## CHAPTER EIGHT

### RECOMMENDATIONS

The following extensions of this experimental study are recommended for further research into the development of a dynamic control methodology:

- An extensive evaluation of the fundamental frequencies associated with the unsteady separating boundary layer. Since these frequencies are expected to change with respect to angle of attack as the airfoil is pitching, it would be worthwhile to study this aspect using a technique such as wavelet transforms. A wavelet transform allows determination of flow frequencies in both space and time.
- Control input, based on the information obtained from the unsteady flow frequencies. This analysis could be accomplished through hot-wire and pressure measurements, as well as application of real-time flow visualization to evaluate the control effects on shear layer and dynamic stall vortex development.
- Development of an interactive dynamic control method. Such a method would measure the frequencies in the flow, evaluate these frequencies using

the wavelet transform, and then input control based on the determined frequencies.

## BIBLIOGRAPHY

Ahuja, K. K. and Burrin, R. H. (1984) "Control of Flow Separation by Sound," AIAA Paper No. 84-2298.

Albertson, J. A., Troutt, T. R., Siuru, W. D., and Walker, J. M. (1987) "Dynamic Stall Vortex Development and the Surface Pressure Field of a Pitching Airfoil," AIAA Paper No. 87-1333.

Albertson, J. A., Troutt, T. R., and Kedzie, C. R. (1988) "Unsteady Aerodynamic Forces at Low Airfoil Pitching Rates," AIAA Paper No. 88-2579.

Arena, A. V. and Mueller, T. J. (1980) "Laminar Separation, Transition, and Turbulent Reattachment Near the Leading Edge of Airfoils," AIAA J., Vol. 18, No. 7, pp 747-753.

Bar-Sever, A. (1989) "Separation Control on an Airfoil by Periodic Forcing," AIAA J., Vol. 27, No. 6, pp 820-821.

Bhattacharjee, S., Scheelke, B., and Troutt, T. R. (1986) "Modification of Vortex Interactions in a Reattaching Separated Flow," AIAA J., Vol. 24, No. 4, pp 623-629.

Birnbaum, W. (1923) "Die tragende Wirbelfläche als Hilfsmittel zur Behandlung des ebenen Problems der Tragflügel theorie," Zeitschrift für angewandte Mathematik und Mechanik (ZAMM) 3, pp. 290-297.

Bradley, R. G. and Wray, W. O. (1974) "A Conceptual Study of Leading-Edge Vortex Enhancement by Blowing," J. Aircraft, Vol. 11, No. 1, pp 33-38.

Browand, F. K. (1986) "The Structure of the Turbulent Mixing Layer," Physica, Vol. 18D, pp 135-148.

Browand, F. K. and Troutt, T. R. (1980) "A Note on the Spanwise Structure in the Two-Dimensional Mixing Layer," J. Fluid Mech., Vol. 97, pp 771-781.

Browand, F. K. and Troutt, T. R. (1985) "The Turbulent Mixing Layer: Geometry of Large Vortices," J. Fluid Mech., Vol. 158, pp 489-509.

Browand, F. K. and Weidman, P. D. (1976) "Large Scales in the Developing Mixing Layer," J. Fluid Mech., Vol. 76, pp 127-144.

Brown, G. and Reshko, A. (1974) "On Density Effects and Large Structure in Turbulent Mixing Layers," J. Fluid Mech., Vol. 64, pp 593-704.

Campbell, J. F. (1976) "Augmentation of Vortex Lift by Spanwise Blowing," J. Aircraft, Vol. 13, No. 9, pp 727-732.



Carr, L. W. (1988) "Progress in Analysis and Production of Dynamic Stall," J. Aircraft, Vol 25, No. 1, pp 6-17.

Carr, L. W. and McAlister, K. W. (1983) "The Effect of a Leading-Edge Slat on the Dynamic Stall of an Oscillating Airfoil," AIAA Paper No. 83-2533.

Carr, L. W., McAlister, K. W., and McCroskey, W. J. (1977) "Analysis of the Development of Dynamic Stall Based Upon Oscillating Airfoil Experiments," NASA TN-8382.

Cherry, N. J., Hillier, R., and Latour, M. P. (1984) "Unsteady Measurements in a Separated and Reattaching Flow," J. Fluid Mech., Vol. 144, pp 13-46/

Collins, F. G. (1981) "Boundary-Layer Control on Wings Using Sound and Leading-Edge Serrations," AIAA J., Vol. 19, No. 2, pp 129-130.

Cook, R. J. (1987) "Similarity Conditions for Flows about Pitching Airfoils," FJSRL-TM-87-003.

Crighton, D. G. (1981) "Acoustics as a Branch of Fluid Mechanics," J. Fluid Mech., Vol. 106, pp. 261-298.

Crow, S. C. and Champagne, F. H. (1971) "Orderly Structure in Jet Turbulence", J. Fluid Mech., Vol 48., Part 3, pp 547-591.

Currier, J. and Fung, K-Y, (1991) "An Analysis of the Onset of Dynamic Stall," AIAA Paper No. 91-0003.

Francis, M. S. and Keese, J. E. (1985) "Airfoil Dynamic Stall Performance with Large-Amplitude Motions," AIAA J., Vol. 23, No. 11, pp 1653-1659.

Gad-el-Hak, M. (1986) "The Use of the Dye-Layer Technique for Unsteady Flow Visualization," J. of Fluids Eng., Vol. 108, No. 3, pp 34-38.

Gad-el-Hak, M. and Bushnell, D. (1991) "Status and Outlook of Flow Separation Control," AIAA Paper No. 91-0037.

Gad-el-Hak, M. and Ho, C.-M. (1986) "Unsteady Vortical Flow Around Three-Dimensional Lifting Surfaces,"

Ham, N. D. (1972) "Some Recent MIT Research on Dynamic Stall," J. Aircraft., Vol. 9, No. 5, pp 378-379.

Ham, N. D. and Garelick, M. S. (1968) "Dynamic Stall Considerations in Helicopter Rotors," J. Am. Hel. Soc., Vol. 13, No. 2, pp 40-50.

Harper, R. W. and Flanigan, R. E. (1948) "Investigation of the Variation of Maximum Lift for a Pitching Airplane Model and Comparison with Flight Results," NACA TN-1734, October, pp 1-22.

Helin, H. E. and Walker, J. M. (1985) "Interrelated Effects of Pitch Rate and Pivot Point on Airfoil Dynamic Stall," AIAA Paper No. 85-0130.

Herbst, W. B. (1985-a) "Dynamics of Air Combat," J. Aircraft, Vol. 20, No. 7, pp 594-598.

Herbst, W. B. (1985-b) "Supermaneuverability," Workshop on Unsteady Separated Flows, pp 1-8.

Ho, C. M. and Huang, L. S. (1982) "Subharmonics and Vortex Merging in Mixing Layers," J. Fluid Mech., Vol. 119, pp 443-473.

Ho, C. M. and Huerre, P. (1984) "Perturbed Free Shear Layers," Ann. Rev. Fluid Mech., Vol. 16, pp 365-424.

Hsiao, F., Shyu, R. and Chang, R. (1990) "Forcing Level Effect of Internal Acoustic Excitation of the Improvement of Airfoil Performance," AIAA Paper No. 90-4010.

Huang, L. S., Maestrello, L., and Bryant, T. D. (1987) "Separation Control Over an Airfoil at High Angles of Attack by Sound Emanating From the Surface," AIAA Paper No. 87-1261.

Jumper, E. J., Dardis, W. J., and Stephen, E. J. (1988) "Toward an Unsteady Flow Airplane," AIAA Paper No. 88-0752.

Jumper, E. J., Schreck, S. J., and Dimmick, R. L. (1987) "Lift-Curve Characteristics for an Airfoil Pitching at Constant Rate," J. Aircraft, Vol. 24, No. 10, pp 680-687.

Kamalu, N. (1989) Visualization Techniques for Understanding Particle Dispersion in Free Shear Flows, PhD Dissertation, Washington State University, Pullman, WA.

Katz, J. (1981) "A Discrete Vortex Method for the Non-Steady Separated Flow Over an Airfoil," J. Fluid Mech., Vol. 102, pp 315-328.

Kibens, V. (1979) Mechanics of Sound Generation by Flows, Ed. E.-A. Muller, p 174. Springer.

Klinge, J., Schreck, S., and Luttges, M. (1991) " " AIAA Paper No. 91-3264

Kramer, M. (1932) "Die Zunahme des Maximalauftriebes von Tragflugeln bei plotzlicher Anstell winkelvergroberung (Boeneffekt)," Zeitschrift fur Flugtechnik und Motorluftschiffahrt (ZFM) 23, pp. 185-189.

Lasheras, J. C., Cho, J. S., and Maxworthy, T. (1986) "On the Origin and Evolution of Streamwise Vortical Structures in a Plane Free Shear Layer," J. Fluid Mech., Vol. 172, pp 231-258.

**Lippisch, A. (1935)** "Versuche zur Sichtbarmachung von Stromlinien," Jahrbuch der Vereinigung für Luftfahrtforschung (VLF), pp. 118–127.

**Lissaman, (1983)** "Low-Reynolds Number Airfoils," Ann. Rev. Fluid Mech., Vol. 15, pp 223–239.

**Luttges, M. W., Robinson, M. C., and Kennedy, D. A. (1985)** "Control of Unsteady Separated Flow Structures on Airfoils," AIAA Paper No. 85–0531.

**Maestrello, L. (1986)** "Active Transition Fixing and Control of the Boundary Layer in the," AIAA J., Vol. 24, No. 10, pp 1577–1581.

**McCroskey, W. J. (1982)** "Unsteady Airfoils," Annual Review of Fluid Mechanics, Vol. 25, No. 1., pp. 285–311.

**McLaughlin, T. (1992)** Private communication. PhD Dissertation August 1992, University of Colorado, Boulder, CO.

**Monkewitz, P. A. (1988)** "Subharmonic Resonance, Pairing, and Shredding in the Mixing Layer," J. Fluid Mech., Vol. 188, pp 223–252.

**Moore, F. K. (1958)** "On the Separation of the Unsteady Laminar Boundary Layer," IUTAM Symposium, Boundary layers, H. Görtler, ed., pp 296–311.

Mueller, T. J. and Batill, S. M. (1982) "Experimental Studies of Separation on a Two-Dimensional Airfoil at Low Reynolds Numbers," AIAA J., Vol. 20, No. 4, pp 457-463.

Oster, D. and Wygnanski, I. (1982) "The Forced Mixing Layer Between Parallel Streams," J. Fluid Mech., Vol. 123, pp 91-130.

Panda, J. (1991) Private communication

Reynolds, W. C. and Carr, L. W. (1985) "Review of Unsteady, Driven, Separated Flows," AIAA Paper No. 85-0527.

Roberts, L., Hesselink, L., Kroo, I., and Wood, N. J. (1985) "The Control of Vortical Flows Over a Delta Wing," Workshop - II on Unsteady Separated Flows, FJSRL-TR - pp 317-322.

Roos, F. W. and Kegelman, J. T. (1986) "Influence of Excitation on Coherent Structures in Reattaching Turbulent Shear Layers," AIAA Paper No. 86-0112.

Roshko, A. (1954) "On the Development of Turbulent Wakes from Vortex Streets," NACA Report 1191.

Rott, N. (1956) "Unsteady Viscous Flow in the Vicinity of a Stagnation Point," Quart. Appl. Math., Vol. 13, pp 444-451.

Sears, W. R. and Telionis D. P. (1975) "Boundary Layer Separation in Unsteady Flow," SIAM J. Appl. Math., Vol. 28, pp 215-235.

Schlichting, H. (1955) Boundary-Layer Theory, McGraw Hill Book Company, New York.

Seginer, A. and Salomon, M. (1986) "Performance Augmentation of a 60-Degree Delta Aircraft Configuration by Spanwise Blowing," J. Aircraft, Vol. 23, No. 11, pp 801-807.

Silverstein, A. Katzoff, S., and Hootman, J. A. (1938) "Comparative Flight and Full-Scale Wind-Tunnel Measurements of the Maximum Lift of an Airplane," NACA Report 618.

Stephen, E., et al (1989) "Extended Pitch Axis Effects on the Flow about Pitching Airfoils," AIAA Paper 89-0025

Stermer, J. (1991) Private Communication, U. S. Air Force Academy Aeronautics Laboratory, CO

Strickland, J. H. and Graham, G. M. (1986) "Dynamic Stall Inception Correlation for Airfoils Undergoing Constant Pitch Rate Motions," AIAA J., Vol. 24, No. 4, pp 678-680.

Tordella, D. and Christiansen, W. H. (1989) "Spectral Observation in a Forced Mixing Layer," AIAA J., Vol. 27, No. 12, pp 1741-1743.

Troutt, T. R. Scheelke, B., and Norman, T. R. (1984) "Organized Structures in a Reattaching Separated Flow Field," J. Fluid Mech., Vol. 143, pp 413-427.

Van den Berg, B. (1981) "Role of Laminar Separation Bubbles in Airfoil Leading -Edge Stalls," AIAA J., Vol. 19, No. 5, pp 553-556.

Walker, J. M. and Chou, D. C. (1987) "Forced Unsteady Vortex Flows Driven by Pitching Airfoils," AIAA Paper No. 87-1331.

Walker, J. M., Helin, H. E., and Chou, D. C. (1985) "Unsteady Surface Pressure Measurements on a Pitching Airfoil," AIAA Paper No. 85-0532.

Walker, J. M., Helin, H. E., and Strickland, J. H. (1985) "An Experimental Investigation of an Airfoil Undergoing Large Amplitude Pitching Motions," AIAA Paper No. 85-0039.

Whitford, R. (1987) Design For Air Combat, Jane's Publishing Company Limited, New York, NY.

Winant, C. D. and Browand, F. K. (1974) "Vortex Pairing: The Mechanism of Turbulent Mixing-Layer Growth at Moderate Reynolds Number," J. Fluid Mech., Vol. 63, Part 2, pp 237-255.



Wood, N. J. and Roberts, L. (1988) "Control of Vortical Lift on Delta Wings by Tangential Leading-Edge Blowing," J. Aircraft, Vol. 25, No. 3, pp 236-243.

Wu, X. H., Wu, J. Z., and Wu, J. M. (1991) "Guiding Principles for Vortex Flow Control," AIAA Paper No. 91-0617.

Zaman, K. B. M. Q., Bar-Sever, A., and Mangalam, S. M. (1987) "Effect of Acoustic Excitation on the Flow over a Low-Re Airfoil," J. Fluid Mech., Vol. 182, pp 127-148.

Zaman, K. B. M. Q. and McKinzie, D. J. (1991) "Control of Laminar Separation Over Airfoils by Acoustic Separation," AIAA J., Vol. 29, No. 7, pp 1075-1083.

Zaman, K. B. M. Q. and Rice, E. J. (1992) "On the Mechanism of Turbulence Suppression in Free Shear Flows Under Acoustic Excitation," AIAA Paper No. 92-0065.

## APPENDIX A

The following is a list of programs used in this study. They are located on the MassComp MC-5500, located at the Frank J. Seiler Research Laboratory.

- |    |                      |                       |
|----|----------------------|-----------------------|
| 1. | Pressure acquisition | PRESS_ONE.F           |
| 2. | Hot-film acquisition | HWIRE.F               |
| 3. | Pressure reduction   | PRESS_CONV.F          |
| 4. | Hot-film reduction   | RDSTATIC.F or RDDYN.F |